u^{b}

Graduate School for Cellular and Biomedical Sciences

University of Bern

Engineering Absorbable Fiber Reinforced Bone Substitute Materials

PhD Thesis submitted by

Elias Tarek Constantin Mulky

from **Sempach LU**

for the degree of

PhD in Biomedical Engineering

Supervisor
Prof. Dr. Martin Frenz
Institute of Applied Physics
Faculty of Science of the University of Bern

Co-advisor
Dr. Reto Luginbuehl
Blaser Swisslube

Accepted by the Faculty of Medicine, the Faculty of Science and the Vetsuisse Faculty of the University of Bern at the request of the Graduate School for Cellular and Biomedical Sciences

Bern,   Dean of the Faculty of Medicine

Bern,   Dean of the Faculty of Science

Bern,   Dean of the Vetsuisse Faculty Bern

Licence

This thesis is licensed under a Creative Commons Attribution 4.0 International License (CC BY 4.0 DEED): https://creativecommons.org/licenses/by/4.0/

Fall down seven times
stand up eight.
— Japanese Proverb

To my parents, who made it possible.

Abstract

The aim of this thesis, embedded in the clinically relevant field of absorbable bone substitute materials, specifically calcium phosphate cements reinforced with poly-l-lactic-acid fibers, was to investigate the factors influencing the compressive mechanical properties of these cements, and to develop novel methods to improve the compressive strength. These investigations were grouped into work packages (WP). The first WP examined the dispersibility of the fibers within the cement matrix. Here, a novel method based on particle assisted sonication was developed to cut, disperse, and mix the fibers together with the cement precursor to manufacture a homogeneous composite. Using this method, a four-fold reinforcement in compressive strength was achieved, compared to pristine cement samples. This method formed a basis for the subsequent WP. The second WP was a systematic screening of the factors influencing the compressive strength and composition of the cement. Factors considered were fiber volume fraction, fiber diameter and dispersity. The latter was investigated using a novel method developed to determine the fiber density in the fracture area. Fiber dispersity was found to be the main contributing factor composite reinforcement, resulting in a three-fold increase in compressive strength compared to cement samples reinforced with undispersed fiber meshes. The final WP was a systematic investigation of the fiber-matrix interfacial properties by comparing plasma coating, a widely used method to reduce the contact angle of materials to a calcium chelating functional coating. This coating resulted in a 50% increase in adsorption of barium as exemplary divalent species compared to the control group, and in a twofold increase in interfacial stiffness, compared to the control group. These results form a systematic study of the factors influencing the mechanical properties of fiber reinforced bone cements and enable further optimizations to be investigated in this area.

Contents

Contents

Prologue Part I

1 | Introduction

This doctoral thesis is an outlined compilation of publications embedded within the field of absorbable [1], fiber reinforced calcium phosphate (CaP) based bone cements.

Bone cements are implantable materials used to fill gaps within the human osseous tissue that are too large to be bridged by endogenous processes; the influence of this gap size was investigated by Claes and co-workers [2]. Of these, the calcium-phosphate based cements (CPC) provide the benefit of being innately osteoconductive, meaning they provide guidance for the surrounding tissue to form new bone around and on the implant surface. Furthermore, if manufactured from absorbable CaP, they are gradually absorbed and replaced with newly formed, endogenous bone. The two reviews by Legeros provide an overview of the conductivity, degradation and resorption mechanisms of CaP [3, 4]. This minimizes risks stemming from foreign body interactions at a later stage and allows for full integration and healing of the site. These CPCs are used clinically for various procedures such as following tumor resectomies, traumatic complex fractures, prosthesis implantation, in plastic surgery and within the dental field. A comprehensive treatment of the applications in the field can be found in the works of Dorozhkin [5] and Ginannoudis and co-workers [6].

The mechanical properties of CPCs are inferior to those of composite bone[1] they are designed to replace. For instance, the compressive strength of injectable bone void fillers available on the market ranges between 0.6 MPa for fast resorbing CaPs and 40 MPa for dense, slow resorbing Hydroxyapatite 6 based CaPs. Examplary studies of the mechanical properties can be found in the works of Linhart and Kurien and Co-workers [7, 8]. A typical, widely used Brushite - β - TCP based cement such as ChronOS inject by Synthes GmbH has a compressive strength of around 5 MPa [9]. In comparison, values between 1.5 and 45 MPa have been reported for cancellous (spongy) bone and between 19 and 209 MPa for cortical (dense) bone by Ginebra and co-workers [10]. These mechanical properties are a consequence of the micro and nanostructure of these CPCs. In most cases, they are composed of randomly oriented loosely connected ceramic micro- and nano crystallites that form a porous, randomly oriented

---

[1]Composite bone: a section of bone containing both cortical and cancellous tissue

microstructure, an example is illustrated in figure 1.1. The lack of interconnectivity, and the high stiffness of the crystallites result in the macrostructure being brittle, and prone to fracturing with little warning. These CPCs can therefore only be used in areas that are non-load bearing or requires extensive stabilization with other, non-absorbable implants such as metallic screws and plates. Examples of such stabilization is shown in the surgical guides for both ChronOS inject, and Hydroset Injectable HA Bone Substitute by Stryker [9, 11] These can be the source of additional morbidity risks and often require removal and additional recovery time for the cavities left by these implants to heal completely. Implants remaining within tissue carry the risk of a sepsis, but also weaken the surrounding bone due to the stress shielding effect of the implant on the tissue due to the high stiffness of the implant compared to the bone surrounding it. Often, these implants need to be removed after the lifetime of the part is exceeded as shown in investigations by de Ruiter and co-workers for total knee prosthesis, and in the study by Prentice and co-workers on total hip arthroplasty patients [12, 13].
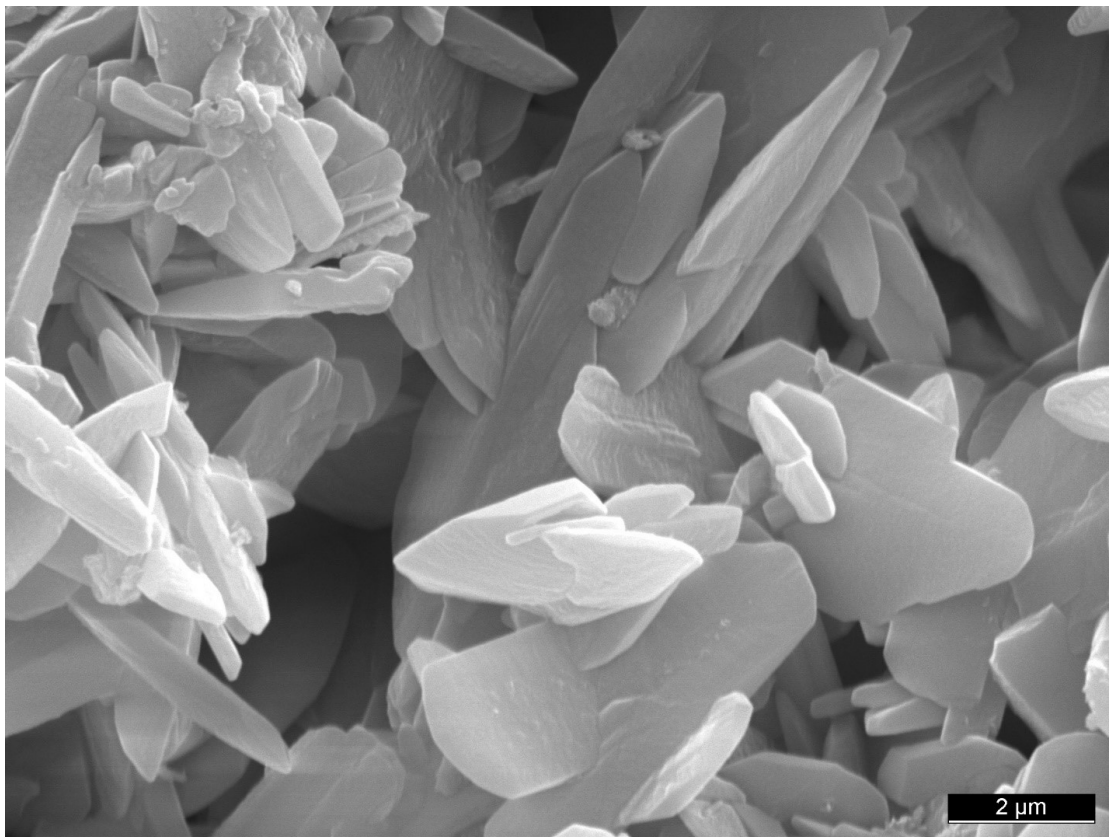
Figure 1.1: SEM micrograph of an exemplary CPC (Brushite) microstructure, highlighting the randomly oriented interconnected crystallites that form a porous network.

CPCs with improved mechanical properties, ideally matching the surrounding bone, could minimize the need for stabilization or in some cases, remove it entirely. A widely applied strategy to improve the mechanical properties of brittle materials is to embed tough, ductile fibers within a brittle matrix, to form a fiber reinforced composite (FRC). For example, bone

itself is a highly ordered hierarchically structured FRC based on the tight interconnection and ordering of collagen-based fibrils with CaP[2] nano crystallites as shown in Figure 1.2. This complex hierarchical ordering is responsible for the exceptionally high strength, toughness, and elastic modulus of human bone. This is achieved by having ordered layers of tough and elastic collagen, that can absorb sudden shocks, and calcium phosphate nanocrystallites that are bonded to the edges of the collagen filaments and provide the necessary stiffness to withstand the weight of a human body. A possible solution to increase the mechanical fracture strength of the bone substitute material is engineering a CPC composite that contains a tough elastic phase, which is homogeneously distributed within the material. This reduces the brittleness of otherwise porous CPCs by inhibiting crack propagation on one hand and acting in a shock absorbing manner on the other. While mimicking the hierarchically structured system of the human bone is desirable, currently, to the author's knowledge, no techniques are available to manufacture these hierarchically structured composites beyond laboratory scale (i.e. in the order of g/day at most) or suitable for in-situ preparation. A simpler composite system that uses randomly oriented but homogeneously distributed fibers could provide sufficient benefits to mechanical strength.
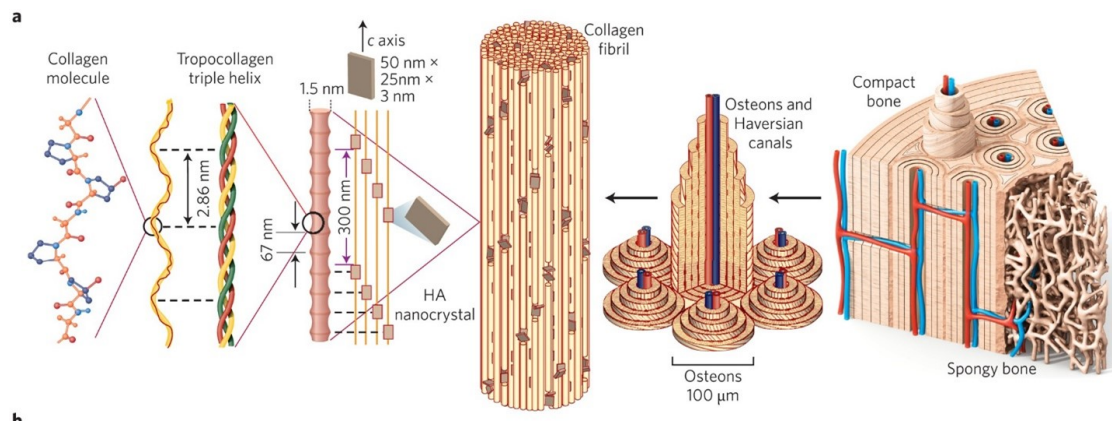
Figure 1.2: Hierarchical structure of bone, illustrating the composite nature of bone. Notable is especially the structure of collagen bone fibril composed of alternating units of (Bio) Hydroxyapatite (HA) nanocrystals (red box) and tropocollagen fibers. Image from Wegst and co-workers [14], reused with permission under copyright.com license no. 5070791132079

While fiber reinforced calcium phosphates have been studied and are available on the market, an exemplary formulation is shown by Kim and co-workers for the Norian cement by Synthes [15]; they either rely on fibers in the micrometer regime such as in the work by Xu and co-workers [16], or they rely on fragments of fibrous meshes or mats as reinforcement as done in the work by Bao, Zuo and co-workers [17, 18]. The systems that incorporate micrometer fibers are more difficult to compare with their biological counterparts that have fibers with diameters in the nanometer regime. Furthermore, smaller diameters allow for a larger number of fibers to be distributed per fiber volume fraction, allowing for more pores to be filled with crack inhibiting fibers. The systems with fragmented meshes have a reduced contact area

---

[2]In this case, a special form of hydroxyapatite called bioapatite

with the CaP matrix, due to the voids that form within the meshes and the resulting fiber-fiber interactions. Also, the fibers used in these studies are generally polymers that are more hydrophobic than their surrounding matrix, which can result in a reduced adhesion of the matrix phase to the fibrous phase. In contrast, collagen filaments mentioned earlier have a significantly lower water contact angle, as shown in the study by Elliot and co-workers [19] .

The scope of the fibrous materials discussed in this work is limited to absorbable materials, which are generally of polymeric nature. This poses limits on the strength and stiffness of the fibers used since absorbable polymers such as Poly Lactic Acid (PLA) are weaker compared to many non-absorbable fibers such as carbon fiber as shown in the studies by Engelberg, Ku, and co-workers [20, 21]. This limitation in scope is due to the fact that non-absorbable micro- and nanofibers can remain in the tissue after the matrix is degraded, which can result in inflammation at the site or even fibrous encapsulation in an area where osseous tissue should form as shown for carbon fibers by Rajzer and co-workers [22], an overview of the challenges associated with the use of nanomaterials can be found in the work by Egli and co-workers [23].

This manuscript is organized as follows:

1. The main methods used in this work are outlined.

2. The fiber dispersing and CPC mixing method is presented and discussed.

3. The influence of the fiber content, diameter and dispersion is analyzed.

4. A novel surface functionalization and its influence on the fiber-matrix interface is shown.

5. The manuscript is concluded and set into context with possible future work.

2 Aim of the Thesis and Hypotheses

2.1 Aim

It is the aim of this thesis to systematically investigate the influence of separated, homogeneously distributed nanometer diameter fibers in a CaP matrix on the compressive fracture strength of the resulting CPC-fiber composite.

The scope of this work includes the following:

1. Developing a novel method to separate electrospun continuous nanofiber meshes into dispersed discontinuous fibers and mix the precursors to form a CaP – fiber composite that minimizes the fiber-fiber interactions.

2. Investigating the influence of the fiber diameter, content, and dispersity, i.e. the influence of meshes compared to discontinuous fibers on the final cement composition and the consequences for the mechanical strength.

3. Develop a novel functionalization for the fibrous phase, that allows for a water contact angle reduction, and through the chelation of Calcium, potentially increase the amount of CaP that can form and remain on the fibrous surface. The effect of this functionalization on the mechanical strength of the fiber-matrix interface will also be investigated.

2.2 Hypotheses

Three main hypotheses were investigated within the framework of this thesis:

1. CaP particles can act as cutting and dispersing moieties for electrospun fiber meshes.

2. Fiber dispersion within the cement matrix is the main contributor to the compressive reinforcement of the CaP matrix with more fibers spread within a volume resulting in a more pronounced reinforcement effect.

3. The use of chelating groups on the surface increases the adhesion of the cement matrix beyond the effect of wettability alone.

Methods Part II

3 Manufacturing Methods

3.1 The Cement Matrix

In this section, the absorbable calcium phosphates used during this work and their manufacturing method is introduced. The selection procedure and criteria for the materials used in this work are also outlined. For a more comprehensive treatment on the topic of CaP the reader is referred to the works of Bohner, Döbelin and Dorozhkin [24, 25, 26, 27, 28].

One of the most prevalent types of absorbable bone cements are calcium-orthophosphate based cements (CPC), Most commonly used are β-Tricalcium phosphate, Hydroyapatite (HA), Calcium deficient Hydroxyapatite (CDHA), and Brushite (DCPD) [24, 26, 27, 29] and most self-setting cements available on the market for biomedical application either set in an Apatite or Brushite form, an assessment of which is given by Bohner and co-workers[26]. They differ in their ratios of Calcium (Ca), to phosphate PO_4, oxygen (O) and Hydrogen (H). These ratios are given in the work of Dorozhkin [28]. This ratio defines the pH under which these are formed or transformed into, their stability within aqueous media of different pH, (Figure 3.1) [30] and in turn, in vivo as shown by Apelt and co-workers [31]. Compact bone can reach compression strengths 100-400 MPa and tensile strengths of 70-150 MPa as shown in the study by Carter and co-workers [32].

The mechanical properties of bulk manufactured CPCs are poorly suited for load bearing applications; this is due to their ceramic, porous and polycrystalline nature which results in samples of low compressive strength (10.7 ± 2.0 MPa for brushite, 75.0 ± 4.2 MPa for hydroxyapatite), and even lower tensile strengths (1.3 ± 0.3 MPa, 3.5 ± 0.9 MPa) as shown by Charrière and co-workers [33]. Increasing the cement density by reducing the porosity allows for an increase in mechanical properties, for example HA reaching 395 ± 42 MPa with a compressive modulus of 8.4 ± 0.4 GPa in dense compact sintered form as reported by Bose and co-workers [34] at the cost of absorbability and integration within the bone structure. Furthermore, these highly compacted CPCs must be shaped, compacted at high pressures, and sintered at temperatures above 1000 °C 38 prior to the surgical intervention. In this form they are also ill-suited for corrections by the surgeon due to their brittleness. This makes them
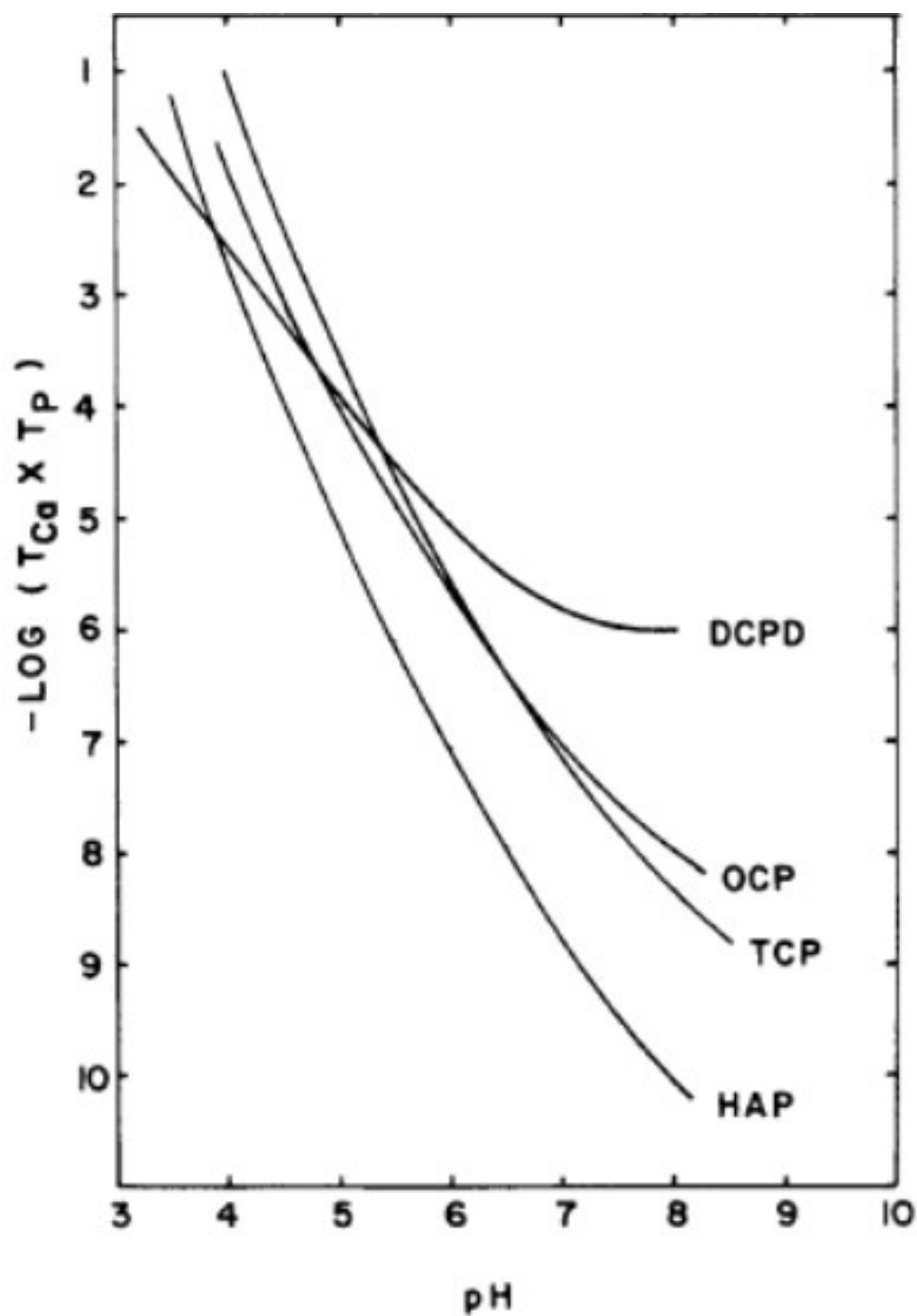
Figure 3.1: Isothermal solubility curves of a selection of CaPs. Data was plotted for 37 °C temperature and 0.1 mol/L ionic strength. These plots indicating the stability of the CaPs in an acidic medium, i.e. a lower solubility indicating a higher stability. Plot is shown as the log of the molar concentration (T) product of Calcium and Phosphate as a function of the pH. Diagram taken from Johnsson and co-workers [30] reused with permission.

unsuitable for applications in trauma surgery where in-situ molding to the cavity geometry is required. The absorption of such compacted, sintered cements is slow to non-existent as shown in the study by Costantino and co-workers [35]. For the scope of this work, the focus lies on non-compacted, self-setting, non-sintered CPCs.

A Brushite self-setting cement is desirable as end product, since these types of cements are absorbed more rapidly (8 weeks) as shown by Theiss and co-workers [36] than their apatitic counterparts with an absorption time of 6 months as shown by Apelt and co-workers [31], making it suitable for further investigations in vitro and in vivo. Furthermore, the significantly lower compressive strength of brushite compared to apatite cements would result in higher benefits from fiber reinforcement compared to apatite formulations. Thus, this work focused on a self-setting brushite forming cement. To obtain the required mix containing Brushite, the correct conditions were necessary.

1. The correct stoichiometric ratio had to be followed, i.e. 1:1 of each Calcium, Phosphate, and sufficient water.

2. The correct pH had to be maintained to precipitate the correct phase from the precursors. The necessary pH can be obtained from the solubility diagram (Figure 3.1) When using β-TCP as precursor, the pH had thus to remain below 5, and when using HA, it had to remain below 4.

Two formulations were mainly used in this work: one based on the formulation of ChronOS inject [31], mainly as proof of concept, and another based on hydroxyapatite nanoparticles as precursor based on a formulation by Barralet [37], where the nanoparticles acted as a base for the first part of this work, namely the development of a novel method to cut and disperse polymeric nanofibers. All cements were manufactured by manual mixing of the components or by use of an electric mixer and were allowed to set for at least 3 days.

3.2   The Fibrous Phase

In this section, the fibers used during this work and their manufacturing method is introduced the selection procedure and criteria for the materials in this work are outlined as well.

The fibers used for reinforcement should fulfill a set of requirements to sufficiently reinforce the surrounding ceramic matrix these requirements are:

- Absorbability: within the scope of this work are absorbable fibers only since the reinforced CPCs should be completely absorbable. Their absorption time should be at least of the same duration as the surrounding matrix, to retain the reinforcement throughout the lifetime of the implant.

- Manufacturing constraints: the fibers should remain stable during the setting reaction

within the acidic medium for minutes to hours within the pH range that is present during the setting reaction (pH 3-6 as shown in the previous chapter).

- Mechanical properties: the tensile strength of the fibers should be significantly higher than that of surrounding matrix, and the modulus at least as high as that of the surrounding matrix to induce a reinforcement effect.

- Dimensions: the aspect ratio i.e. length divided by the diameter (for circular cross sections) of the fiber should at least be as high as the ratio between elastic moduli of the fiber and the matrix, with longer fibers being beneficial as long as fiber entanglement does not occur as defined by Robinson and co-workers [38], furthermore they should be of diameters in the micro- or even nanometer range to increase the number of fibers in contact with the matrix given a constant volume fraction.

- Fiber Surface: the adhesion with the matrix should be sufficiently high to allow for a maximization of the work of fracture, however it should remain within the pull-out failure range of the composite.

- Manufacturable in sufficient quantities: a quantity of multiple grams of fiber per day should be manufacturable to allow for a meaningful amount of bulk test samples.

The fibers and methods to manufacture these that fulfill the abovementioned criteria are limited. Regarding the manufacturing method, electrospinning is one of the few methods that allows manufacturing of fibers with micro- and nanometer diameters in quantities outlined above. Electrospinning is outlined in the following section. Electrospinning is however generally limited to polymer fibers. Of those that are absorbable, Poly Lactic Acid (PLA) and Poly Glycolic Acid (PGA) possess the highest tensile strengths (11-85, 57- 69 MPa measured by Athanasiou and co-workers [39]) and moduli (1.5-2.7, 5-7 GPa, observed by Canal and co-workers [40]), however, it has been shown by You and co-workers [41] that PGA and its copolymers degrade rapidly in vitro (within 2-4 weeks), while PLA remains stable within that period, thus PLA was chosen as fiber model system for this work.

3.2.1 Electrospinning

Electrospinning is a technique for manufacturing polymeric fibers that relies on using an electric field to draw long, "endless" filaments. The manufacturing parameters of these filaments can be varied to generate fibers with controlled diameters generally ranging between 5 μm and 50 nm such as in the works by Bhardwaj, Lavielle, Reneker and co-workers [42, 43, 44], making it a suitable technique to manufacture the fibers required for this work. The following section outlines the technique in the framework of this thesis. The section starts with a brief introduction into its origins, followed by the main principles governing the technique. Finally, the materials and parameters investigated throughout this study are described.

One of the earliest systematic descriptions is by Boys [45], who investigated the effects of

an electrical field on natural polymers such as sealing wax or shellac, while investigating different techniques for drawing fibers [1]. He describes the formation of an electrospun mat in the following quote: "…If sealing-wax is employed, and a sheet of paper laid for it to fall on, the paper becomes suffused in time with a delicate rosy shade produced by innumerable fibres separately almost invisible. On placing the fingers on the paper, the web adheres and can be raised in a sheet as delicate and intricate as any spider's-web …". An early patent by Formhals [46] describes the collection of oriented electrospun fibers on a rotating setup, similar to the one used in this work (see also the illustration in Figure 3.2). With improved characterization methods and a deeper understanding of fluid mechanics the technique found a resurgence in 1996 where Reneker and Chun electrospun and quantified fibers with diameters in the nanometer diameter [44] and laid the groundwork for establishing parameter ranges for consistent fiber generation. Since then, the technique has been widely used to a wide variety of applications, such as filters, functional textiles, an overview of which is given by Chung and co-workers [47], artificial skin scaffolds, which are reviewed by Keirouz and co-workers [48] and more recently for transparent face masks as shown in the press release by Empa, Switzerland [49]. A more comprehensive outline of the history of electrospinning can be found in the book by Andrady [50].

Governing Principles

The mechanics and governing principles have been described elsewhere in detail [44, 51, 52, 53], and for applications in the field of medicine the reader is referred to the work of Akins [54]. For a more recent review on the state of the art of the technology, the widely cited review by Xue and co-workers can be consulted [55]. Of note are for example the books by Agarwal and co-workers and Andrady and co-workers [56, 50]. These principles and mechanics are abbreviated and paraphrased from these works in the following section for the readers comprehension and convenience.

Electrospinning occurs when a polymer liquid solution or melt is under the influence of an electric field, when the strength of that field is higher than the retarding force of liquid surface tension. This is visible by the formation of a so-called Taylor cone, where the solution is ejected from its tip. This occurs when the half angle of the cone reaches 49.38 ° as observed by Taylor [57]. The ejected material then travels towards the collector as a liquid jet. Generally, at low viscosities, the jet disintegrates into individual droplets, a phenomenon called electrospraying. At higher viscosities, the polymer chains can entangle, and a fiber is formed. Through instabilities occurring during flight, these fibers change their movement from going in a straight line towards the collector to a circular whipping motion. This causes the fibers to extend in length and shrink in diameter by one to three orders of magnitude, allowing for diameters in the nanometer scale.

---

[1]Of note is also his detailed description of the use of bow and arrow to draw thin fibers from inorganic materials such as quartz
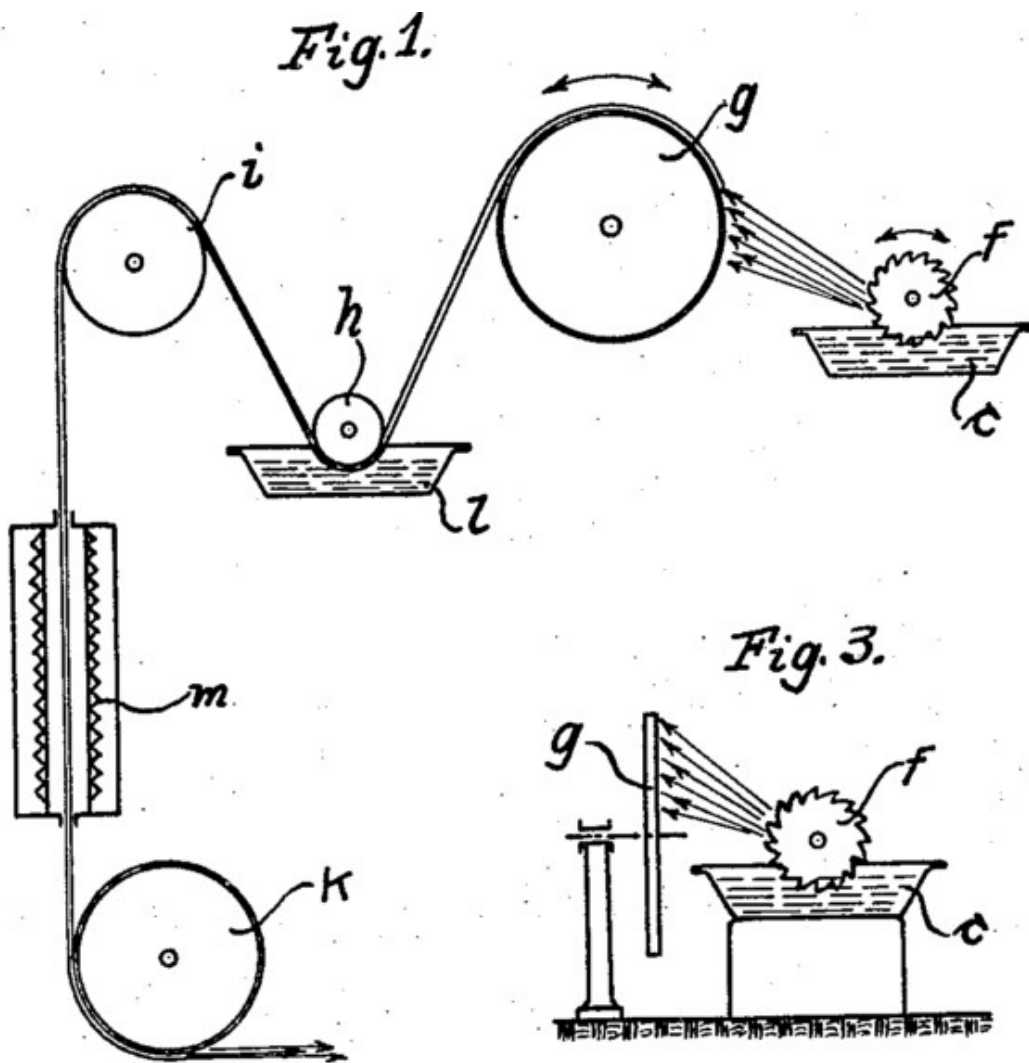
Figure 3.2: Illustration of the electrospinning setup patented by Formhals [46], Fig. 1 shows a setup where the electrospun fibers are collected on the cylindrical surface of a rotating disc. Fig 3 depicts the setup rectangular to Fig 1 with the fibers being dispersed on the face of the spinning disc, similar to the setup used in this work. Illustration taken with permission as public domain.

The goal of the electrospinning process for this work was to manufacture fibers from polylactic acid, within a specified range of diameters e.g., 250 nm and 2 μm. For this purpose, a suitable set of manufacturing parameters had to be determined. Even though the governing principles of the process are known, the parameters are often determined empirically due to their sensitivity and interaction terms between them, resulting in prediction difficulties. The factors influencing these parameters and the parameters used in this work are outlined as follows:

1. Molecular weight or molar mass of the polymer: correlates with the chain length of the polymer and determines the spinnability of the polymer, its mechanical and degradation properties among others. Solutions with higher weights can be spun at lower concentrations and are generally stronger, tougher and have a higher elastic modulus, with diminishing effects (asymptotic relationship) at very high weights. On the other hand, they are more difficult to dissolve and result in higher viscosity solutions than their low weight counterparts as described in the work by Nunes and co-workers [58]. In this work, PLA of a molar mass of 200 kDa was used.

2. Solvents: These dissolve the polymer and determine the degree of charge accumulation that can occur on the droplet during the spinning process. Depending on the solvent volatility, the surface topography can also be modified e.g., to form pores e.g. as shown in the work by Yazgan and co-workers [59]. Generally, a mixture of solvents is used for spinning. Non-polar solvents such as chloroform can dissolve the polymers that are often non-polar themselves, while polar solvents such as Dimethyl Formamide (DMF) or protic solvents such formic acid are used to increase the charge density, which decreases the radius of the spun fibers. The determination of the suitable solvent mix is highly complex, and determined empirically in general as shown in various such as by Bordes, Fridrikh, Lavielle, Van Der Schueren, Yao and co-workers [60, 61, 43, 62, 63] . In this work, solutions of Chloroform: N-N Dimethylformamide (DMF): Formic Acid at a ratio of 8:1:1 were used with polymer concentrations between 5% and 9% (w/w).

3. Humidity: influences the solidification kinetics of the fiber as shown in the works of Armentano, Simonet and co-workers [64, 65] and fiber morphology as shown in the study by Yazgan and co-workers [59]. A low humidity can result in the fiber drying rapidly, often at the syringe tip while a high humidity can result in a rapid charge dissipation and hindering the spinning process. In this work, ambient conditions were used (20-60 % rH)

4. Electric field strength: a minimum (dependent on the solution) usually in the order of kV/cm is required to achieve a stable jet. Within the stable parameter range, the fiber diameter can be varied to a degree, at too high strengths, branching and bead formation can occur due to decreased charge density. In this work, fields between 0.5 and 1 kV/cm were used.

5. Distance: a minimum distance is required to achieve drying and the whipping instabilities. At too high distances the required voltages become very high, and charge

leakage into the surrounding air can occur, halting the spinning process. In this work the distances were varied between 10 and 20 cm.

6. Flow rate: should be sufficient to allow for a stable taylor cone to form. The flow rates in this work ranged between 10-30 μl/min.

7. Current: should be sufficient to maintain the charge density. Throughout this work 0.1 mA was used.

8. Temperature: should be sufficiently high for drying to occur and to achieve the desired viscosity for spinning. This work was conducted under ambient conditions, at temperatures between 19 and 24 ° C

9. Collector type: a large variety of possibilities has been reported, the simplest being an aluminum foil. For this work a rotating drum to achieve a degree of fiber orientation has been chosen 72. In this work, a 20 cm diameter collector rotating at 1340 rpm was used, corresponding to a speed of 140 m/s.

3.3 Composites and interfaces

3.3.1 FRCs

To improve the mechanical properties of CPCs, approaches for fiber reinforcement of cements applied in other fields were analyzed. Among those investigated were reinforcement strategies used for concrete, which is a material comparable to CPCs in terms of its brittleness, porosity and polycrystallinity. For instance in a study by Betterman and co-workers [66] a FRC was manufactured using a mortar matrix reinforced with Polyvinyl alcohol fibers with diameters between 12 and 41 μm, lengths between 4 and 12 mm and volume fractions between 1 and 4% (v/v). The FRC was subjected to tensile and pull-out testing. It was observed that the specimens with the highest fiber volume fraction had more than twice the peak tensile stress compared to the samples with the lowest fiber volume fractions. This effect called crack bridging, is explained by the fibers serving as "bridges" between the initial cracks forming during the application of the load stress and is illustrated in figure 3.3.
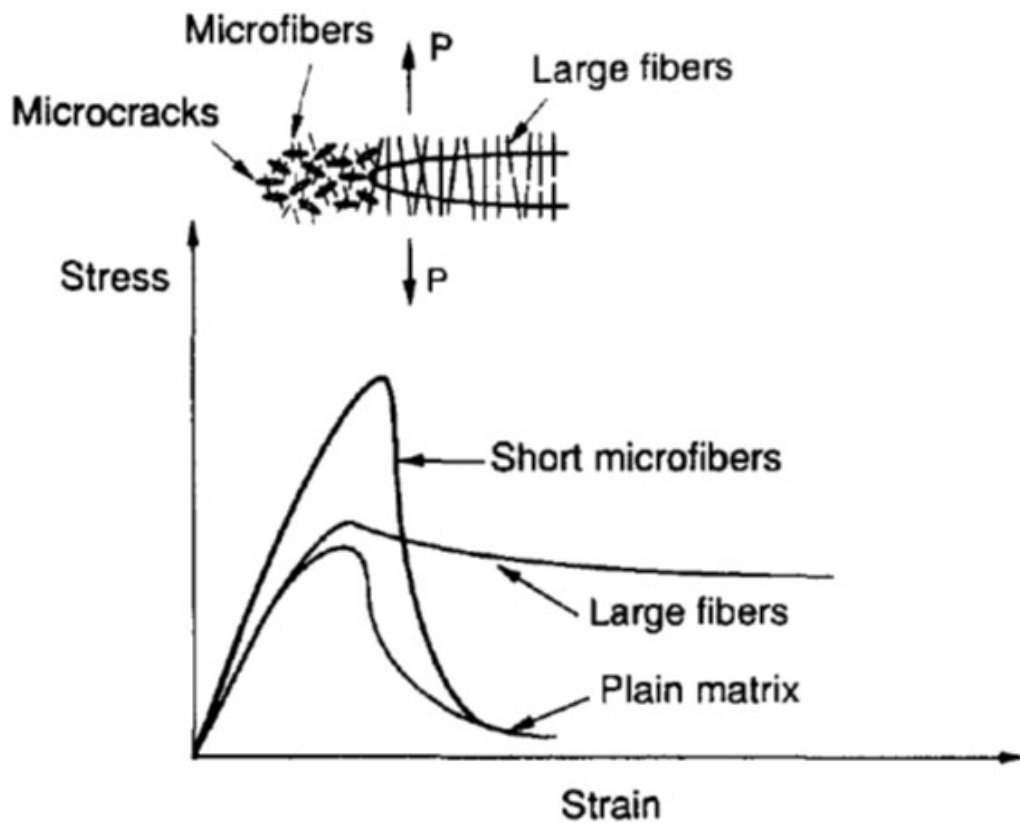
Figure 3.3: Illustration of the influence of the fiber length on crack bridging and fracture behavior. Image obtained from Betterman and co-workers [66] and reused with permission under copyright.com license no. 5234351280149.

In the case of a discontinuous, porous matrix, such as a CPC, it can be hypothesized that if the fiber diameter is within the order of the building blocks of a (discontinuous) matrix, these fibers can occupy areas that would otherwise result in pores in a pristine during the setting reaction. these pores can act as crack initiation areas, and the presence of fibers would reduce and bridge these areas, resulting in a higher peak strength. In this work, the fiber diameters used for reinforcement used were therefore within the size range of the CaP crystals i.e. between 200 nm and 1 μm.

An overview of current reinforcement strategies is given by Ashby, Brandt, Xu and co-workers [67, 68, 16].

3.3.2 Interfaces

The failure modes of an FRC are illustrated in figure 3.4. When the interfacial strength between the fibers and the matrix is weak, the mode is generally by fiber pull-out or by fiber-matrix debonding. In samples with stronger interfaces, fiber failure and matrix cracking is observed. For a comprehensive treatment of fracture behavior of composites, the reader is advised to consult the book by Anderson [69]. To optimize the stress transfer from the matrix to the fiber, a stronger interface can therefore be desirable.

1. Fiber Pull-Out.
2. Fiber Bridging.
3. Fiber/Matrix Debonding
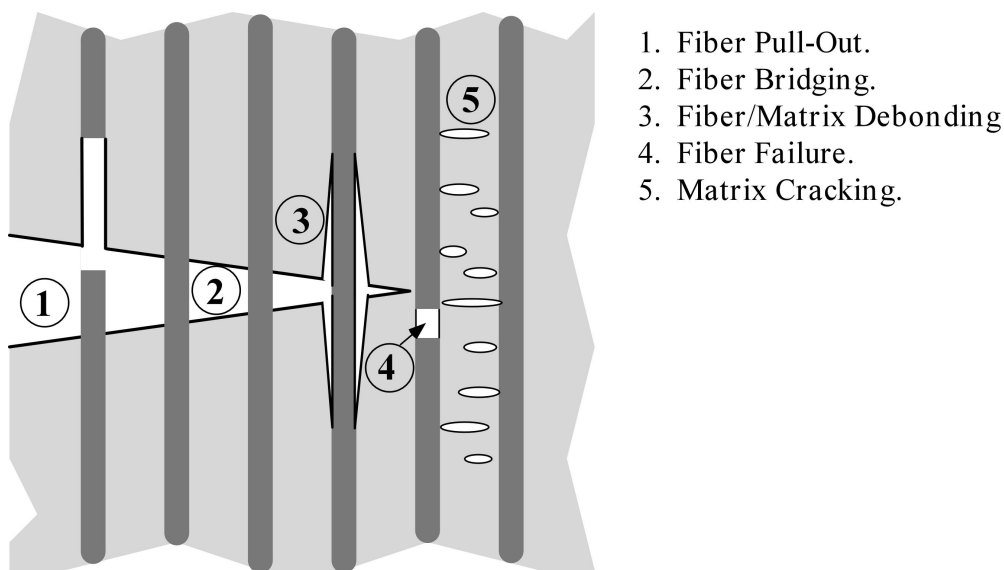4. Fiber Failure.
5. Matrix Cracking.

Figure 3.4: Illustration of the different fracture modes of fiber reinforced composites. Image from the book by Anderson (figure 6.15) [69], obtained and reused with permission by the author (e-mail communication [70]).

Interfacial strengthening can be performed by modifying the surface energy of fibers such that they match that of the matrix more closely or vice versa. Examples for such reinforcement strategies are the widely used plasma treatements such as in the work of Maenz, Graupner and co-workers [71, 72]. Another strategy is the grafting of functional groups onto the desired

surface for instance to promote the adhesion of the desired species onto the surface. examples are show in in the works by Caspar, Guex and co-workers [73, 74].

In this work both plasma treatment and the functionalization of a calcium chelating group onto the fiber surface was investigated.

3.4 Analysis techniques

In this section, the main analysis techniques used in this work are outlined. The equipment used is mentioned in the respective publications.

3.4.1 Bulk and Fracture Analysis

In this work, the primary analysis method used was scanning electron microscopy (SEM) due to the sample dimensions being in the sub-micrometer range. Optical microscopy was used to for fiber counting and length determination due to the large surface area that could be covered. For Porosity and overall surface area determination, gravimetric and gas adsorption techniques, which are standard techniques used for these analyses.

3.4.2 Surface Analysis

X-ray Photoelectron Spectroscopy (XPS) was used for precise determination of adsorbed species, while Energy dispersive x-ray spectroscopy was used in conjunction with SEM to analyze the composition of cement residue on the fibers. For roughness analysis, white light interferometry was applied which is a non contact method to measure surface roughness.

3.4.3 Mechanical Testing

Compressive testing was used for the cements due to the tests resilience towards manufacturing defects and fractures already present in the composite, which results in a lower sample variance compared to flexural testing for example. Furthermore the small sample dimensions allowed for more samples to be manufactured resulting in a higher number of repeats. For interfacial analysis pull-out testing was used which is a standard technique used for these analyses and is described in the previous chapter.

3.5 Statistics

In general, a sample size of at least 5 was used, especially for mechanical testing. This was due to the long times needed to generate sufficient FRC samples. Deviations are indicated in this work where applicable. Analysis of variance was used for significance testing.

Publications Part III

4 Fiber Cutting and Dispersion

4.1 Context

An optimal mix between the fibrous and the cement matrix phase is a prerequisite for a mechanically strong bone cement, this optimal distribution can be defined as minimizing the fiber-fiber interaction. Thus, following disentanglement and cutting into discontinuous pieces, the individual fibers should be separated by the matrix. For a cement prepared and placed in situ, no preferred orientation is given. Thus, isotropic distribution of the fibers i.e. fibers in all directions equally probable. To achieve such a mixture for a suitable cement precursor, the electrospun fibers must be disentangled, cut, and mixed with the cement matrix precursors in such a way that this mix is retained after setting.

For electrospun fibers in the sub-micro and nanometer diameter range, no straightforward solution exists to disentangle and mix the cement precursor in sufficient quantities of g/day. The manuscript describes the different methods known and their advantages and drawbacks. From the possible range of methods sonication was selected as it was previously used for cutting purposes in the work by Sawawi and co-workers [75] however only by prior reduction of the mechanical strength of the fibers using UV light. Furthermore, it was employed for coating fibers with particles as was done in the work of Perelshtein and co-workers [76] leading to the assumption that with a higher concentration of cement precursor particles a suitable mix could be achieved. To investigate this method systematically the following factors were investigated in this manuscript:

1. What influence does the dispersion medium have on the disentanglement and cutting of tough polymer fiber mats?

2. The effect/influence of particles (size, concentration) on the cutting efficiency, and can the particles act as cutting moieties?

3. How well do the particles remain mixed with the fibers or do they separate?

4. Do the fibers remain separated during and after the cement reaction?

The manuscript demonstrates that the dispersion medium plays an important role to allow cutting and dispersing the individual fiber fragments together with the precursors, furthermore it elucidates the mechanisms that have a significant effect on the length and ones with a low influence. It shows the possibility of using sonication as dispersion and homogenization technique for particles and fibers at both high and low concentration, and that the fibers remained separated after performing the cement reaction. This method allows for a more tailored approach for in situ preparation of cements with variable mechanical properties depending on the reinforcement required.

4.2 Contribution of the author

Experimental design and protocol were a collaborative effort between Elias Mulky (EM), Gökçe Yazgan (GY), Katharina Maniura-Weber (KM), Giuseppino Fortunato (GF), Reto Luginbuehl (RL), and Ana-Maria Buehlmann-Popa (AMBP). Most of the manufacturing experiments and analysis and were performed by EM except for fiber spinning and analysis of the meshes sonicated with ethanol and deionized water, which was performed by GY, particle size analysis, mechanical testing, and BET analysis (See also acknowledgments section in the manuscript). Statistical analysis was conducted collaboratively between EM and AMBP. The main manuscript writing was performed mainly by EM, RL and AMBP. All figures except for 2a and b (prepared by GY) were prepared by EM.
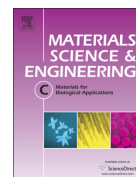
Article reused with permission from Elsevier.

4.3 Fabrication of biopolymer-based staple electrospun fibres for nanocomposite applications by particle-assisted low temperature ultrasonication

MATERIALS
SCIENCE &
ENGINEERING
C

CrossMark

Fabrication of biopolymer-based staple electrospun fibres for nanocomposite applications by particle-assisted low temperature ultrasonication

Elias Mulky [a,b], Gökçe Yazgan [b,c], Katharina Maniura-Weber [b], Reto Luginbuehl [a], Giuseppino Fortunato [c,*], Ana-Maria Bühlmann-Popa [c]

[a] RMS Foundation, Chemistry & Biology, Bischmattstrasse 12, Bettlach, Switzerland
[b] Empa, Swiss Federal Laboratories for Materials Science and Technology, Laboratory for Materials–Biology Interactions, Lerchenfeldstrasse 5, 9014 St Gallen, Switzerland
[c] Empa, Swiss Federal Laboratories for Materials Science and Technology, Laboratory for Protection and Physiology, Lerchenfeldstrasse 5, 9014 St Gallen, Switzerland

ARTICLE INFO

ABSTRACT

We demonstrate the fabrication of staple polymer-based fibres by the ultrasound-assisted processing of electrospun meshes. Bioabsorbable Poly-L-Lactic Acid (PLLA) was electrospun from organic solvent mixtures, yielding continuous fibres with diameters in the range of 244 ± 78 nm. Subsequently, the obtained fibres were sonicated at low temperatures in the presence of nanoparticles in order to obtain fibres with small aspect ratios. The influence of the dispersion medium, the sonication process parameters (temperature and time) and the dimensions of the particles used on the respective length distribution of the obtained nanofibres was investigated. Hexane was identified as an optimal dispersion medium for the system studied in this work. When a cooling bath temperature of 0 °C was used, a slight increase in the obtained fibres' average length and distribution was observed as compared to cooling at -80 °C (54 ± 43 μm vs 44 ± 31 μm). Moreover, in the presence of hydroxyapatite and hydrophilic and hydrophobic TiO_2 nanoparticles in the dispersion medium longer fibres were obtained (44 ± 31 μm, 63 ± 47 μm, and 51 ± 52 μm). Finally, the application of the obtained PLLA-fibre–hydroxyapatite (HA) nanoparticle precursors for the fabrication of a fibre-reinforced Brushite-based cement with high compressive strength is shown. This method of obtaining nanoscaled fibre-reinforced materials opens up a wide range of perspectives for the fabrication of composites for tissue engineering applications.

© 2014 Published by Elsevier B.V.

1. Introduction

Dispersed short discontinuous fibres, also known as staple fibres, are widely used as additives in polymeric materials and cement-based matrices to engineer fibre reinforced composites (FRCs) [1–3]. With the increasing interest in micro- and nano-scale composites – especially in the field of bone and tissue engineering – the required raw materials and resulting structures are fabricated in micrometre to nanometre scale to improve mechanical properties or to mimic biological features and elicit specific biological reactions [4–6]. Electrospinning is a very versatile method to produce nano- to micron-sized fibres from a wide range of polymeric and inorganic materials [7–10]. This process typically yields oriented or random non-woven fibre mats [7,11,12]. Electrospinning is used in many applications [13], including tissue engineering [14–17], drug delivery [8], or high performance membranes and textiles [18–21]. The process typically does not yield staple fibres, but it generates meshes and spindles with endless, partially fused fibres [22].

Therefore, subsequent processing steps are required to cut and unbundle into staple fibres of desired length, which can be further dispersed into relevant polymer or inorganic matrices. Different processes for the production of staple fibres with diameters down to 5 μm have been described; however few investigations on the scission of submicron sized fibres have been conducted. Stoiljkovic and co-workers processed electrospun microfibres from polystyrene-co-butadiene containing n-butyl methacrylate and Coumarin as a photocrosslinker. By irradiating the resultant fibre meshes with UV light under a mask the dissolution of non-irradiated areas in THF could be achieved, generating staple fibres of 20 to 150 μm in length dependent on the photomask used [23]. This process is thus suitable only for fibres containing photosensitive groups. Poly-L-Lactic Acid-co-polyethylene oxide staple fibres in the range of 10 μm were obtained by freezing the nanofibre meshes in ethanol using liquid nitrogen, followed by mechanical cutting using a motor driven blade [24]. High shear homogenization was applied for the milling of high molecular weight styrene-co-4-vinylbenzyl 2-brompropionate nanofibre meshes [25]. Greenfeld and collaborators observed the appearance of discrete short fibres up to a length of 1 mm when electrospinning low molecular weight polymethyl-methacrylate (PMMA) (15 kDa) [26]. In a recent work, Sawawi and co-workers

* Corresponding author.
E-mail addresses: reto.luginbuehl@rms-foundation.ch (R. Luginbuehl), giuseppino.fortunato@empa.ch (G. Fortunato).

described the use of ultrasonication as a method for the scission of poly-styrene and PMMA fibres down to 10 μm in length [27]. They have also shown the application of this method for the milling of UV/ozone pre-treated Poly-L-Lactic Acid (PLLA) fibres.

Sonication was also applied to coat microfibre based cotton bandage fabrics with metal oxide nanoparticles such as Al_2O_3 or MgO [28]. It has been predicted that the addition of nanoparticles enhances the sonication effect by providing nucleation sites for cavitation bubbles, thus increasing the sonication efficacy [29], but to our knowledge the effect of nanoparticles on the outcome of nanofibre cutting by ultrasonication has not yet been investigated.

The goal of the present work was to demonstrate the potential of particle-assisted low-temperature ultrasonication for the fabrication of submicron- to nanometre diameter staple fibres from the use in bioma-terials applications, i.e. of biopolymers such as PLLA (a bioabsorbable polymer with a high tensile strength of 70 MPa and a glass transition temperature of 60 °C [30]), without any additional chemical pre- or post-treatments. By performing the procedures well below the glass transition temperature of the materials, the fibres are expected to be brittle enough to be cut under the complex action of the ultrasonic waves, while retaining relevant morphological features such as diameter and surface structure, as well as mechanical characteristics [31,32]. The effect of the dispersion media, ultrasonication temperature and time on the cutting efficiency was evaluated. The nanoparticles were expected to act as cutting moieties and provide additional nucleation sites, thus improving the sonication yield. Moreover, we hypothesized that this approach would allow the simultaneous, homogeneous disper-sion of particles and fibres. The morphology of the staple fibres was characterized by optical and scanning electron microscopy. The staple fibres/nanoparticle dispersions were then used to fabricate a calcium phosphate-based cement that can be used as a bone substitute material. The distribution of the fibres in the composite and its mechanical prop-erties were also evaluated.

2. Materials and methods

All solvents were obtained from commercial providers in ACS quality and were used without further purification. Poly-L-Lactic Acid (PLLA, Biomer L9000, Mw: 200 000 kDa), was obtained from Biomer Biopolyesters (Germany). The titanium dioxide (TiO_2) nanopowder, P25, and octylsilane coated, hydrophobic TiO_2-T805, was provided by Evonik/Degussa (Germany), and had a nominal particle diameter of 21 nm, as indicated by the manufacturer. Hydroxyapatite (HA) nano-particles were purchased from M K Impex Corp (Canada) and the nom-inal particle diameter was 30 nm as indicated by the manufacturer.

2.1. Electrospinning

A stock solution of 5.6% (w/w) PLLA in chloroform:DMF (8:1 w/w) was prepared (shaken at 200 rpm at room temperature for at least 15 h). After complete dissolution, concentrated formic acid was added at a ratio of 9:1 (w/w) to an aliquot of stock solution and incubated for 20 min; the obtained solution was used immediately for electrospinning.

The electrospinning equipment was an in-house built device, consisting of a syringe pump (KD scientific), a variable high voltage power source (AIP Wild AG Switzerland), and an in-house built rotating collector. The whole system was placed in a Faraday cage. A +15/−5 kV potential, with a maximum current of 0.1 mA, was applied between the needle tip (18 G gauge) and collector. The tip–collector distance was set at 18 cm. The rotating speed of collector (20 cm diameter) was constant at 1340 rpm. The whole system was controlled by the LabView™ soft-ware. The collected fibres were removed using tweezers and placed on an aluminium foil for storage and post-processing. Prior to process-ing, the fibre meshes were cut to approximately 0.5 cm × 1 cm sections perpendicular to the fibre length orientation using a surgical blade (KLS Martin Group, Germany).

2.2. Fabrication of staple fibres

The probe sonication was performed with a sonicator (Branson Dig-ital Sonifier Model 450D) equipped with a 1.27 cm tip, a fixed frequency applied of 20 kHz and a maximum output of 400 W. A 30 mL glass flask containing 20 mL of n-hexane was immersed into a bath containing a mixture of dry ice/acetone and cooled to a temperature of −80 °C. The bath temperature was maintained constant during the process by periodically refilling the coolant mixture. Subsequently a weighed sam-ple of aligned PLLA fibre mesh was transferred to the flask together with a corresponding quantity of HA nanoparticles, as to obtain v/v ratios between 2:1 and 1:4 respectively. A similar protocol was applied when using TiO_2 particles, but only a 1:1 v/v ratio was investigated. The sonication tip was immersed in the flask keeping a gap of 5 mm ver-sus the bottom of the flask. The amplitude was set to be 90%. Pulse/pause time was set to be 2/2 sec to allow sufficient cooling of the disper-sion during sonication. The sonication experiments in hexane were repeated 3 times.

Three dispersion media were tested for sonication: a) pure water b) ethanol:water 1:4 (v/v) and c) hexane. The experiments involving water-based mixtures were conducted in an ice/water bath at 0 °C. In the case of hexane, the experiments were conducted at −80 ° C in an ethanol/dry ice bath and a comparison experiment was done at 0 °C.

For the materials used in the fibre reinforced cement, multiple batches of 50 to 120 mg PLLA fibres were sonicated together with 400 to 1000 mg of with HA particles at a fixed fibre to a particle ratio of 1:3 (v/v) for 20 min and at a temperature of −80 °C. The resulting fibre/particle dispersion was air dried under a fume hood under ambi-ent conditions for at least 15 h.

2.3. Cement manufacturing

An aqueous solution containing 1.7 M monocalcium phosphate monohydrate (Innophos Inc., USA) and 0.06 M disodium dihydrogen pyrophosphate (Sigma Aldrich, Switzerland) was prepared with ultra-pure water. Subsequently, the solution was mixed with the HA/PLLA dry mass at a ratio of 2:1 (w/w). The resulting slurry was mixed for 2 min with a spatula to obtain a cementeous paste, which was trans-ferred into Teflon cylinders of 10 mm in diameter and 12 mm in height. The cement was left to set for 3 days. The resulting PLLA fibre content was calculated to be 5% (v/v) in the final composite cement.

2.4. Nanoparticle characterization

The nanoparticles were characterized in suspensions of isopropanol, as a reference, and hexane, as a dispersion medium used for sonication, to study their agglomeration behaviour. The suspensions were sonicat-ed for 5 min in an ultrasonic bath (Bandelin Sonorex digital) and then analysed using a laser diffractometer particle size analyser (Beckman Coulter LS13320 PIDS), according to the manufacturer's instructions. Sonication was applied throughout the measurement.

2.5. Fibre characterization

The fibres were characterized by scanning electron microscopy (SEM). Meshes were cut into size, while sonicated samples were pre-pared by collecting aliquots from the bottom of dispersion fluids with a glass pipette and applying a few drops to steel SEM sample holders. The samples were air dried under the fume hood under ambient condi-tions for at least 15 h. During solvent evaporation, the shortening of the meniscus of the dispersion fluid caused fibre agglomeration. The dried samples were sputter coated with 7 nm gold (Polaron Equipment Ltd. E5100). SEM analysis (SEM, Hitachi S-4800) was performed using a voltage of 2 kV and 10 μA current intensity.

Before the analysis by optical microscopy (using an Keyence VHX 1000 instrument) the fibres were aligned by sliding a coverslip over a

glass slide on which 300 μL dispersion was deposited. At least 250 individual fibres from 6 different images were measured for the determination of the fibre length.

2.6. Compression characterization of the FRC cements

The cylinders were subjected to compression tests using a static compression testing machine (MPM Zwick 1474). At least 3 cylinders were measured. Following fracture, the cements were placed on a sample holder, coated with a 15 nm thick layer of gold using a sputter coater (Baltec SCD 050) and analysed by SEM (Zeiss MA 26).

2.7. Porosity measurements

Porosity was calculated according to the equation below, where the porosity ϕ is calculated by taking the ratio between the specific gravity of the measured scaffold (mass of the scaffold m, divided by its volume V) and the specific gravity of the dense material (Brushite / Brushite + PLLA) ρ_s, and subtracting the result from 1.

$$\phi = 1 - \frac{\dfrac{m}{V}}{\rho_s}$$

2.8. Specific surface area analysis

The specific surface area measurements were conducted by drying the samples under an N_2 flow at 40 °C for at least 12 h, then conducting a BET (Brunauer–Emmet–Teller) analysis using a gas adsorption measurement device (Tristar II Plus, Micromeritics GmbH, Germany), according to the manufacturer's instructions.

2.9. Contact angle measurement

The contact angle of high purity water, ethanol, ethanol:water 4:1 (v/v) and hexane was measured on aligned nanofibre meshes and polymer films. All samples were conditioned in a controlled atmosphere (50% RH for 3 days). The polymer films were fabricated by solution casting on a glass support. The polymer film was peeled off the glass slide and measurements were conducted on the smooth side that was in contact with the glass.

2.10. Statistics

The statistical analysis was conducted using one-way ANOVA. The analysis was performed using Origin 8.1 software. p values < 0.05 were considered as significant.

3. Results and discussion

3.1. Electrospinning

The acid-containing polymer solutions were spun during 2 h on a high-speed rotating collector; however the quality of the fibre alignment was lower than that reported in literature. Moreover, at process durations longer than 150 min a secondary fibre web was formed around the collector. The former is due to the decrease of the electrostatic field strength between the needle and the collector. The latter phenomenon is due to the increase in the thickness of the deposited mesh, which acts as an insulator. A similar observation has been reported earlier by Katta and collaborators who spun Nylon 6 fibres for over 40 min [33]. The fibres exhibited a smooth surface structure and very little bead formation was observed in the mesh (Fig. 1). The average diameter of the obtained PLLA fibres was calculated based on SEM micrographs and was found to be 244 ± 78 nm. The small diameter is

attributed to the high dielectric constant of formic acid (57.2 at 298 K) (DMF, 36.7; chloroform, 4.8) which increases the net charge density and thus the repulsive force on the polymer jet, leading to a decreased fibre diameter [36,37].

3.2. Nanoparticle agglomeration

According to the manufacturer, the pure TiO_2 nanopowder P25 and the octyl silane coated TiO_2 hydrophobic nanopowder T805, which were used throughout our investigations, have an average primary particle diameter of 21 nm by size vs number ratio; 90% of the particles fall in the size range of 9–38 nm. The HA nanoparticles have a nominal average size of 30 nm in diameter. In order to account for the influence of the dispersion media and eventual aggregation effects, the size of the nanoparticles was determined after sonication in isopropanol or hexane by laser diffractometry, estimating the size vs number ratio. Indeed, both types of nanoparticles (TiO_2 and nano HA) were found to be agglomerated. For the TiO_2 (P25) particles the average diameter of the agglomerates was 105 ± 77 nm in isopropanol and 96 ± 89 nm in hexane. The average particle size of T805 was found to be 106 ± 63 nm in isopropanol and 80 ± 44 nm in hexane. The agglomeration of P25 TiO_2 is reported in literature, namely that these particles do not exist in a monodispersed form, but mainly as aggregates with an average diameter of approximately 0.1 μm [38]. In an apolar liquid such as n-hexane, the dispersion quality is further improved, as the agglomerate clusters are broken down in the sonication process and re-agglomerates are less formed in media with lower surface tension such as hexane. In addition, silane coated nanoparticles on the other hand (TiO_2 T805) exhibit a low surface energy as well. This was indicated both through the smaller measured average particle size in hexane as compared to P25 and through the colour of the dispersion medium in hexane resulting in a stable opaque white dispersion when T805 particles were added. TiO_2 P25 on the other hand changed colour from opaque to clear within minutes. For nano-HA agglomerates of 3030 ± 2055 nm in isopropanol and 2796 ± 1676 nm in hexane were measured, which leads to the conclusion that the HA clusters could not be broken down by pre-processing through sonication, and remained in an agglomerated form. In both cases, the averages between the dispersion media were determined not to be significant.

### 3.3. Engineering of staple fibres by sonication

Different process parameters were investigated with respect to their influence on the length of the resulting staple PLLA nanofibres. Specifically, we analysed the influence of the dispersion media, the co-sonication of fibres and nanoparticles and their respective ratios, as well as the effect of temperature and sonication time.

3.4. Influence of the dispersion medium

The ultrasonication was conducted in pure water, ethanol/water 1:4 (v/v) and hexane in order to account for the role of the dispersion medium on the outcome of the process. Meshes sonicated in pure water clumped after 10 min of sonication (Fig. 2a) and no separation of the fibres was observed. SEM micrographs of fibres treated in ethanol/water showed that the meshes were disintegrated with a number of cut fibres (Fig. 2b), but the majority of fibres were still entangled and continuous. Sonication in hexane resulted in the best separation: the meshes were fully dispersed and the fibres were cut with a high efficiency (Fig. 2 c, d).

Static contact angle measurements were performed on both casted solid film of PLLA evaporated from the previously described electrospinning solution and on electrospun nanofibre meshes. The water contact angle was found to be 72° ± 2 on the solid PLLA and 134° ± 4 on the nanofibre mesh. The difference can be explained by the effect of the nanostructured topography of the electrospun mesh
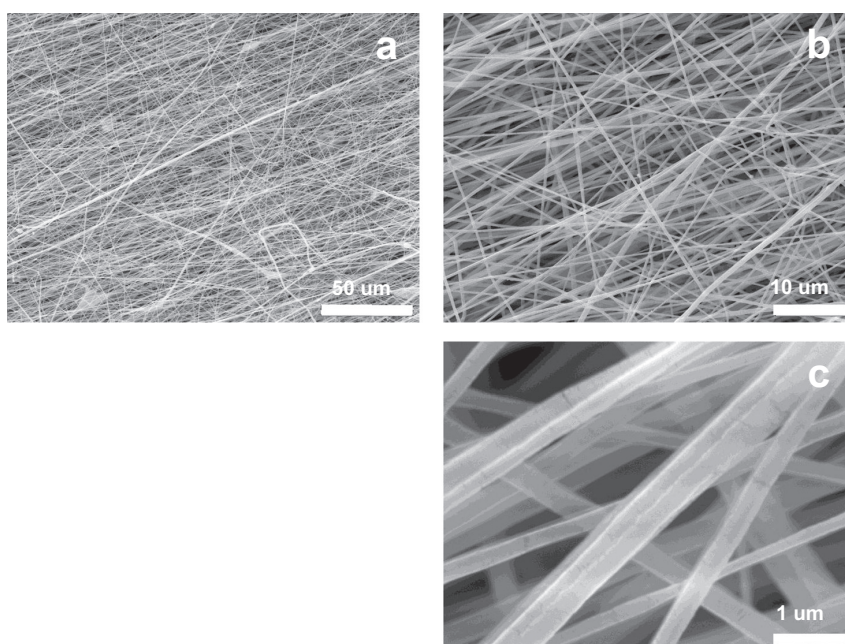
Fig. 1. SEM micrographs of pristine PLA nanofibres as spun on a rotating collector imaged at a) low, b) intermediate and c) high magnifications.

as reported by others [34,35]. In comparison, pure ethanol, ethanol/water 4:1 and hexane wetted both fibre mesh and film surface completely (contact angles < 5°). A key influence on the scission and dispersion of the fibres was the interaction between PLLA fibres and the dispersion media, i.e. the surface energy and hydrophobicity/hydrophilicity contrast. Indeed, when using water, which exhibits a static contact angle of 134° ± 4 on the PLLA meshes, the dispersion and fragmentation efficiencies were very low. This is possibly due to the fibre–fibre adhesion being energetically more favourable than the fibre–water interaction [27]. Since with each sonication cycle the

membranes are folded up, less water penetrates into the membrane, leading to a lack of cavitation bubble formation. It is possible that the ozone/UV exposure used as pre-treatment to cut PLLA fibres previously reported by Sawawi et al. [27] introduced −OH groups on the surface of the PLLA fibres, increasing their wettability with respect to water. This pre-treatment, however, irreversibly degrades PLLA fibres by oxidizing the ester bonds of the polymer, leading to a reduction of molecular weight and a significant reduction of the mechanical properties of the polymer. A study by Yixiang and co-workers showed a reduction of 47% in the ultimate tensile strength of PLLA derived nanofibres upon
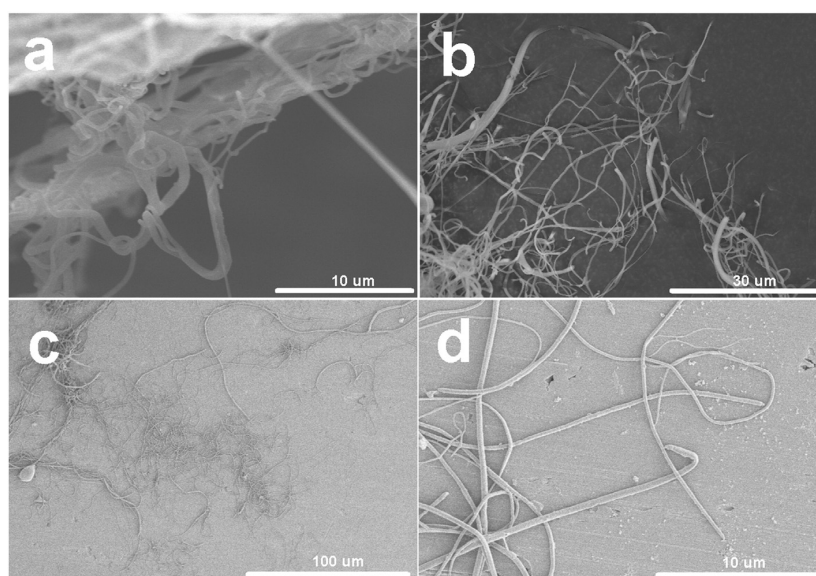
Fig. 2. SEM micrographs illustrating the influence of the dispersion media on the fibre morphology: a) PLA nanofibres sonicated in DI water for 10 min at 0 °C, b) PLA nanofibres sonicated in EtOH:H₂O, 1:4 for 10 min at 0 °C and c) and d) PLA fibres sonicated in hexane at −80 °C for 30 min at low and high magnifications, respectively, on steel 2.54 mm ø SEM sample holders).

31

exposure of the polymer to UV irradiation [39]. As such it is important to have processing alternatives that allow the fibres to maintain their mechanical integrity. In comparison, hexane, ethanol and a water/ethanol ratio of 1:4 were found to wet the PLLA surface completely. Indeed, it was previously reported that these solvents penetrate PLLA meshes more readily than pure water and displace any air pockets remaining within the meshes [40]. However PLLA is partially soluble in ethanol and thus processing the fibres in ethanol-containing medium leads to a partial dissolution at the surface and a subsequent agglomeration of the fibres. No degradation of PLLA was observed when using hexane as a dispersion medium. Additionally hexane has a melting point at −96 °C, which still allows for the process to be conducted in dispersion at −80 °C. The low vapour pressure of hexane also has a beneficial influence on the process outcome, since it allows for efficient cavitation. At lower temperatures the vapour pressure of the dispersion medium is lower, and the pressure difference between the outside and inside of the cavitation bubble is higher, resulting in a stronger implosion, further increasing the fibre fragmentation probability [41]. Indeed, we also evaluated pentane as a dispersion medium, but the separation of the fibres was unsatisfactory (results not shown). This leads to the conclusion that from the dispersion media examined in this work, hexane is the most suitable for sonication-assisted fragmentation of PLLA-based fibres.

3.5. Influence of particle type, size and particle to fibre ratio

PLLA nanofibres were sonicated in hexane, at −80 °C without and with nanoparticles as milling additives. Three types of particles, hydrophilic (P25) and hydrophobic (T805) TiO_2 and HA, having nominal diameters of 21 nm (TiO_2) and 30 nm (HA), respectively, were added to the fibre suspension in hexane before sonication. The morphology of the resulting staple fibres was analysed by SEM (Fig. 3). The length of the fibres obtained in different conditions was estimated based on optical microscopy images. The agglomerates observed after sonication were excluded from the quantitative analysis.

The nanoparticles penetrated into the fibre meshes, separating the fibres but not necessary leading to disentanglement. Indeed, SEM micrographs at higher magnifications showed that most particles filled the gaps between the fibres (Fig. 3). This may be due to either a re-agglomeration of cut fibres after sonication, i.e. during sample preparation, or to the fact that the sonication process separated the meshes only in part, but did not disentangle individual fibres. To examine that effect, we investigated the glass slides after measurements by SEM (Figs. 4–8). While a number of agglomerates remained, the separated staple fibres were clearly visible. This suggested that indeed, a re-agglomeration may take place. The effect of re-agglomeration during drying had been described before by Sawawi and co-workers [27]. They found that cut polystyrene fibres were highly agglomerated after drying, although the fibre aspect ratios (3–20) were an order of magnitude smaller than that achieved in the present work. Furthermore, the number of individual fibres visible by optical microscopy favours the hypothesis of drying-induced re-agglomeration. The addition of TiO_2 nanoparticles significantly affected the average fibre length of the fibres (p < 0.05) whether in hydrophilic or hydrophobic form. While sonication without particles yielded a fibre average length of 39 ± 37 µm, HA nanoparticle assisted sonication was not significant as compared to the "no-particle" case with a fibre length of 44 ± 31 µm. The addition of hydrophilic TiO_2 led to a fibre length of 63 ± 47 µm while in the hydrophobic case 51 ± 52 µm was measured. More interesting, a broader distribution of the respective fibre lengths was observed in the case of the TiO_2 assisted sonication as compared to the reference without particles (box plots in Fig. 9). The influence of the fibre:particle (v/v) ratio was studied in detail for the case of the HA nanoparticles, since they are relevant for the application explored in this work (FRC synthesis). When varying the volume ratios of fibre to particles between 2:1 and 1:4 no clear trend was observed. For example, for a 2:1 v/v particle to fibre ratio the obtained nanofibres' average length was 62 ± 45 µm, whereas when using an eight fold lower particle ratio (1:4) the yielded average length was 61 ± 44 µm and a ratio of 1:1 resulted in an average length of 44 ± 31 µm. In all cases the averages were higher than in the no particle case (39 ± 38 µm). It can thus be hypothesized that the particles provide more preferential sites for cavitation bubble nucleation and thereby "protect" the fibres, thus lowering the fragmentation efficiency. The slightly lower agglomerate size of T805 as compared to P25 (80 ± 44 vs 96 ± 89 nm) led to a lower fragment length average (51 ± 52 vs 63 ± 47) which is attributed to the decrease in cavitation threshold for well wetted particles (T805 in hexane) as compared to particles with a mismatch in wetting properties as compared to the
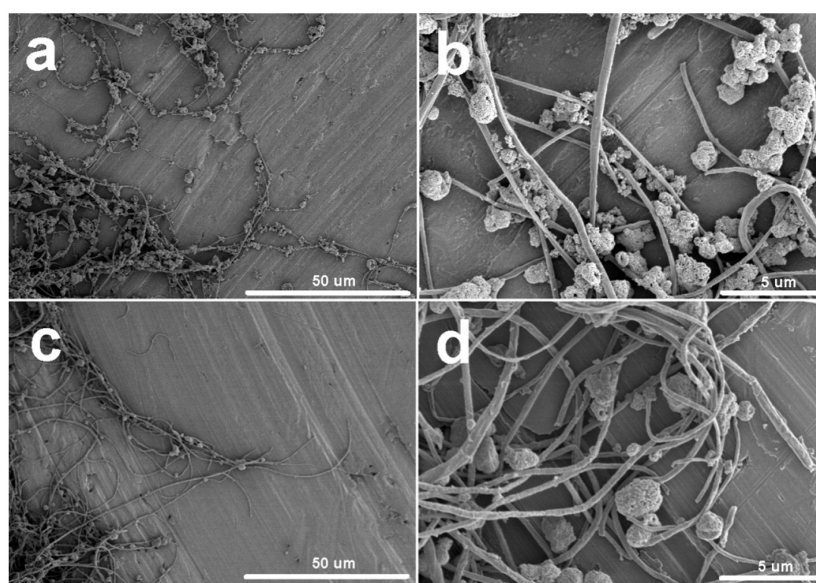
Fig. 3. SEM micrographs of: a) and b) PLLA fibres sonicated with TiO_2 P25 particles at low and high magnifications, respectively (hexane, 30 min, −80 °C, 1:1 fibre:particles v/v ratio) and c) and d) PLLA fibres sonicated with HA nanoparticles at low and high magnifications, respectively (hexane, 30 min, −80 °C, 1:1 fibre:particles v/v ratio).
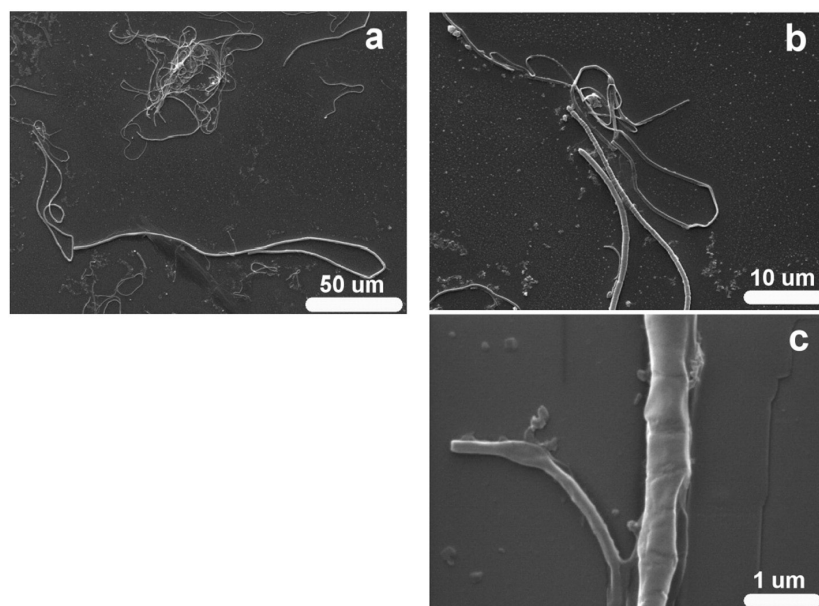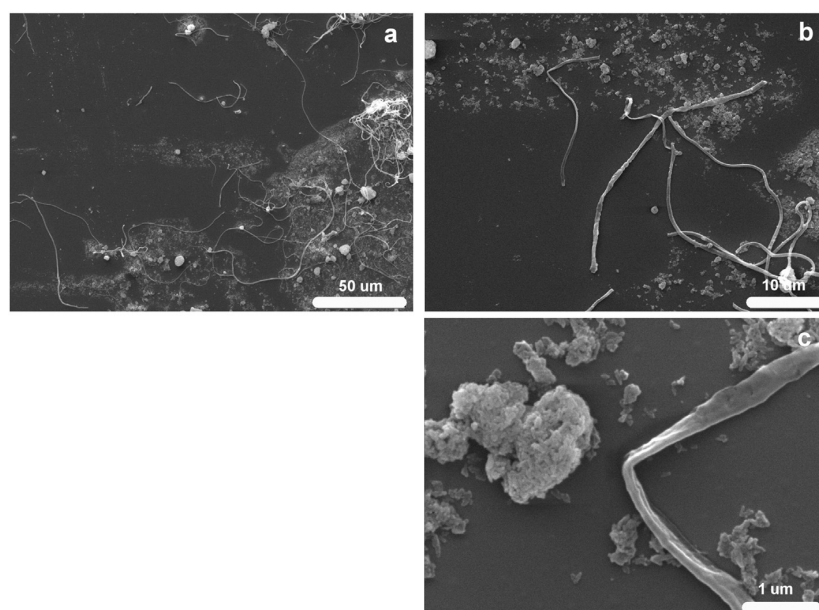
Fig. 4. SEM micrographs of PLLA fibres sonicated without particles at a) low, b) mid and c) high magnifications, respectively (hexane 30 min, −80 °C, on glass slide).

dispersion medium (P25 in hexane), resulting in an increase in fragmentation efficiency. Recent reports have shown that the addition of particles decreases the cavitation threshold [29,42]. As such, the fragmentation of the fibres due to the eventual mechanical impact of the particles does not seem to be a major factor contributing to the scission. This conclusion is supported by the results of additional experiments mentioned above in which the fibres to nanoparticle ratio was altered between 1:4 and 2:1 (v/v). The short neck area and ragged edges as depicted in Fig. 8 hint to a fracture originating from erosion rather than through tensile failure. However, a combination of erosion and subsequent failure through bending or shear cannot be excluded,

since elasticity of the fibre is also a factor as e.g. PCL fibres do not fragment when beyond their glass transition temperature.

3.6. Influence of sonication temperature and time

The influence of sonication temperature and time was studied in detail for the case of the fragmentation of PLLA fibres in hexane, in the presence of HA nanoparticles (fibre:particle ratio of 1:1). The temperature-induced changes were analysed at different bath temperatures of 0 °C (ice/water) and −80 °C (dry ice/ethanol). The temperature in the bath was maintained constant, but an important increase
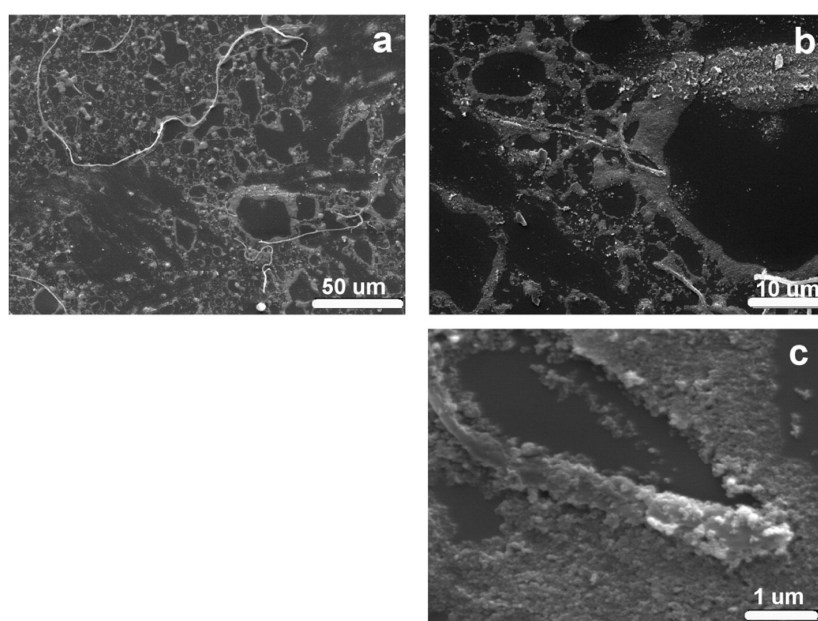

Fig. 5. SEM micrographs of: a), b), and c) PLLA fibres sonicated with HA particles at low, medium and high magnifications, respectively (hexane, 30 min, −80 °C, 1:1 fibre:particles v/v ratio on a glass).
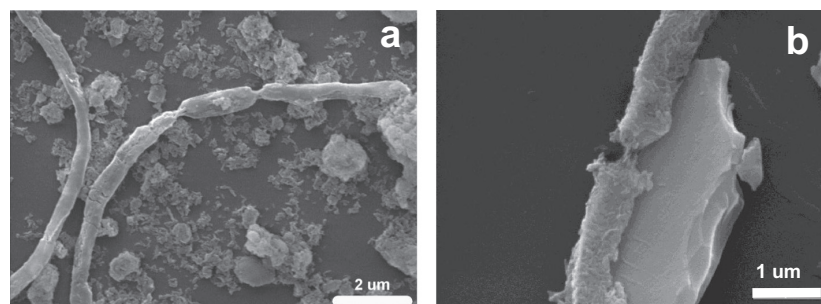
33
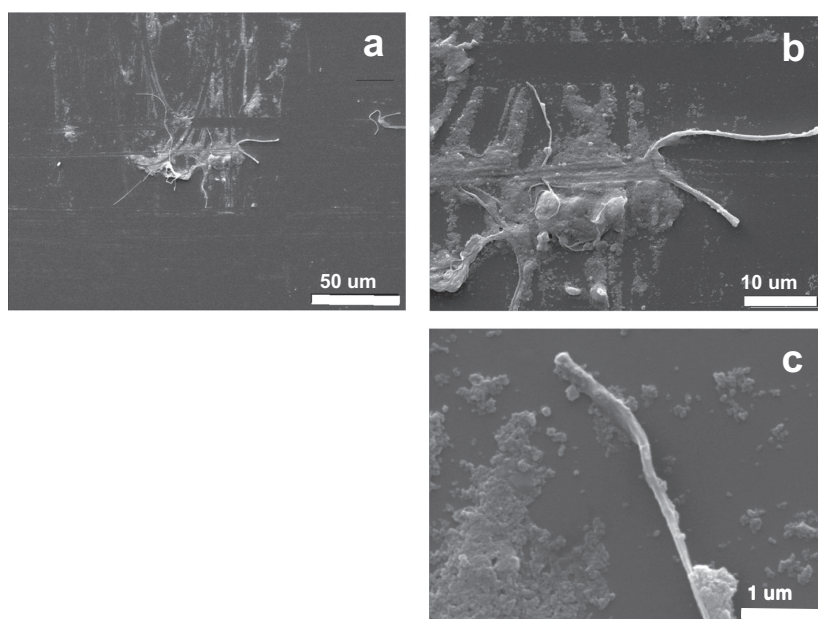
Fig. 6. SEM micrographs of: a), b), and c) PLLA fibres sonicated with hydrophilic P25 TiO$_2$ particles at low, medium and high magnifications, respectively (hexane, 30 min, −80 °C, 1:1 fibre:particles v/v ratio on).

in the dispersion medium temperature during the process was observed: from −71 °C to −31 °C when using a cooling bath of −80 °C and from 3 °C to 22 °C in the case of the 0 °C bath. This can be explained by lower processing temperatures that lead to a reduction in ductility of the PLLA fibres, since PLLA exhibits a glass transition temperature of ~50 °C. Below the T$_g$ the polymer behaves as a brittle solid and is more prone to strain induced fractures [31,32], thus resulting in a higher likelihood of short fibres being produced. Further support comes from unpublished sonication experiments on electrospun PCL, a hydrophobic elastic polymer, which has a T$_g$ of −60 °C. The PCL meshes could not be cut in any of the dispersion media mentioned previously using cooling baths with a temperature of −80 °C. The temperature measurements conducted inside the vials indicated a temperature increase (up to −30 °C) during sonication, well above the T$_g$ of PCL. This supports the conclusion that the dispersion medium temperature must be considerably lower than the glass transition temperature in order to allow the dispersion and fragmentation of amorphous or semi-crystalline polymers.

Fig. 7. SEM micrographs of PLLA fibres sonicated with hydrophobic T805 TiO$_2$ particles at a) low, b) mid, and c) high magnifications, respectively) (hexane, 30 min, −80 °C, 1:1 fibre:particles v/v ratio on glass slide after separation).

Fig. 8. SEM micrographs showing two partial fibre fractures (PLLA fibres sonicated with HA particles at low, medium and high magnifications, respectively) (hexane, 30 min, −80 °C, 1:1 fibre:particles v/v ratio on glass slide) showing eroded areas of a partially fractured PLLA fibre.

At −80 °C the process was conducted for 10, 20, 30, and 60 min giving average fibre lengths of 77 ± 51 μm, 63 ± 49 μm, 44 ± 31 μm and 35 ± 28 μm, respectively. The average fibre length decreased as a function of sonication time (Fig. 9). Statistical analysis showed significant differences for all sonication times. At 0 °C the samples were sonicated for 30 min. The obtained fibre length was significantly different (p < 0.05), with a decrease from 54 ± 43 μm to 47 ± 23 μm in the ice/water bath and dry ice/ethanol respectively. Moreover, a wider distribution of the cut nanofibres' length was observed at higher temperatures (Figs. 9c and 10c). It is possible that at a certain minimum length range – or aspect ratio – the short fibres do not allow for building up of a high enough local tensile stress, sufficient to induce stress fractures. However, the fractures originate in local pitting or erosion, which is produced by microjets from the collapsing bubbles, rather than in a strain or ultimate strength fracture. Indeed, ductile fibres such as PLLA, exhibit

a higher resistance towards pitting and erosive wear. Our results are in agreement with previous reports which have shown that the bending effect and local pitting lead to an asymptotic decrease of fibre length in time [27].

3.7. Engineering of a fibre reinforced composite cement

As mentioned above, fibre reinforced composite cements were engineered using the PLLA fibres fragmented by HA-nanoparticle assisted sonication. Compression tests with the reinforced cements (Fig. 11a, b) resulted in a compressive strength of 4.7 ± 0.5 MPa for the fibre containing cement versus 2.7 ± 0.7 MPa for the control sample (prepared without nanofibres, Fig. 11c, d). This is a significant increase in compressive strength (90%). SEM imaging of a fractured cement revealed a homogeneous dispersion of the fibre/nanoparticle precursor
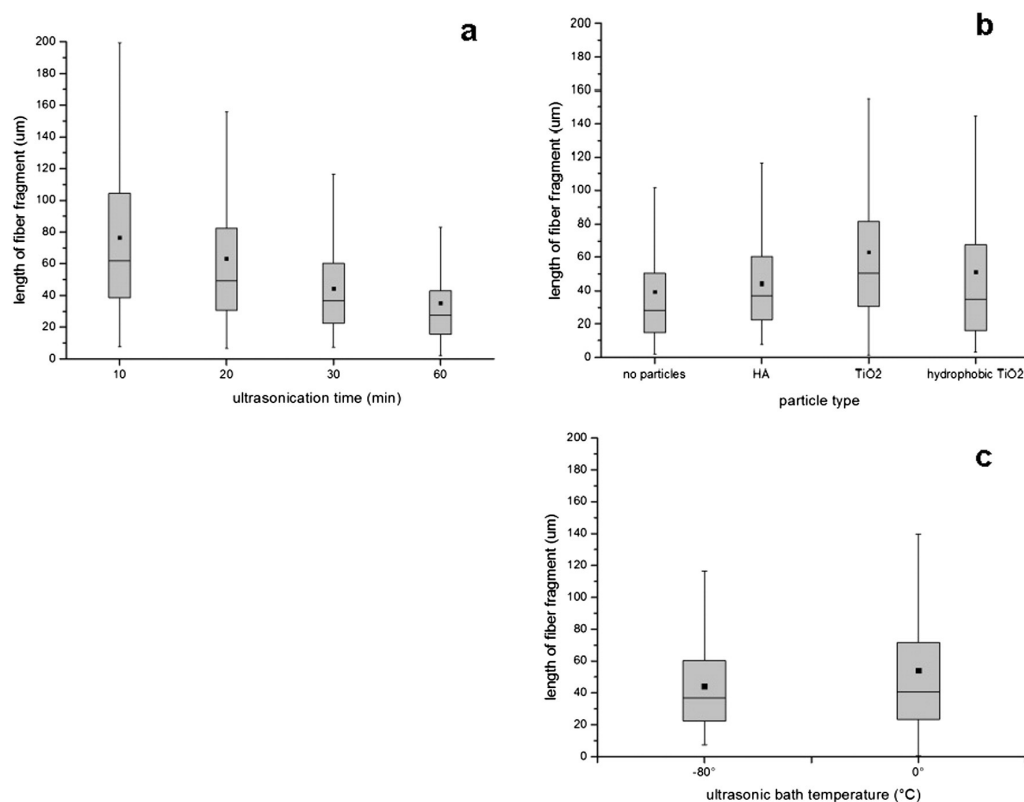
Fig. 9. Box plots illustrating the fibre length distributions as a function of the ultrasonication conditions: a) different types of nanoparticles, in hexane, at −80 °C, at 1:1 fibre:particle v/v ratios, b) different bath temperatures and c) different sonication times (a) and c) investigated in the presence of HA nanoparticles, in hexane, and a 1:1 fibre:particle v/v ratio).
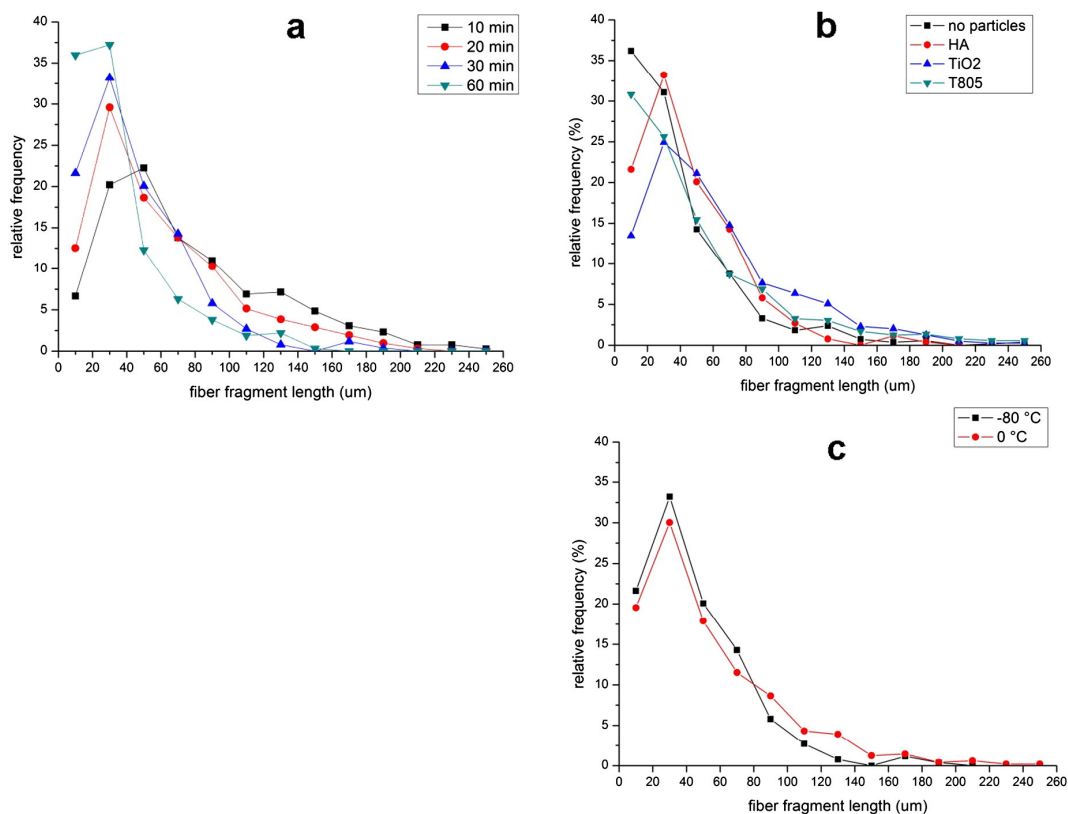
Fig. 10. Histograms depicting the relative fibre length distributions as a function of a) time, b) particle type, and c) temperature, n > 250.

in the cement. Porosity was calculated to be 59% for the reference cement, as compared to 52% for the reinforced composite.

BET measurements showed a specific surface area of 14 m^2/g for the reference cement, as compared to 9 m^2/g for the reinforced cement. This result is in agreement with what can be expected for fibre reinforcement, shown by Xu and co-workers, who integrated knitted vicryl microtextiles into HA cement and obtained a significant increase in flexural strength [43]. This is in contrast to the result observed by Zuo et al.
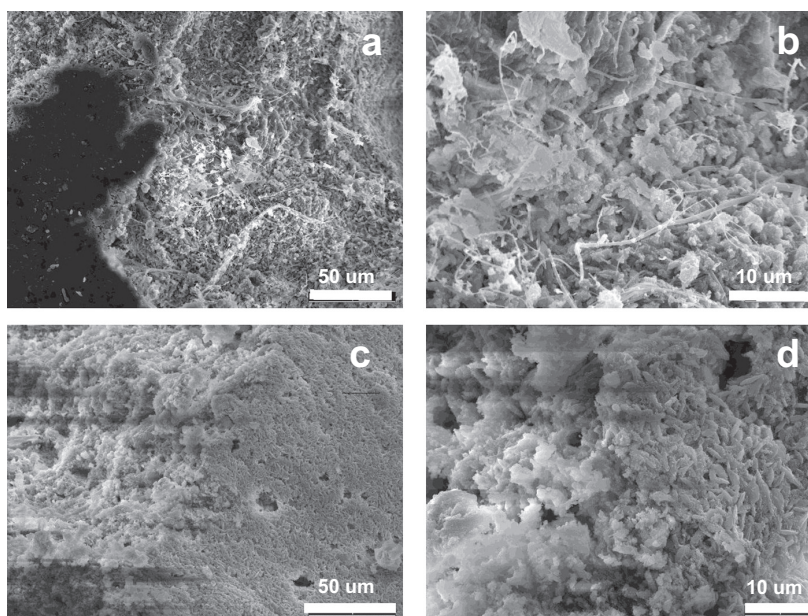

Fig. 11. SEM micrographs of PLLA fibre reinforced cement at a) low and b) high magnifications. As comparison a cement without fibres at c) low and d) high magnifcations.

[44] or Gorst et al. [45], who both incorporated non-processed electrospun meshes into HA cement and found a decrease in compression strength. In the present work, the reinforcement emerges from the finely distributed fibres bridging micro-sized cracks and faults within the cements, thus contributing to compressive strength. It also shows the advantage of nanoparticle-assisted sonication of fibres, since this process yields a highly homogeneous intercalation of particles into fibre meshes, leading to their disintegration and fibre separation. Despite the manual mixing procedure, no significant fibre agglomeration was visible in the set cement, which was confirmed by SEM measurements (Fig. 11a, b). This indicates that the fibre–particle precursor remains stable during mixing, subsequent dissolution and recrystallization during the setting time of the cement. It can be assumed that the HA suspension adheres sufficiently to the fibres such that the forces required for the fibres to reagglomerate are higher than the forces applied during the mixing process, thus keeping the fibres dispersed within the resulting cement matrix. The unreinforced cement has a 13% higher porosity and 55% higher surface area as compared to the reinforced cement. The presence of the fibres reduces the porosity of the cement, which contributes to its higher mechanical strength. One can assume that the fibres act as pore fillers during the setting process. The influence of the sonication process on the porosity or pore size seems unlikely, since no visible particle deagglomeration was observed during sonication (section 3.2.). Since no sonication is applied during the cement setting and mixing itself, a contribution of the sonication process to that seems unlikely.

4. Conclusion

Staple PLLA nanofibres were produced by electrospinning and subsequent sonication at low temperatures. We investigated the effect of dispersion medium type, temperature, time and the use of nanoparticles on the length of the individual fibres that were cut using sonication, without any chemical or pre-treatments. The most efficient fragmentation of the PLLA fibres was obtained in hexane, a high-vapour pressure dispersion medium that efficiently wet the fibres and allowed the formation of cavitation bubbles within the meshes. Additionally we have demonstrated that lower temperatures resulted in shorter fibres and narrower length distributions. Increased sonication time resulted in an asymptotic decrease of fibre length and a narrowing of fibre length distribution. The addition of nanoparticles reduced the efficiency of the fragmentation process and fibres with higher average lengths were obtained. This effect was independent of the fibre-to-particle ratio. Moreover, by particle-assisted sonication a good distribution of the particles between the nanofibres was obtained. This effect further allowed the homogeneous dispersion of the fibre–particle precursor within a HA-based matrix, making the technique suitable for the fabrication of fibre-reinforced cements. We have thus demonstrated in this work the successful production of a PLLA-Brushite composite cement with high compressive strength. The method presented is thus a promising technique for the fabrication of FRCs with very good mechanical properties, which can be further integrated in biomedical products.

Acknowledgments

References

[1] H.H.K. Xu, F.C. Eichmiller, A.A. Giuseppetti, J. Biomed. Mater. Res. 52 (2000) 107–114.
[2] E. Pirhonen, Institute of Biomaterials, Tampere University of Technology, Tampere, 2006, pp. 80.
[3] J.J. Beaudoin, Handbook of Fiber-reinforced Concrete, Noyes Publications, Ottawa, 1990.
[4] C. Canal, M.P. Ginebra, J. Mech. Behav. Biomed. Mater. 4 (2011) 1658–1671.
[5] E.P. Giannelis, Adv. Mater. 8 (1996) 29–35.
[6] D.R. Paul, L.M. Robeson, Polymer 49 (2008) 3187–3204.
[7] H. Yan, L. Liu, Z. Zhang, Mater. Lett. 65 (2011) 2419–2421.
[8] J. Peng, Z. Qian, B. Wang, S. Fu, G. Guo, F. Luo, R. Li, D. Wu, J. Nanosci. Nanotechnol. 11 (2011) 3659–3668.
[9] L. Yao, C. Lee, J. Kim, Fibers Polym. 11 (2010) 1032–1040.
[10] A. Greiner, J.H. Wendorff, Angew. Chem. Int. Ed. 46 (2007) 5670–5703.
[11] M. Simonet, O.D. Schneider, P. Neuenschwander, W.J. Stark, Polym. Eng. Sci. 47 (2007) 2020–2026.
[12] J.C. Yang, S.Y. Lee, W.C. Tseng, Y.C. Shu, J.C. Lu, H.S. Shie, C.C. Chen, Macromol. Mater. Eng. 297 (2012) 115–122.
[13] Z.M. Huang, Y.Z. Zhang, M. Kotaki, S. Ramakrishna, Compos. Sci. Technol. 63 (2003) 2223–2253.
[14] S.G. Kumbar, R. James, S.P. Nukavarapu, C.T. Laurencin, Biomed. Mater. 3 (2008).
[15] K. Sombatmankhong, N. Sanchavanakit, P. Pavasant, P. Supaphol, Polymer 48 (2007) 1419–1427.
[16] S. Liao, B. Li, Z. Ma, H. Wei, C. Chan, S. Ramakrishna, Biomed. Mater. 1 (2006) R45–R53.
[17] B. Holmes, N.J. Castro, L.G. Zhang, E. Zussman, Tissue Eng. B Rev. 18 (2012) 478–486.
[18] J.M. Deitzel, J. Kleinmeyer, D. Harris, N.C. Beck Tan, Polymer 42 (2001) 261–272.
[19] S. Lee, S.K. Obendorf, J. Appl. Polym. Sci. 102 (2006) 3430–3437.
[20] C.A. Fuenmayor, S.M. Lemma, S. Mannino, T. Mimmo, M. Scampicchio, J. Food Eng. 122 (2014) 110–116.
[21] P. Gibson, H. Schreuder-Gibson, D. Rivin, Colloids Surf. A Physicochem. Eng. Asp. 187–188 (2001) 469–481.
[22] A.L. Andrady, Science and Technology of Polymer Nanofibers, John Wiley & Sons, Hoboken, New Jersey, 2008.
[23] A. Stoiljkovic, S. Agarwal, Macromol. Mater. Eng. 293 (2008) 895–899.
[24] M. Thieme, S. Agarwal, J.H. Wendorff, A. Greiner, Polym. Adv. Technol. 22 (2011) 1335–1344.
[25] C. Yoshikawa, K. Zhang, E. Zawadzak, H. Kobayashi, Sci. Technol. Adv. Mater. 12 (2011).
[26] I. Greenfeld, E. Zussman, J. Polym. Sci. B Polym. Phys. 51 (2013) 1377–1391.
[27] M. Sawawi, T.Y. Wang, D.R. Nisbet, G.P. Simon, Polymer 54 (2013) 4237–4252.
[28] I. Perelshtein, G. Applerot, N. Perkas, J. Grinblat, E. Hulla, E. Wehrschuetz-Sigl, A. Hasmann, G. Guebitz, A. Gedanken, ACS Appl. Mater. Interfaces 2 (2010) 1999–2004.
[29] C.H. Farny, T. Wu, R.G. Holt, T.W. Murray, R.A. Roy, Acoust. Res. Lett. Online 6 (2005) 138–143.
[30] G.L. Fiore, F. Jing, V.G. Young Jr., C.J. Cramer, M.A. Hillmyer, Polym. Chem. 1 (2010) 870–877.
[31] S. Kalia, S.-Y. Fu, Polymers at Cryogenic Temperatures, Springer, 2013.
[32] G. Hartwig, Polymer Properties at Room and Cryogenic Temperatures, Plenum Press, 1994.
[33] P. Katta, M. Alessandro, R.D. Ramsier, G.G. Chase, Nano Lett. 4 (2004) 2215–2218.
[34] P.B. van Wachem, T. Beugeling, J. Feijen, A. Bantjes, J.P. Detmers, W.G. van Aken, Biomaterials 6 (1985) 403–408.
[35] P.N. Thanki, E. Dellacherie, J.-L. Six, Applied Surface Science 253 (2006) 2758–2764.
[36] L. Van Der Schueren, B. De Schoenmaker, O.I. Kalaoglu, K. De Clerck, Eur. Polym. J. 47 (2011) 1256–1263.
[37] N. Lavielle, A. Hébraud, G. Schlatter, L. Thöny-Meyer, R.M. Rossi, A.M. Popa, ACS Appl. Mater. Interfaces 5 (2013) 10090–10097.
[38] A. Mills, S. Le Hunte, J. Photochem. Photobiol. A Chem. 108 (1997) 1–35.
[39] D. Yixiang, T. Yong, S. Liao, C.K. Chan, S. Ramakrishna, Tissue Eng. A 14 (2008) 1321–1329.
[40] A.G. Mikos, M.D. Lyman, L.E. Freed, R. Langer, Biomaterials 15 (1994) 55–58.
[41] H.M. Santos, C. Lodeiro, J.-L. Capelo-Martínez, The Power of Ultrasound, Ultrasound in Chemistry, Wiley-VCH Verlag GmbH & Co. KGaA, 2009. 1–16.
[42] T. Tuziuti, K. Yasui, M. Sivakumar, Y. Iida, N. Miyoshi, J. Phys. Chem. A 109 (2005) 4869–4872.
[43] H.H.K. Xu, J.B. Quinn, S. Takagi, L.C. Chow, Biomaterials 25 (2004) 1029–1037.
[44] Y. Zuo, F. Yang, J.G.C. Wolke, Y. Li, J.A. Jansen, Acta Biomater. 6 (2010) 1238–1247.
[45] N.J.S. Gorst, Y. Perrie, U. Gbureck, A.L. Hutton, M.P. Hofmann, L.M. Grover, J.E. Barralet, Acta Biomater. 2 (2006) 95–102.

5 Reinforcement of CaP Cement

5.1 Context

In the previous chapter, a novel method for cutting and dispersing and mixing electrospun fibers with cement precursors was introduced and a proof of concept of the set reinforced cement was manufactured and mechanically characterized which showed the significance of fiber dispersion on the mechanical strength of the cement. The range of required fiber content and diameter to achieve a good reinforcement was not determined. Furthermore, the fibers act as fillers within the cement and can influence the cement reaction as shown by Engstrand and co-workers [77]. Finally, the fiber distribution within the cement was characterized to quantify the effect of the fiber dispersity within the cement. To the best of knowledge, no straightforward method exists to characterize the distribution of these fibers. The following manuscript therefore had the following goals: 1) characterize cements with low and high fiber content and nano and micron sized fiber diameter and investigate their influence on the mechanical and cement setting properties 2) develop a novel method to analyze the fiber dispersion within the matrix by graphic analysis of the fracture surface With regard to the fiber diameter and content it was found that a low concentration of nanofibers (5%) was sufficient to induce a 4 fold increase in compressive strength, with higher concentrations or larger diameters being less beneficial. Furthermore, it was observed that the cement composition was altered by the presence of the dispersed fibers, an effect that was not observed within the controls, confirming the influence of the filler as reaction modifier. A novel method of characterizing the fiber dispersion based on a Voronoi surface analysis was developed, where indeed the nanofibers showed a higher dispersity compared to the microfibers or control. Finally, it was observed that the failure of the material was primarily by pull-out, and little residue was observed on the surface of the pulled-out fibers, which raised the question for the following manuscript regarding an increased adhesion of the CaP to the fibers. The upper limit was determined by the miscibility of the cement components with the matrix. The lower was set based on the ratio achieved in the previous publication.

5.2 Contribution of the author

Experimental design and protocol and were devised a collaborative effort between EM and RL. Most of the manufacturing experiments and analysis were performed by EM except for the following, which were conducted as collaborative effort between EM and the respective subject matter experts: Mechanical testing, Voronoi analysis and XRD measurements (See also acknowledgments section in the manuscript). Statistical analysis was performed by EM. The main manuscript writing was collaboratively performed by EM, KM, Martin Frenz (MF), GF and RL. All figures were prepared by EM.

Article reused with permission license no. 5234360972916 from copyright.com

5.3 Absorbable mineral nanocomposite for biomedical applications: Influence of homogenous fiber dispersity on mechanical properties

Absorbable mineral nanocomposite for biomedical applications: Influence of homogenous fiber dispersity on mechanical properties

Elias Mulky,[1,2] Katharina Maniura-Weber,[2] Martin Frenz,[3] Giuseppino Fortunato,[4] Reto Luginbuehl[5]

[1]RMS Foundation, Bischmattstrasse 12, Bettlach, Switzerland

[2]Laboratory for Biointerfaces, Lerchenfeldstrasse 5, Empa, Swiss Federal Laboratories for Materials Science and Technology, St Gallen 9014, Switzerland

[3]Institute of Applied Physics, University of Bern, Sidlerstrasse 5, Bern 3012, Switzerland

[4]Laboratory for Biomimetic Membranes and Textiles, Lerchenfeldstrasse 5, Empa, Swiss Federal Laboratories for Materials Science and Technology, St Gallen 9014, Switzerland

[5]Department of Biomedical Material Research, University of Bern, Bern 3002, Switzerland

Abstract: Electrospun micro- and nanosized fibers are frequently used as reinforcing elements in low temperature ceramic composites for biomedical applications. Electrospinning of fibers yield, however, not individual fibers, but rather fiber-mats that are difficult to separate. Most investigations have been performed on diced mats and highly nonhomogenous composites. We examined the influence of dispersed electrospun single micro- and nanometer fibers on the mechanical properties of calcium phosphate cement composites. Absorbable poly-L-lactic-acid was electrospun yielding fibers with diameters of 244 ± 78 nm, named nanofibers (NF), and 1.0 ± 0.3 μm, named microfibers (MF). These fibers were cut using a particle assisted ultrasonication process and dispersed with hydroxyapatite nanoparticles and composites of low (5%) and high (30%) NF/MF content were engineered. The homogeneity of the fiber distribution was investigated by analyzing fracture areas regarding the number of fibers and Voronoi area size distribution. Variation of fiber distribution was significantly lower in the NF group as compared to the MF group. For composites containing 5% NF (V/V), an eightfold increase in the compressive fracture strength, and for the 30% NF (V/V) a threefold increase compared was measured. The composite containing 5% NF was identified as optimal regarding fiber distribution and strength. Our new method of engineering these composites allows for high volume fractions of NF with low variation in fiber distribution to be incorporated into composites, and shows the importance of using single filaments as reinforcing agents. © 2017 Wiley Periodicals, Inc. J Biomed Mater Res Part A: 106A: 850–857, 2018.

Key Words: absorbable, calcium phosphate cement, composite, nanofibers, electrospinning

INTRODUCTION

Calcium phosphate cements (CaP) are frequently used as defect fillers for human bones.[1] They are well-accepted by the bone tissue and are absorbed within specified time frame based on their formulation.[2] The drawback of CaP are, however, their poor mechanical properties,[3] which limits their use to nonload bearing situations. That drawback can be overcome by introducing reinforcing elements in form of fibers.[4–6] The resulting mechanical properties of such so-called fiber reinforced composites (FRC) outperform typically those of the matrix or fibers alone. In particular, in cements, the aggregation of crystalline nano- and microparticles forms a brittle, porous bulk structure. Under load,

these cements tend to fracture without a prior discernible change in geometry or mechanical properties, resulting in a sudden significant loss of mechanical properties.

Nowadays, fibers are widely used as additives in cements. Von Gonten and colleagues[7] used a polyglycolic acid based multifilament fiber meshes with single filament diameters of 17 μm to reinforce a hydroxyapatite (HA) based matrix resulting in a composite with the work of fracture (29 N/m) equal to that of poly-methyl-methacrylate (PMMA) (28 N/m) in flexural strength. In a similar approach, Xu et al. used a variety of different discontinuous filaments of Aramid, E-glass, or polyglycolic acid with diameters in the order of tens of micrometers and lengths

between 3 and 200 mm to reinforce HA. They described an up to fourfold increase in fracture strength as compared to their pristine cement control.[6] However, at fiber contents above 5%, the fibers entangled which lead to phase segregation within the cement and consequently to a lower reinforcement and even a decrease in strength. This is a prime example for the importance of homogeneous fiber dispersion for yielding matrix reinforcement. In that context, it can be conjectured that decreasing the fiber diameters while keeping the total fibrous volume constant allows for a significantly larger part of the cement matrix to be in contact with the fibers. The consequence is an increased reinforcement provided that the fiber aspect ratio is constant or larger than in the case of larger diameter fibers.[4,8,9]

Electrospinning is a well-established technique to engineer micro- and nanometer-sized fibers from a large selection of polymeric and inorganic materials.[10–13] The process typically yields directionally or randomly oriented fibers which are collected in the form of nonwoven fleece.[10,14,15] Such mats are however not suited for reinforcement as they cannot be homogenously dispersed in or penetrated by the matrix material such as calcium phosphate based cements. It has been shown that their effect in composites is minimal or nonexisting even they were chopped into multifilament segments prior to use.[16] The direct engineering of short, staple fiber like fibers by electrospinning has been demonstrated.[17] It either results in rather slow process (solution flow rate of 0.5 μL/min), or is restricted to polymers with rather low molar mass in the range of 15 kDa.[18] In order to produce strong composites, polymers with high molar mass are desirable in the production of mechanical competent composites.[19] In order to obtain staple fibers from electrospinning process at high yield, postprocessing is required to separate and cut these meshes into single separated filaments. We recently demonstrated that electrospun poly-ʟ-lactic-acid (PLLA) fibers can be separated and cut to staple fiber like precursors by using a particle assisted sonication process.[20]

It is the aim of the present work to show the effect of fiber dispersion in calcium phosphate based cements on the fracture strength. Our approach lies in engineering composites containing HA nanoparticles as base and use them for particle assisted sonication allowing for high intercalation and penetration of the fibrous phase yielding a homogenous distribution. The resulting particle/fiber mixture is reacted with MCPM and water to obtain a rapidly degradable monetite/brushite cement.[21,22] Electrospun PLLA fibers with diameters of 250 nm (nanofiber [NF]) or 1000 nm (microfiber [MF]) were used as fibers. These diameters were chosen to study the influence of fiber dispersity within the same volume fraction at low (5%) and high (30%) concentrations. Cements containing diced electrospun mats served as negative control. Furthermore, the influence of the fiber content on the phase composition of the CaP based cement was evaluated by comparing the composites with pristine cement of similar water content. The resulting composites were comprehensively characterized regarding compressive strength, crystalline phase composition as well as fiber dispersity.

MATERIALS AND METHODS

All solvents were obtained from commercial providers in ACS quality and were used without further purification. PLLA (Biomer L9000, Mm: 200,000 Da) was obtained from Biomer Biopolyesters (Krailing, Germany). Chloroform, N-N-dimethylformamide (DMF), formic acid, and disodium dihydrogen pyrophosphate, were purchased from Sigma Aldrich (Buchs, Switzerland). Hydroxyapatite (HA) nanoparticles were purchased from MKnano (Missisauga, ON, Canada) and mono calcium phosphate monohydrate (MCPM) particles (Regent 12xx) were purchased from Innophos Inc. (Cranbury, NJ).

Fiber processing

The polymer fibers were manufactured by electrospinning. The protocol for electrospinning was described in previous work[20] and adapted for the present study: Briefly, 5.6% (w/w) of PLLA for NF production and 8.9% (w/w) PLLA for MF production were dissolved in a solution containing chloroform:DMF at a ratio of 8:1 (w/w). The solutions were mixed for at least 15 h at room temperature on an orbital shaker (200 rpm) prior to use. After complete dissolution of the PLLA, an aliquot of stock solution was separated for immediate use for electrospinning and concentrated formic acid was added slowly while mixing to achieve a ratio of 9:1 (w/w) of stock solution to formic acid. The resulting solution was incubated again for 20 min on the orbital shaker.

Electrospinning was performed with an in-house built device, consisting of a syringe pump Aladdin 1000 (World Precision Instruments, Sarasota, FL), a variable high voltage power source CPS Series (AIP Wild AG, Oberglatt, Switzerland), and an in-house built rotating collector which allowed for predominate fiber orientation. The complete system was placed in a Faraday cage. A +15/−5 kV potential, with a maximum current of 0.1 mA, was applied between the 18G, blunt needle tip (BD Braun, Bethlehem, PA) and collector with a tip-collector distance of 18 cm. The rotating speed of the 20-cm diameter collector was constant at 1340 rpm. An in-house programmed LabVIEW[TM] application was used to control the electrospinning process. Collected fibers were removed from the collector using a surgical blade and metal tweezers and wrapped in aluminum foil for storage before postprocessing.

Fiber analysis

The fibers were analyzed using scanning electron microscopy (SEM). The samples were coated with 7 nm of gold using a sputter coater Polaron. E5100 (Polaron Equipment Ltd., Hertfordshire, United Kingdom). SEM analysis was conducted on a Hitachi S-4800 (Hitachi Ltd., Tokyo, Japan) using a voltage of 2 kV and 10 μA of current. The diameters of at least 10 fibers from three separate images were measured per batch.

Composite processing

The protocol for composite engineering was described in detail in a previous work and adopted accordingly.[20] Briefly, the collected fiber meshes were removed from the aluminum wrapping with tweezers and diced to approximately 1 ×

43
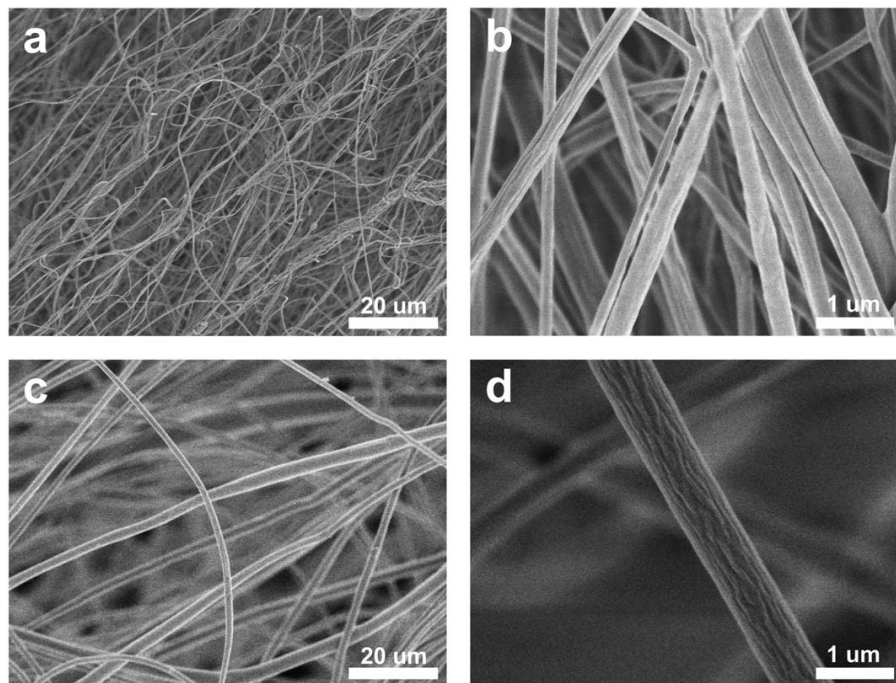
FIGURE 1. SEM micrographs of pristine PLA NF (a, b) and MF (c, d) as spun on a rotating collector imaged at low (a, c) and high (b, d) magnification. Visible is the smooth structure of the NF (b), and the wrinkled structure of the MF (d).

1 cm^2 sections using a surgical blade no 11, sterile (KLS Martin Group, Mühlheim, Germany), preferentially perpendicular to the main fiber orientation. Subsequently, the patches were transferred into a 30 mL glass flask containing 20 mL of *n*-hexane. The flask was then immersed in a dry ice/acetone bath and cooled to −80°C. The bath temperature was maintained constant during the process by periodically refilling the coolant mixture. HA nanoparticles with a nominal diameter of 30 nm were added at a ratio of 5:1 w/w for the cement precursor containing 5% v/v of fibers and 9:10 w/w for the cement precursor containing 30% v/v of fibers, respectively. Sonication was performed by immersing a 1.27 cm sonicator

tip (Branson Digital Sonifier Model 450D, 20 kHz fixed frequency, 400 W output power, Emerson, Ferguson, MO) for 30 min in 2/2 s on/off cycles at an amplitude of 90%. Multiple batches of 50 to 80 mg PLLA fibers were sonicated summing up samples of up to 1000 mg (fibers and HA particles). In a final step, MCPM was added at a ratio of 16:13 HA-fiber premix to MCPM and sonicated again for 5 min. The resulting fiber/particle dispersion was drained of excess hexane using a filter, and air dried in a fume hood under ambient conditions for at least 15 h.

An aqueous solution containing 0.06M disodium dihydrogen pyrophosphate, which slows the setting reaction and
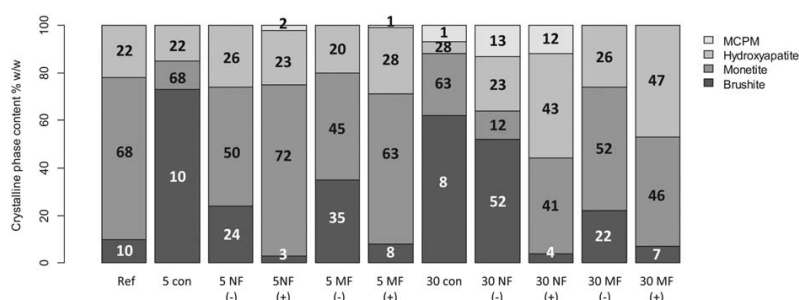
FIGURE 2. XRD analysis of the relative (% mass) crystalline content of the sonicated composites. Brushite and monetite are the products, while MCPM and HA are the starting materials. There is a trend of decrease in reactivity with increased fiber dispersion and fiber content. The numbers in the bars refer to respective mass fraction. 5/30, fiber volume fraction; Con, control denoting equivalent water addition as the respective composites; (−), nonsonicated samples; (+), sonicated samples.

44
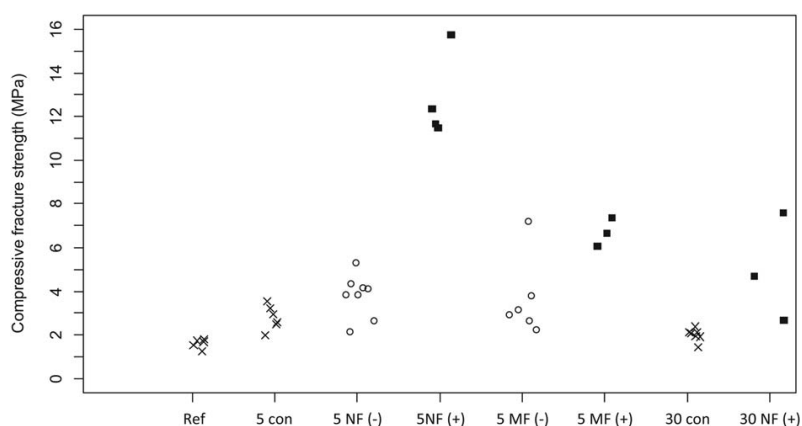
FIGURE 3. Compressive strength of the different samples. Notable is the consistently higher fracture strength of the sonicated composites when compared to their nonsonicated counterparts or the pristine cements. Pristine samples are indicated by an x; the nonsonicated composites by empty circles; and the sonicated composites by filled squares. Con, control denoting equivalent water addition as the respective composites; (−), nonsonicated samples; (+), sonicated samples.

maintains moldability during handling,[23] was prepared with deionized water (>18 MΩ, in-house supply). This liquid was mixed with the HA/PLLA/MCPM at ratios of 9:4, 8:4, and 7:4 dry powder mixture to liquid ratio (w/w). The ratios were calculated for the composite to have a fiber content of 0, 5, and 30% v/v, respectively. Additional pristine (containing no fibers) cements with powder to liquid ratios of 8:4 and 7:4 were produced as controls, corresponding to the added liquid of the composites containing fibers at 5 and 30% v/v. The resulting slurry was mixed for 2 min with a spatula to obtain a cement paste, which was transferred into custom-made Teflon cylinders of 5 mm diameter and 7 mm height. The cement allowed for setting and curing during 3 days in a fume hood under dry conditions.

Nonsonicated controls were produced by dicing PLLA fiber meshes to 10 × 10 mm² sections, and mixing them with HA and MCPM at the ratios as indicated above. The cement paste was mixed manually using a spatula and vortexed for 15 s.

Compositional analysis of the cements

The different crystalline calcium phosphate phases were analyzed using X-ray diffraction analysis (XRD). The samples were prepared by manual milling in an agate mortar (Agar Scientific Ltd, Stansted, UK). The resulting powders were spread in a cylindrical PMMA sample holder. Samples containing <1 g total mass were processed by adding acetone to the powder mass to form a slurry and spread directly in the sample holders. All XRD measurements were either performed on a X'Pert Pro MPD (Panalytical, Almelo, The Netherlands) or on a Bruker D8 ADVANCE (Bruker Corporation, Billerica MA) diffractometer. Ni-filtered CuK_2 X-ray source was used and spectra were acquired between 4.01° and 59.99° with a step size of 0.016°. The peaks were semiquantitatively analyzed by Rietveld refinement using BGMN software (http://profex.doebelin.org). Crystalline models of the BGMN database were used.

Mechanical characterization of the cements

Static compressive strength was determined on a Zwick 1474 universal testing machine (Zwick GmbH, Ulm, Germany) using cylindrical samples of 5 mm diameter and 7 mm height. Fracture was determined to be at the point of maximum compressive force.

Fracture plane analysis

All fracture planes of the samples were coated with gold using a sputter coater SCD 050 (Baltec, Pfäffikon, Switzerland) prior to SEM analysis using a Zeiss MA 26, (Zeiss AG, Oberkochen, Germany). The fiber distribution in the composite materials was analyzed by acquiring 10 micrographs at 2000-fold magnification in random areas on one sample of each group. The micrographs were analyzed using the Fiji distribution of the imageJ software, Version 1.50i (National Institute of Health, Bethesda). The fibers were marked at the exit points from the cement and counted manually on each image using the cell-counting package of imageJ. In addition, the protocol for Voronoi/Delaunay analysis was adapted from Bertoncelj et al.[24] for use on a rough surface. Briefly, the Voronoi surface around each fiber is the area that is closer to that fiber than to any other fiber. It was iteratively measured using the imageJ plugin. The values used for analysis were the following. (a) Average number of fibers over all images $\bar{x}(f)$ was used as measure to differentiate between the dispersity between NFs- and MFs. (b) Standard deviation of number of fibers $\sigma(f)$ was used to measure the variation between the number of fibers within the images. (c) Coefficient of variation of fibers $\gamma(f)$ is the standard deviation of the fiber number divided by average number of fibers. (d) Voronoi surface area v is the area containing all points closer to one fiber than to any another. (e) Area homogeneity coefficient $\gamma(v)$ is the average coefficient of variation for the Voronoi surface areas. (f) Standard deviation of the area homogeneity coefficient $\sigma(\gamma(v))$, which indicates how homogeneous the composite is overall between the images.
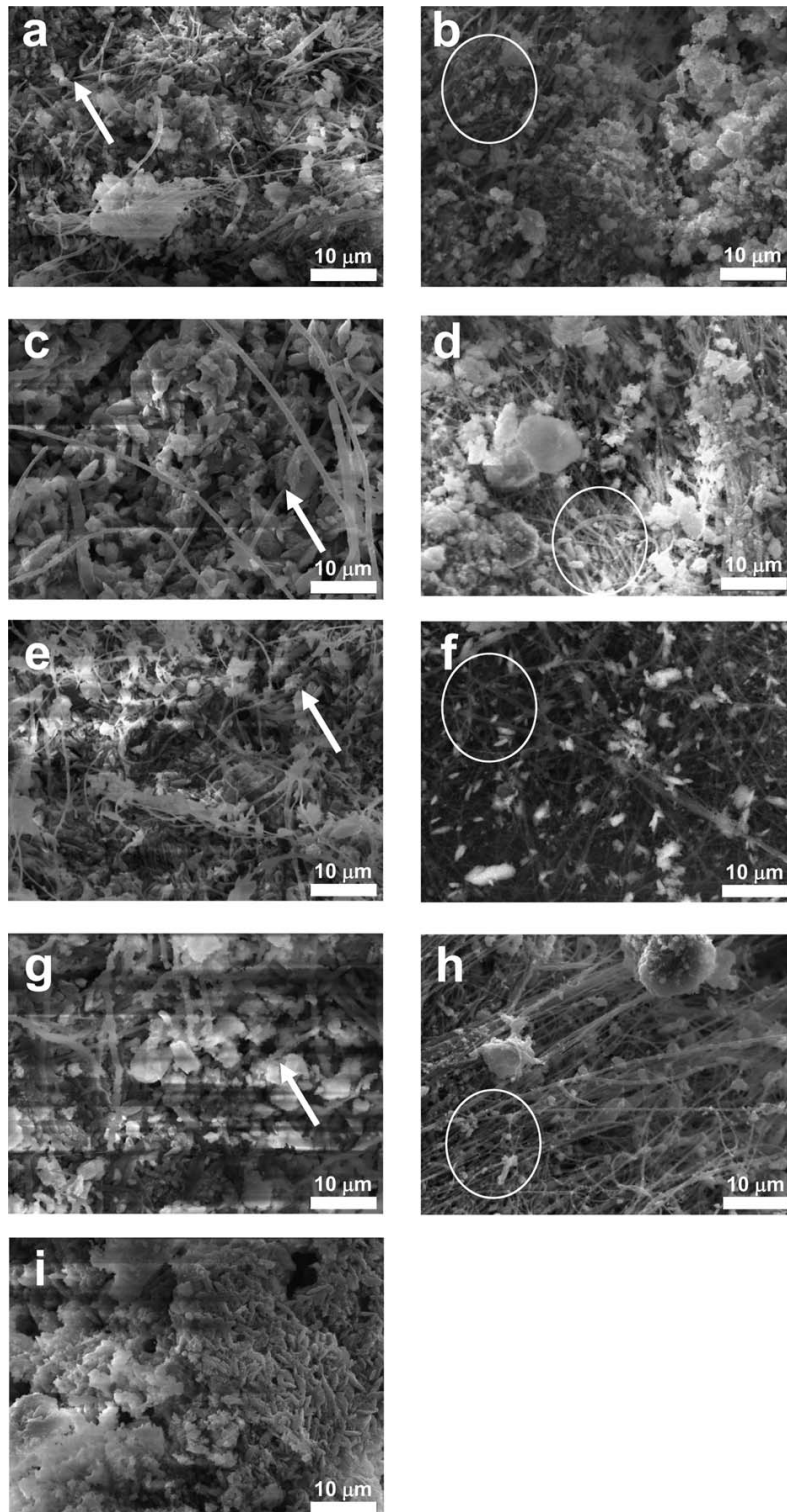
FIGURE 4. SEM micrographs of PLLA fiber reinforced cements with (a) 5% v/v NF, (c) 5% v/v MF, (e) 30% v/v NF, (g) 30% v/v MF content, visible as single fibers exiting the cement at the fracture area (white arrows as highlighted examples) and (i) no fiber content. The respective negative controls (b), (d), (f), (h) containing nonsonicated cut electrospun mats which are visible as fiber bundles exiting the fracture area (white ovals as highlighted examples).

46
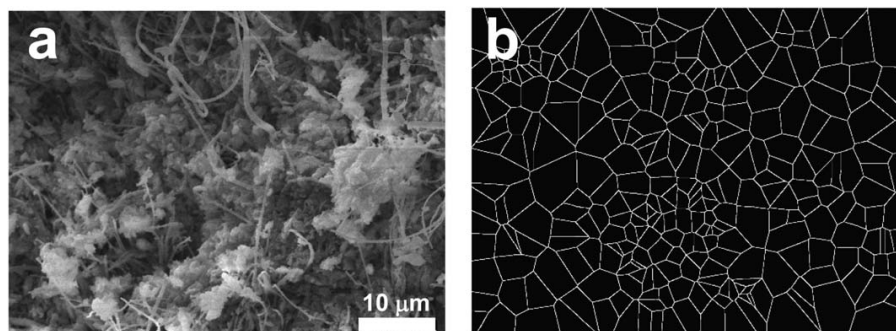
FIGURE 5. Fracture area micrograph of composite with 5%v/v nanofibers (a) and its corresponding Voronoi diagram (b).

Statistical analysis

The statistical analysis was conducted using one- or two-way analysis of variance where appropriate. Sample sizes and repetitions are indicated in the methods section of the respective experiment. The analysis was performed using Origin 8.1 software. p values <0.05 considered as significant.

RESULTS AND DISCUSSION
Fiber manufacturing

The acid-containing polymer solutions were spun for 5 h on a high-speed rotating collector. The NF exhibited a smooth surface morphology. Very little bead formation was observed in the mesh [Fig. 1(a,b)]. The MF [Fig. 1(c,d)] on the other hand, exhibited a slightly rougher surface. This wrinkling along the fiber axis is due to the interaction of the fiber jet with humidity from the environment[25] which in the current case was observed to be between 45 and 60%. The average diameter of the obtained PLLA fibers was determined based on SEM micrographs and was found to be 0.24 ± 0.08 μm for the NF and 1.0 ± 0.2 μm for the MF. These fibers were postprocessed to be used in the composites.
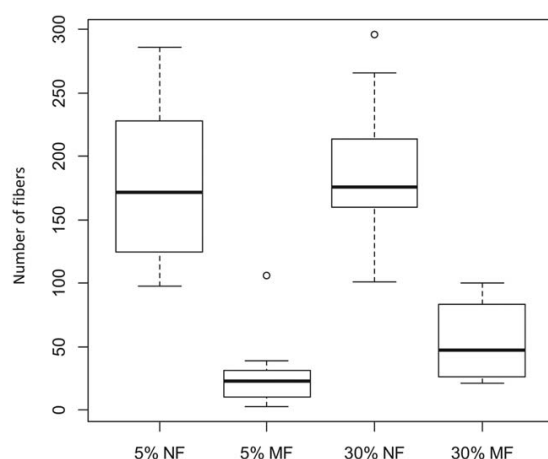
FIGURE 6. Average number of fibers per image on the fracture area of the sonicated composites. Notable is the similar high number in the nanofiber composites.

Composite processing

The powder phases containing the cement and the fiber phase were mixed with the liquid phase to create a cement. It was observed that when being poured into 1.5 mm diameter forms, the moldability was in the following order: pristine cement >5% sonicated >30% sonicated >5% nonsonicated >30% nonsonicated whereas NF or MF containing fraction did not matter. It was noted that the liquid to powder ratio had to be increased for complete wetting from the initial 4:9 (w/w) for pristine cements to 4:8 (w/w) for 5% fiber and 4:7 (w/w) for 30% fiber content. This change in moldability is due to fiber agglomeration during the mixing process of samples with high fiber contents and is in agreement with the observation by Martinie et al.[26] Agglomeration was also observed by Xu et al.[6] during HA reinforcement with a fiber volume fraction of 9.5% v/v. Regardless of fiber distribution, it is necessary to take the fiber content into account when adding the aqueous phase.

Composition analysis of the cements

The reactivity, defined as residual amounts of HA and MCPM, of the cement decreased with increased fiber content as measured with XRD. An example of the refinement is shown in the Supporting Information in Figure S1. There is trend that the fraction of unreacted HA and MCPM increased with fiber content and sonication (Fig. 2). No significant difference in the reactivity in between the MF group was observed. Furthermore, it was observed that a notable amount of MCPM was present in the samples containing 30% of NF, and in samples with increased water content. Thus, it can be hypothesized that reactivity of the MCPM is reduced in the surrounding of the fibers. Due to the significantly larger surface area of the NF composites (a calculated 16× surface increase compared to the microphase) the effect is more pronounced in composites containing NF.

XRD analysis of the products dicalcium phosphate dihydrate (brushite) and dicalcium phosphate anhydrous (monetite) revealed a lower content of brushite in the cements containing sonicated fibers when compared to pristine cements. The nonsonicated composites however contained increasing contents of brushite with increased fiber content. Again, it can be hypothesized that the presence of fibers

TABLE I. Average Number of Fibers as Determined Manually from the SEM Micrographs[a]

	5% NF	5% MF	30% NF	30% MF
Average number of fibers per image $\bar{x}(f)$	180	25	190	55
Standard deviation $\pm \sigma(f)$	60	28	54	30
Coefficient of variation $\gamma(f)$	0.3	1.1	0.3	0.6
Voronoi surface area (μm^2) $\bar{x}(v) \pm \sigma(v)$	16 ± 6	440 ± 740	14 ± 5	66 ± 36
Area homogeneity coefficient $\gamma(v) \pm \sigma(\gamma(v))$	1.0 ± 0.3	0.7 ± 0.4	0.8 ± 0.1	0.7 ± 0.2

[a]Voronoi surface areas as measured by software and calculated values as derived from section "Fracture plane analysis."

inhibits the uptake of water by influencing the cement reaction toward monetite formation. The increased content of both monetite and brushite correlated with an increase in strength, while an increase in HA content led to a decrease in strength in the FRCs.

Mechanical characterization of the composites

All composites were tougher than the corresponding pristine cements. While pure HA has been observed to have a significantly higher compressive strength of up to 70 MPa compared to brushite or monetite, (up to 10 MPa),[3] the mixture of both phases resulted in a significantly lower compressive strength of <2 MPa for the pristine cements. The increase in composite strength can therefore be attributed to the presence of the reacted components rather than to the amount of HA present.

Analysis of the mechanical properties resulted in an increase in compressive strength of the FRC as compared to the pristine cement or the nonsonicated counterparts (Fig. 3). The results of the sonicated composites were significant regarding to both fiber content and fiber diameter. Especially notable was the 5% v/v NF cement achieved the highest (eightfold) reinforcement of all groups as compared to the pristine cement. This is in accordance with the results reported by Pirhonen,[5] who observed a peak in flexural strength at approximately 7.5% polyglactin fiber content in a HA composite. Our results show that already 5% of fibers (v/v) is sufficient to achieve a measurable increase in compressive strength in the cement (for both NF and MF). Increasing the fiber content to 30% did not yield an increased strength of the composite as compared to the 5% content, and in the case of the nonsonicated controls and MF, plastic deformation was observed. We assume that the fragments of the mats present within these composites greatly influenced the compressive modulus of the composite. Therefore, the influence of the fiber phase on the compressive modulus is dominant at 30% volume content.

Fracture analysis

Analysis of the fracture areas [Fig. 4(a–h)] showed a significant amount of unclad fibers dangling from the fracture area. It can therefore be concluded that the primary mechanism of composite fracture is mainly by fiber pull-out, which is to be expected since PLLA fibers are more hydrophobic (water contact angle of 70°[27]) as compared to the more hydrophilic CaP matrix. Analysis of the fiber distribution on the fracture area (see Fig. 5 and Table I) showed that the average number of nonaggregated fibers per image

was significantly higher in the 5 and 30% NF composites (180 ± 60, 190 ± 54) as compared to the number of fibers on the fracture areas of 5 and 30% MF composites, (25 ± 28, 55 ± 30). The variation in number of fibers between the images of the same group divided by the average fiber number (coefficient of variation) was significantly lower in the NF composites (0.3, 0.3), as compared to the MF composites (1.1, 0.6). The results were significant regarding fiber diameter but not regarding the fiber content. Additional analysis showed that no significant differences were observed between the 5 and 30% NF groups while the difference between the 5 and 30% MF was significant. Due to the manual processing of the composites, it is possible that they were not completely homogeneous. It can be assumed that the fracture areas analyzed were areas with lowest reinforcement, containing the lowest number of fibers. Furthermore, due to the low number of samples analyzed for their fracture areas, it is possible that the 30 NF sample contained a low amount of fibers at the fracture site. The Voronoi areas were similar in the NF group (16 ± 6, 14 ± 5), and significantly different within the MF group (440 ± 740, 66 ± 36). It can be assumed from the lower variation of the 30% NF/MF group compared to the 5% NF/MF that at lower fiber concentrations, the effect of clustered fibers is more pronounced. The nonsonicated cements showed a strong inhomogeneity, that is, areas with only fibers and areas with only cements, and were therefor excluded from evaluation. It can be thus concluded that a more homogeneous distribution of the fibers can be achieved when using fibers with a smaller diameter, allowing a better intermixing of the components and thus a superior reinforcement. For microfiber composites, the sonicated materials were comparable to the nonsonicated controls, indicating that while the introduction of fibers increases the compressive strength of the composites, the fiber dispersity of NF is the dominating factor contributing to the compressive strength of the composite.

CONCLUSION

Absorbable fiber reinforced calcium phosphate based cements were produced via electrospinning, subsequent sonication followed by cement reaction. We found that the highest impact of fiber volume content on the mechanical and structural properties of the fiber reinforced cement was obtained for the 5% v/v fiber fraction. Regardless of fiber content the NF enabled a higher fracture strength as compared to the MF. An inhibition of water uptake to form brushite was observed when fibers were added to the

cement mixture. The sonicated NF samples had a higher compressive strength when compared to their nonsonicated counterparts, while the sonicated MF samples had a similar compressive strength when compared to their nonsonicated counterparts. This was independent of crystalline and water content and indicates that indeed the fiber distribution has a large influence on the fracture strength of the composites. Additionally, at high fiber content of 30% (w/w), the composite fracture strength was reduced, but still significantly higher than the pristine cement. The analysis of the fracture area revealed the most homogenous fiber distribution for the 5% sonicated NF. We have thus demonstrated that a good dispersion of NF enhances the fractural strength of calcium phosphate based cements.

REFERENCES

1. Döbelin N, Luginbühl R, Bohner M. Synthetic calcium phosphate ceramics for treatment of bone fractures. Chimia 2010;64:723–729.
2. Legeros RZ. Biodegradation and bioresorption of calcium phosphate ceramics. Clin Mater 1993;14:65–88.
3. Charrière E, Terrazzoni S, Pittet C, Mordasini P, Dutoit M, Lemaître J, Zysset P. Mechanical characterization of brushite and hydroxyapatite cements. Biomaterials 2001;22:2937–2945.
4. Beaudoin JJ. Handbook of Fiber-Reinforced Concrete. In: Ramachandran VS, editor. Building Materials Science Series Ottawa: National Research Council of Canada/Noyes Publications; 1990. p 332.
5. Pirhonen E. Fibres and Composites for Potential Biomaterials Applications. Tampere: Institute of Biomaterials, Tampere University of Technology; 2006. p 80.
6. Xu HHK, Eichmiller FC, Giuseppetti AA. Reinforcement of a self-setting calcium phosphate cement with different fibers. J Biomed Mater Res 2000;52:107–114.
7. Von Gonten AS, Kelly JR, Antonucci JM. Load-bearing behavior of a simulated craniofacial structure fabricated from a hydroxyapatite cement and bioresorbable fiber-mesh. J Mater Sci 2000;11:95–100.
8. Proctor BA. A review of the theory of GRC. Cem Concr Compos 1990;12:53–61.
9. Zollo RF. Fiber-reinforced concrete: An overview after 30 years of development. Cem Concr Compos 1997;19:107–122.
10. Yan H, Liu L, Zhang Z. Continually fabricating staple yarns with aligned electrospun polyacrylonitrile nanofibers. Mater Lett 2011; 65:2419–2421.
11. Peng J, Qian Z, Wang B, Fu S, Guo G, Luo F, Li R, Wu D. Preparation and release characteristic of quercetin loaded poly(lactic acid) ultrafine fibers. J Nanosci Nanotechnol 2011;11:3659–3668.
12. Yao L, Lee C, Kim J. Fabrication of electrospun meta-aramid nanofibers in different solvent systems. Fibers Polym 2010;11: 1032–1040.
13. Greiner A, Wendorff JH. Electrospinning: A fascinating method for the preparation of ultrathin fibers. Angew Chem Int Ed 2007; 46:5670–5703.
14. Simonet M, Schneider OD, Neuenschwander P, Stark WJ. Ultra-porous 3D polymer meshes by low-temperature electrospinning: Use of ice crystals as a removable void template. Polym Eng Sci 2007;47:2020–2026.
15. Yang J-C, Lee S-Y, Tseng W-C, Shu Y-C, Lu J-C, Shie H-S, Chen C-C. Formation of highly aligned, single-layered, hollow fibrous assemblies and the fabrication of large pieces of PLLA membranes. Macromol Mater Eng 2012;297:115–122.
16. Zuo Y, Yang F, Wolke JGC, Li Y, Jansen JA. Incorporation of biodegradable electrospun fibers into calcium phosphate cement for bone regeneration. Acta Biomater 2010;6:1238–1247.
17. Fathona IW, Yabuki A. One-step fabrication of short electrospun fibers using an electric spark. J Mater Process Technol 2013;213: 1894–1899.
18. Greenfeld I, Zussman E. Polymer entanglement loss in extensional flow: Evidence from electrospun short nanofibers. J Polym Sci Part B 2013;51:1377–1391.
19. Nunes RW, Martin JR, Johnson JF. Influence of molecular weight and molecular weight distribution on mechanical properties of polymers. Polym Eng Sci 1982;22:205–228.
20. Mulky E, Yazgan G, Maniura-Weber K, Luginbuehl R, Fortunato G, Bühlmann-Popa A-M. Fabrication of biopolymer-based staple electrospun fibres for nanocomposite applications by particle-assisted low temperature ultrasonication. Mater Sci Eng C 2014; 45:277–286.
21. Theiss F, Apelt D, Brand B, Kutter A, Zlinszky K, Bohner M, Matter S, Frei C, Auer JA, von Rechenberg B. Biocompatibility and resorption of a brushite calcium phosphate cement. Biomaterials 2005;26:4383–4394.
22. Desai TR, Sarit B, Bhaduri, Tas AC. A self-setting, monetite (CaHPO$_4$) cement for skeletal repair. In: Advances in Bioceramics and Biocomposites II—30th International Conference on Advanced Ceramics and Composites. Cocoa Beach, FL: Wiley; 2006.
23. Bohner M, Lemaitre J, Ring TA. Effects of sulfate, pyrophosphate, and citrate ions on the physicochemical properties of cements made of β-tricalcium phosphate-phosphoric acid-water mixtures. J Am Ceram Soc 1996;79:1427–1434.
24. Bertoncelj B, Vojisavljevic K, Rihtarsic J, Trefalt G, Huskic M, Zagar E, Malic B. A Voronoi-diagram analysis of the microstructures in bulk-molding compounds and its correlation with the mechanical properties. Express Polym Lett 2016;10:493–505.
25. Yazgan G, Dmitriev RI, Tyagi V, Jenkins J, Rotaru G-M, Rottmar M, Rossi RM, Toncelli C, Papkovsky DB, Maniura-Weber K, Fortunato G. Steering surface topographies of electrospun fibers: understanding the mechanisms. Sci Rep 2017;7:158.
26. Martinie L, Rossi P, Roussel N. Rheology of fiber reinforced cementitious materials: Classification and prediction. Cem Concr Res 2010;40:226–234.
27. Thanki PN, Dellacherie E, Six J-L. Surface characteristics of PLA and PLGA films. Appl Surf Sci 2006;253:2758–2764.

49

6 Fiber Surface Modification

6.1 Context

The fracture mechanism by which a composite fails under stress can give an indication on the limits of the possible reinforcement. In the case of PLA-reinforced CPC it was shown in the previous manuscript that the CPC failure mechanism was by fiber pull-out, giving an indication that the strength of the interface between the fibrous and the matrix phase was weaker than the strength of the fiber. Furthermore, it was observed that the fibers had low to no CaP residual visible on the surface of the fiber which could be a further indication of a weak interfacial bonding. This weak interfacial bonding stems from the mismatch in surface energy between the fibrous and the matrix phase, and a typical method used to increase this interfacial bonding is to reduce the water contact angle, using techniques such as plasma activation or coatings, such as in the works of Bolbasov and Canal and co-workers [78, 79].

Functional groups allow for a stronger, and more specific adhesion of desired species such as what is shown in the works by Guex and Guimond and co-workers [74, 80]. In the case of CaP, it has shown that chelating amino acids play a biological role in the nucleation and growth of CaP on surfaces as shown by Davis and co-workers [81]. From these findings it was therefore the goal of this manuscript to engineer such a selective functionalization on the surface of the fiber and perform a systematic comparison with other contact angle reducing techniques regarding the adsorption of divalent species such as Calcium and its effect on the mechanical strength of the interfacial bond. Furthermore, the role of the surface roughness was quantified to assess its influence on the mechanical strength and take into account its interfering effect.

The results indicated that the divalent species were indeed adsorbed to the functionalized surfaces and had a higher retention after washing compared to the surfaces with reduced water contact angle alone. Furthermore, it was shown that while the interfacial bond strength remained the same, the stiffness of the functionalized interfacial bond was higher compared to the controls or wetting alone, presumably due to the polycrystalline, porous nature of the CaP. These findings show the potential of functionalized coatings to tailor the adhesion of CaP to polymeric surfaces and opens the possibility for novel reinforced biomedical composites

with modified interfaces.

6.2   Contribution of the author

Experimental design and protocol were devised in a collaborative effort by EM, GF, Dirk Hegemann (DH), Jorge Sague (JS) and Roman Heuberger (RH). Manufacturing experiments and wet chemical post processing and analysis were also performed by EM. The following experiment were performed by other subject matter experts/team members: Plasma coating (DH), XPS (RH), white light interferometry (RH) and mechanical testing was performed collaboratively, see also the acknowledgements section. Surface analysis and quantification was performed collaboratively between EM and RH. Statistical analysis was performed by EM. The manuscript writing was performed collaboratively by EM, DH, JS, RH and MF. All figures except Fig 2a-f (RH) were prepared by EM.

6.3 Grafting of calcium chelating functionalities onto PLA monofilament fiber surfaces

Grafting of calcium chelating functionalities onto PLA monofilament fiber surfaces

Elias Mulky (iD), Giuseppino Fortunato (iD), Dirk Hegemann (iD), Jorge Sague, Roman Heuberger (iD), and Martin Frenz (iD)

View Online   Export Citation   CrossMark

ARTICLES YOU MAY BE INTERESTED IN

Formation and characteristics of mixed lipid/polymer membranes on a crystalline surface-layer protein lattice
Biointerphases **15**, 011002 (2020); https://doi.org/10.1116/1.5132390

Polystyrene-block-polyethylene oxide thin films: In vitro cytocompatibility and protein adsorption testing
Biointerphases **15**, 011003 (2020); https://doi.org/10.1116/1.5135062

Rapid detection of urokinase plasminogen activator using flexible paper-based graphene-gold platform
Biointerphases **15**, 011004 (2020); https://doi.org/10.1116/1.5128889

AVS 67th INTERNATIONAL SYMPOSIUM & EXHIBITION
OCTOBER 25-30, 2020
Colorado Convention Center · Denver, Colorado, USA
www.avs.org

15, 011006

Grafting of calcium chelating functionalities onto PLA monofilament fiber surfaces

Elias Mulky,[1] (ID) Giuseppino Fortunato,[2] (ID) Dirk Hegemann,[2] (ID) Jorge Sague,[1] Roman Heuberger,[1,a] (ID)
and Martin Frenz[3,a] (ID)

AFFILIATIONS

[1]RMS Foundation, Bischmattstrasse 12, Bettlach 2544, Switzerland
[2]Empa, Swiss Federal Laboratories for Materials Science and Technology, Lerchenfeldstrasse 5, 9014 St Gallen, Switzerland
[3]Institute of Applied Physics, University of Bern, Sidlerstrasse 5, 3012 Bern, Switzerland

[a]**Authors to whom correspondence should be addressed:** roman.heuberger@rms-foundation.ch and frenz@iap.unibe.ch

ABSTRACT

Polymer surface grafting is widely used in the field of bone regeneration to increase calcium phosphate (CaP) adhesion, with the intent of improving mechanical properties of CaP-polymer composite cements. Reinforcement can be achieved using multiple combined functional groups and/or complex surface geometries that, however, concurrently influence multiple effects such as wetting, roughness, and interfacial strengthening. This study focused on the influence of a chelating group, namely aspartic acid, on the adsorption of divalent ions such as Ba^{2+} or Ca^{2+} onto poly-L-lactic acid (PLA) films. The films were analyzed using contact angle measurements and X-ray photoelectron spectroscopy. The adsorption of CaP and its interfacial mechanical properties were investigated using functionalized PLA monofilaments whose surface roughness was analyzed using white light interferometry. Mechanical analysis was conducted by performing pull-out tests. The surfaces were analyzed using scanning electron microscopy and energy dispersive X-ray spectroscopy. Using aspartic acid as a chelating group resulted in a 50 % increased adsorption of barium, an almost threefold increase in calcium coverage of the fiber compared to the control group and a twofold increase in interfacial stiffness. No significant increase in interfacial strength was determined, most likely due to the weakness of the CaP matrix, which was partially visible as residues on the monofilaments in the postfracture imaging. This study shows the potential of surfaces functionalized with aspartic acid as a simple alternative to complex polypeptide based functional groups for the adsorption of divalent ions such as calcium on poly-lactic acid in bone regenerating applications.

I. INTRODUCTION

In the field of bone regeneration, calcium phosphate (CaP) based cements are widely used due to their excellent biocompatibility and tunable characteristics such as geometry, strength, porosity, setting time, and time to total absorption. However, these CaP cements are generally brittle and of low mechanical strength due to the porous, disoriented polycrystalline nature of the set cement.[1] Reinforcing these cements with polymer filaments can increase fracture strength and reduce the cement brittleness due to the combination of high polymer toughness with the rigidity of the cement phase.[2] To allow for efficient stress transfer, a strong bond between the polymeric filament and the matrix interface is needed to avoid structural rigidity.[3] In fact, an important mechanism contributing to the mechanical strength of bone is the presence of strong hydrogen bonds between the fibrous collagen phase and single crystalline hydroxyapatite (HA) platelets.[4] Of particular interest for biodegradable cements are tough biodegradable polymers based on polyglycolic acid (PGA) or polylactic acid (PLA) with high tensile strengths in the order of 70 MPa and stiffness around 2 GPa. For slow degrading cements and cements reacted using aqueous solutions, PLA is more suitable as a reinforcing agent compared to PGA. This is based on the slower degradation rate of PLA in aqueous media, meaning that the fibers can hold the mechanical integrity of the cement for a longer time. This stems from the higher hydrophobicity of PLA (static water contact angle of 70° up to 120° in electrospun nonwovens) compared to PGA (water contact angle of 40°–60°).[5,6] However, the hydrophobic nature of PLA results in a poor interfacial bond with the hydrophilic CaP cement.[7] To increase the adhesion strength between the CaP cement and PLA filaments, a suitable interlayer has to be introduced between the two phases.

Many methods exist to manufacture the interlayer, such as dip and spin coating, plasma deposition, and wet chemical methods. The latter two are of particular interest since they modify the polymer surface chemically resulting in durable interfaces. In particular, plasma deposition can be performed as a continuous reel-to-reel process as demonstrated by Leal and co-workers with plasma activated continuous polyethylene filaments.[8]

This interlayer can either be engineered to match the surface energy of the CaP more closely, i.e., to increase the hydrophilicity of the PLA, or to specifically adsorb a component of the CaP cement. The first approach, namely, increasing the hydrophilicity of the PLA, can be achieved by depositing different hydrophilic groups onto the surface. For this purpose, the plasma deposition technique is widely used.[9] Such studies were performed by Canal and co-workers[10] who subjected chopped multifilamentous PLA to O_2 plasma and mixed it with CaP to form a PLA–CaP cement. The plasma treatment resulted in an increase in both surface roughness and hydrophilicity of the treated PLA (static water contact angle of 62°). The interfacial strength was indirectly measured by conducting mechanical tests on the treated cements indicating an increase in the work of fracture of the cements containing the treated multifilaments, while the flexural strength remained similar to the pristine cement. This was attributed to the increased contact surface between the CaP and the PLA due to the increased hydrophilicity. Despite the increase in surface roughness resulting from the plasma treatment, the effect was insignificant with regard to the mechanical properties of the interface. Another study was conducted by Maenz and co-workers[11] who subjected polyglycolic-co-lactic acid (PGLA) multifilaments to O_2 plasma, followed by embedding them into CaP cement and measuring the interfacial shear strength using pull-out tests on these samples. This study also showed an increase in polymer hydrophilicity (water contact angle of 5°). Furthermore, a twofold increase in the interfacial shear strength of the treated filaments was measured. The increase was attributed to a combination of effects, namely, an increase in surface roughness of the multifilaments, increased wetting of the multifilaments with the cement, and the formation of chemical bonds between the calcium phosphates and the fibers.

The second mentioned approach, namely, the specific adsorption of a CaP component to the fiber surface, can be achieved by grafting an interlayer of specific cation attracting chelate groups onto the polymer surface. These groups can form a complex with divalent ions such as calcium (Ca^{2+}), which are highly available in a CaP cement precursor solution. The formation of such complexes then results in an increased nucleation and growth of CaP on surfaces containing such groups. In fact, in a study performed by Rautaray and co-workers,[12] an increase in growth of CaP was observed on surfaces containing gold nanoparticles functionalized with aspartic acid (ASP) terminal groups. This growth effect is also attributed to chelating groups such as ASP, naturally present among others on silk fibroin in a study by Kong and co-workers[13] and Schroeder and co-workers.[14] The effects of these groups on the mechanical properties of CaP were reported by Ou and co-workers.[15] They observed a twofold increase in compressive strength in CaP cement treated with silk fibroin solution, compared to untreated samples. This wet chemical approach is more specific regarding the deposited groups compared to plasma deposition. Also, surface roughening can often be reduced or avoided by choosing a suitable reaction.

The aim of this study was to demonstrate the grafting of ASP onto the surface of polymeric fibers, namely, PLA monofilaments to strengthen the PLA–CaP interface and analyze the effect of the treatment on both the adsorption of divalent ions and the mechanical properties of the PLA–CaP cement interface.

II. EXPERIMENTAL SETUP AND METHODOLOGY

PLA (Biomer L9000, Mm: 200 000 kDa) was obtained from Biomer Biopolyesters (Krailing, Germany) in a bead form. A spool with a PLA monofilament with a diameter of 0.8 mm was kindly provided by Perlon Nextrusion AG (Bobingen Germany). The gases used for the plasma processes, i.e., argon, ethylene, and carbon dioxide, were of 99 % purity and obtained from Carbagas (Gümligen, Switzerland). De-ionized water for the water vapor process was obtained from in-house supplies (18 MΩ, Merck KGaA, Darmstadt, Germany). The consumables used in the wet chemistry process, i.e., aspartic acid, barium chloride dihydrate, disodium dihydrogen pyrophosphate, 1-ethyl–3-(3-dimethylaminopropyl) carbodiimide hydrochloride (EDC), ethylenediaminetetraacetic acid (EDTA), hexamethylene diamine (HMD), N-hydroxysuccinimide (NHS), nitrilotriacetic acid (NTA), and sodium hydroxide, were obtained from Merck KGaA (Darmstadt, Germany). HA nanoparticles were purchased from M K Impex Corp (Mississauga, Canada). Monocalcium phosphate monohydrate (Regent 12xx) was purchased from Innophos Inc. (Cranbury, USA). 2-(N-morpholino)-ethane sulphonic acid (MES) was obtained from Carl Roth GmbH + Co. KG (Karlsruhe, Germany). All solvents were obtained from commercial providers in ACS quality and were used without further purification.

A. Sample manufacturing

The polymer sample manufacturing consisted of different steps that are outlined schematically in Fig. 1.

1. Polymer sample preparation

To manufacture flat PLA films used for X-ray photoelectron spectroscopy (XPS) characterization tests [Fig. 1(a)], PLA beads were placed in a square steel frame of 1 mm thickness and an inner diameter of 100 mm, which was covered from both sides with 0.2 mm thick aluminum foil. The form was then heated to 190 °C for 20 min, followed by an additional 20 min of cooling. The processed PLA films were then removed and placed in an aluminum foil for storage. The PLA monofilaments were cut into lengths of 80 mm using a surgical blade.

2. Plasma treatment

Both the flat PLA films and the PLA monofilaments [Fig. 1(b)] were coated using a low-pressure radio frequency (RF, 13.56 MHz) plasma reactor consisting of two plane-parallel electrodes separated by a glass ring (30 cm in diameter, 5 cm in height). To establish a sufficiently high number of functional groups on the surface, protocols from Guex and co-workers[16] and Guimond and co-workers[17] were adapted for the current work and are described in the supplementary materials. The protocols were chosen such that minimal fiber degradation occurred. The finally selected protocol was as follows: RF power input of 60 W; pressure of 0.1 mbar; process
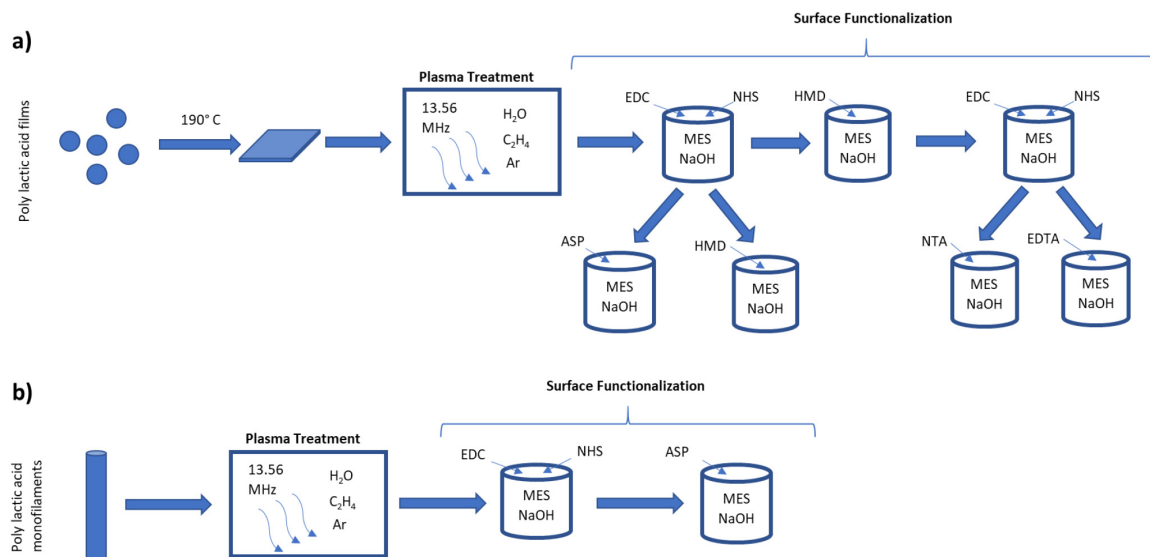
FIG. 1. Schematic of the functionalization treatment of (a) the PLA films and (b) the PLA monofilaments. The wet chemistry components, namely, the sodium hydroxide buffered 2-(N-morpholino)ethanesulfonic acid solution (MES NaOH), as well as the reactants aspartic acid (ASP), 1-ethyl-3-(3-dimethylaminopropyl)carbodiimide (EDC), eEDTA, hexamethylenediamine (HMD), N-hydroxysuccinimide (NHS), and nitrilotriacetic acid (NTA), are shown.

duration of 5 min; and a gas mixture of 36 SCCM H_2O vapor, 6 SCCM C_2H_4, and 50 SCCM Ar. The latter was added to enhance crosslinking and stability of the deposited plasma polymer film.

After plasma treatment, the samples were placed in polyethylene bags filled with argon for transfer to further processing.

3. Surface functionalization

Following the plasma treatment, the prefunctionalized surfaces reacted with aspartic acid by carbodiimide chemistry using a protocol adapted from Edlund and co-workers.[18] Each sample was placed in an individual well of a 24-well plate and immersed in 0.1M MES–NaOH buffer of pH 6 for 30 min (reaction 1). Following that, two solutions, 0.2M of EDC and 0.5M NHS, were dissolved in the MES buffer (Carl Roth GmbH + Co. KG, Karlsruhe, Germany) added sequentially to the reaction and left to react under gentle shaking for 1 h (reaction 2). Afterward, the samples were washed and immersed in an MES buffer of pH 7 and added to a solution of 0.05M of either HMD or aspartic acid (reaction 3). A subset of samples reacted with HMD was subjected again to reactions 1 and 2 and subsequently to a 0.05M solution of NTA or EDTA. The samples were left to react for 2 h, and then removed, washed with de-ionized water, and dried under ambient conditions.

4. Cement matrix engineering

To manufacture the cement samples for the pull-out tests, an aqueous solution containing 0.06M disodium dihydrogen pyrophosphate (Sigma-Aldrich, Switzerland) was prepared with ultrapure water. This solution was mixed with β-tricalcium phosphate and monocalcium phosphate monohydrate powder (16:13 w:w ratio) at a ratio of 3:2 powder to liquid (w:w). The resulting slurry was mixed for 2 min with a spatula to obtain a cementous paste, which was transferred into cylindrical forms of 20 mm in diameter and 30 mm in height. Immediately after, a PLA monofilament was embedded at a depth of 10 mm at the center of the paste. To ensure that the monofilament remained at the defined height and alignment throughout the setting process, it was fixed with a metal clip on the sample form. The resulting samples were left to set and cure for 3 days.

B. Characterization

1. Surface functionalization

The chemical surface analysis was conducted by XPS. To quantify the chelation efficacy, a subgroup of each sample type was immersed in an aqueous 0.1M $BaCl_2$ solution for 1 h, subsequently rinsed with de-ionized water, and their barium content was quantified using XPS. Since calcium is highly abundant in the lab environment as a contaminant (e.g., supplementary material, Fig. 1),[23] a similar but less commonly used element (barium) was chosen to minimize the risk of false positive results during the specific adsorption measurements. XPS measurements were performed either on a PHI 5000 VersaProbe II instrument (Minnesota, USA) or on an Axis Nova (Kratos Analytical, Manchester, United Kingdom). Both instruments were equipped with a monochromatic AlKα X-ray source. Detailed scans of the binding energies

corresponding to C1s, O1s, N1s, and Ba3d were conducted. This was followed by survey scans to obtain an elemental overview and to quantify possible contaminations (example shown in the supplementary material, Figs. 1–7).[23] Spectra were analyzed using CasaXPS software (Version 2.3.18, Casa software Ltd, GB). An iterated Shirley background was subtracted from the signals. The peak fitting was performed using a Gauss/Lorentz line shape, with the FWHM being set to be equal to that of the most dominant component in each scan. Charge correction was applied using a value of 285.0 eV for the aliphatic C1s-peak.

2. Wettability

Hydrophilicity was quantified by measuring the static water contact angle with the sample surface on flat PLA films. To conduct the measurements, a contact angle meter SURFTENS-universal, OEG GmbH (Frankfurt, Germany) was used. The measurements were conducted as follows: de-ionized water was filled into a metered glass syringe, and a sessile water drop of $<10\,\mu l$ volume was deposited on the surface of the sample using a syringe with a flat tip metal needle. The needle was then retracted, and the angle was measured on both sides of the droplet using SURFTENS 4.3 software. Three areas of each of the treatment groups were measured. Samples having contact angles below 45° were considered as hydrophilic.

3. Surface roughness

Three PLA monofilaments from each group, i.e., control, plasma coating, and aspartic acid grafted samples, were analyzed for their surface roughness. Three randomly chosen areas of each sample were analyzed by white light interferometry using an S neox interferometer and confocal microscope (Sensofar, Barcelona, Spain). Prior to the measurement, the samples were blown with nitrogen to remove remaining particulate contaminants. The magnification was chosen to be $50\times$ and the analyzed surface was $0.67 \times 0.26\,mm$ along the monofilament. Three separate areas of each monofilament were analyzed. The data were analyzed using SensoMAP Premium (Version 7.4.8051, Digital Surf, France). From the topography, a polynomial function of the second degree corresponding to the cylindrical filament shape was derived and subtracted to allow a comparison with flat surfaces. The arithmetic mean roughness R_a and waviness parameters were determined on profiles extracted from the topographies. The ratio of the real surface, i.e., the surface encompassing the three-dimensional contour of the sample accounting for the roughness, to projected surface, i.e., the two-dimensional top-down area, was determined to quantify the influence of the surface contribution of the sample roughness. These parameters were determined following the ISO 4287 and 4288 standards.

4. Mechanical characterization of the interfacial strength

The effect of the treatments on the integrity of the monofilaments was determined by measuring the ultimate tensile strength of untreated and treated monofilaments without embedding them into the CaP cement.

The stiffness and strength of the calcium phosphate bonding with the functionalized monofilaments were measured by conducting pull-out tests on monofilaments embedded in CaP cement. The interfacial modulus, which estimates the stiffness of the interfacial bond between the matrix and the monofilaments, was calculated as the value of the slope of the load–displacement curve within the bonded zone. Maximum debonding load was defined as the first maximum in load observed within the debonding zone. The debonding zone was defined as the zone between the start and the end of the interfacial debonding of the monofilament from the cement matrix. This was determined in the load–displacement curve between the point where the value of the slope starts to decrease and the inflection point where the sliding/friction zone starts (schemes describing typical pull-out behaviors are shown in the supplementary material, Fig. 19).[23] This is adapted from the works of Zhan and Meschke[19] and Friedrich and Wang[20] who conducted numerical simulations of pull-out tests for applications in concrete.

The samples manufactured according to Sec. II A 4 were subjected to pull-out tests using a universal testing machine Zwicki-Line Z5.0 (Zwick GmbH & Co. KG, Ulm, Germany) with a preload of $5N$ and an embedding depth of $10\,mm$ determined from a series of preliminary tests with untreated fibers. In all cases during the preliminary tests, linear load–displacement behavior was observed down to a minimum of $8N$. Thus, $5N$, a typical value used within the lab, was kept as a preload value for the following experiments. A speed of $2.5\,mm/min$ was chosen. After the maximum debonding load was measured, the experiment was stopped when the pull-out load reached 10% of the maximum measured strength of each sample. The monofilament groups used were as follows: (1) untreated as control, (2) plasma coated using protocol 3 (water vapor) described in Sec. II A 2, and (3) plasma treated with protocol 3 (water vapor) followed by a functionalization with aspartic acid using the protocols described in Sec. II A 3. At least four replicates were measured for each group. To test for polymer degradation during the treatment, five monofilaments from each group were subjected to tensile testing.

5. Analysis of calcium adsorption on the filament surface after pull-out

a. Postfracture image analysis. After the pull-out experiment, the extracted monofilaments were analyzed for CaP cement residue by stereomicroscopy using a Leica M205A (Leica Microsystems AG, Wetzlar, Germany). Areas with residue on the surface were observed as being matt areas under the white light of the microscope when compared to the shiny areas with low or no CaP content. The filaments were placed on a SEM sample holder such that the areas with the highest CaP concentration were visible for analysis. The samples were coated with 5 nm of palladium, using a sputter coater SCD 050 (Baltec, Pfäffikon, Switzerland), and analyzed using SEM. The magnification was chosen to be $150\times$ at a working distance of $20\,mm$ to allow full width coverage of the imaged filament part. The following areas were selected for analysis: (1) the bottom (tip) of the monofilament, being the deepest embedded area and subjected to the longest period of pull-out; (2) the top (stem), least embedded area and subjected to the shortest

pull-out period; and (3) the center, containing the areas in between. At least four monofilaments of each group were analyzed.

b. Postfracture element analysis. The quantitative calcium content on different areas of the monofilaments was determined by analyzing the pulled-out samples with energy dispersive X-ray spectroscopy (EDX) using an Oxford instruments Xmax-N with the attached AzTec software version 3.3 (Oxford Instruments plc, Abingdon, United Kingdom). From the three locations determined in Sec. II A 4, at least four monofilaments of each sample were analyzed. The scan was done on an area of $750\,\mu m$ width x $560\,\mu m$ height corresponding to the observable diameter of the monofilament. A relative coverage of the area was then determined by image analysis. The images were then analyzed with Fiji bundle of imageJ version 1.52n. The relative coverage was determined by counting the green pixels present in the images, which correspond to the areas where Ca(II) was detected.

C. Statistical analysis

All values reported are averages with their standard deviations. The statistical analysis was conducted using either one- or two-way ANOVA where appropriate. Additionally, a pairwise t-test with Bonferroni correction was conducted to determine significant differences among the different groups. The analysis was performed using R software, version 3.3.2, Python matplotlib library version 3.1.1 and Excel 2016. Principal component analysis was performed with the Analyse-It plugin for Excel, version 5.40.2. Probability values for rejecting the null hypothesis (p) of <0.05 were considered as significant.

III. RESULTS

The functionalization and wettability analyses were conducted on PLA films with the following treatments: the untreated controls, water vapor plasma (Plasma), and the following functional groups functionalized to the polymer film surface using wet chemistry: ASP, HMD, NTA, and EDTA, while the surface roughness, mechanical, and postfracture analyses were conducted on PLA monofilaments with the following treatments: the untreated controls, Plasma, and ASP.

A. Surface functionalization

Analysis of different element concentrations showed that the adsorption of divalent barium from aqueous solution was the highest for ASP (6.4 ± 0.2 at. %), followed by control (4.2 ± 0.7 at. %) and EDTA (2.9 ± 0.4) (see Table I and supplementary material, Table 2).[23] For C1s, Plasma had the highest concentration of C, followed by control and EDTA (73.0 ± 0.6 at. %, 72.2 ± 0.4 at. %, and 64.0 ± 3.3 at. %) [Table I and supplementary material, Figs. 1–3, Table 2].[23] Analysis of the O1s spectrum (Table I and supplementary material, Figs. 4–6, Table 2)[23] showed that HMD and NTA contained the highest oxygen concentration (34.9 ± 0.3 at. % and 34.5 ± 1.2 at. %), followed by EDTA group (30.8 ± 2.5 at. %). Low concentrations of residual chloride (<1 at. %) stemming from the barium chloride salt as well as silicon (glassware), sulfur, and sodium (buffering solution) were measured in all samples.

B. Wettability

The lowest static water contact angle corresponding to the highest hydrophilicity was measured after treatment with EDTA ($32° \pm 10°$), and the highest value corresponding to the lowest hydrophilicity was measured for the control ($77° \pm 6°$).

C. Surface roughness

The quantitative analysis by interferometry (Fig. 2) measured along the length axis of the monofilament showed an R_a of 45 ± 5 nm for the control group, 134 ± 34 nm for the Plasma, and 93 ± 26 nm for the ASP in pull-out direction. Parallel grooves stemming from the monofilament manufacturing process were observed on all monofilaments. Perpendicular to the monofilament length axis, the R_a values were 74 ± 15 nm for the control, 210 ± 45 nm for the Plasma, and 84 ± 26 nm for the ASP. The ratios of real to projected surfaces were as follows: 1.005 ± 0.002 for control, 1.034 ± 0.013 for Plasma, and 1.008 ± 0.001 for ASP.

D. Mechanical characterization of the interfacial strength

The tensile tests showed that all the monofilaments had a tensile strength of 70 ± 3 MPa regardless of the treatment they received.

TABLE I. Overview of the different measurement results performed in this study.

| Sample | Concentration (at. %) | | | | Pull-out tests | | EDX measurements |
	Carbon	Oxygen	Barium	Contact angle	Max. debond. load (N)	Interfacial stiffness (N/mm)	Calcium surface coverage (%)
Control	72.2 ± 0.4	21.2 ± 0.8	4.2 ± 0.7	77° ± 6°	13 ± 4	12 ± 4	11 ± 9
Plasma	73.0 ± 0.6	23.1 ± 0.6	2.1 ± 0.5	71° ± 8°	12 ± 5	16 ± 10	17 ± 10
HMD	61.5 ± 1.3	34.9 ± 0.3	2.1 ± 1.0	42° ± 5°			
ASP	60.6 ± 1.6	30.4 ± 1.1	6.4 ± 0.2	42° ± 5°	17 ± 5	23 ± 7	29 ± 17
NTA	63.3 ± 1.0	34.5 ± 1.2	1.2 ± 0.1	36° ± 6°			
EDTA	64.0 ± 3.3	30.8 ± 2.5	2.9 ± 0.4	32° ± 10°			
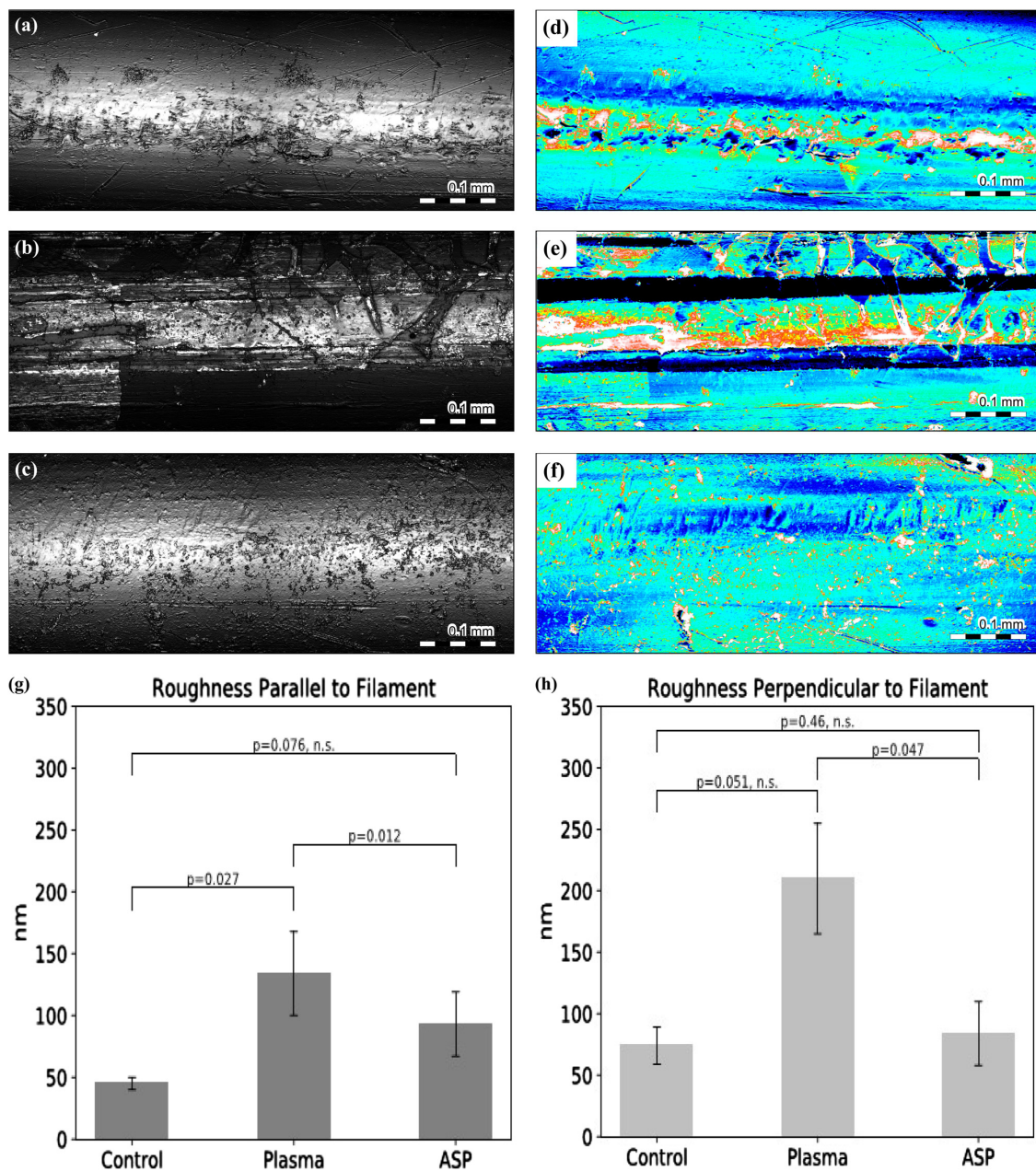
FIG. 2. Optical image at 50× magnification of the monofilaments (a) control, (b) Plasma, and (c) ASP. Color plot of the topography of the monofilaments (d) control, (e) Plasma, and (f) ASP. The darker colors (blue/violet) denote the valleys (indicated exemplarily with solid arrows), and the lighter colors (yellow red white) denote the peaks of the surface (indicated exemplarily with dotted arrows). Bar plots of the surface roughness of the filaments parallel (g) and perpendicular (h) to the filament axis; n.s. indicates nonsignificance.
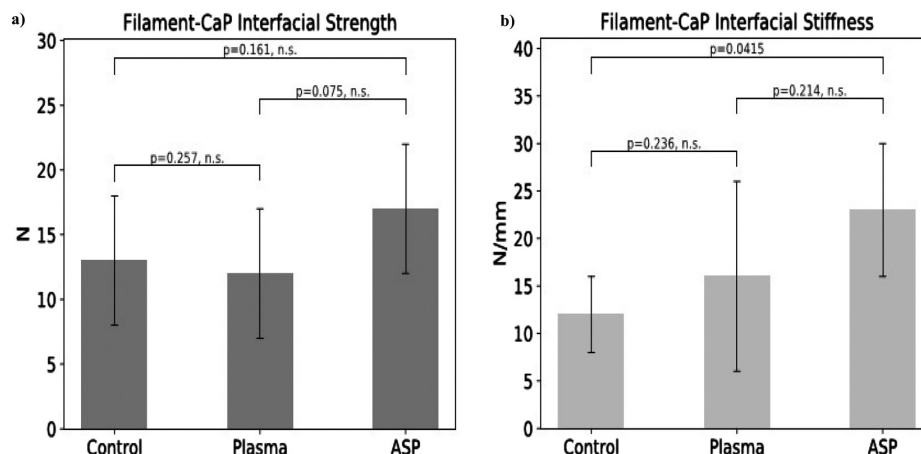
60

FIG. 3. Bar plots of the interfacial strength (a) and stiffness (b) of the different treatments. n.s. indicates nonsignificance.

The interfacial stiffness values measured were 12 ± 4, 16 ± 10, and 23 ± 7 N/mm for the control, Plasma, and ASP group, respectively. The differences between control and ASP were significant ($p = 0.03$). The values for maximum debonding load were 13 ± 2, 12 ± 5, and 17 ± 5 N (Table I, Fig. 3) for the control, Plasma, and ASP group, respectively. The maximum debonding loads measured showed a broad scattering with the differences being not significant ($p = 0.27$). Debonding occurred generally within 1 mm (approximately 10 %) of displacement. One filament (CTRL 5) of the control group was embedded approximately 1.5 mm deeper (supplementary material, Fig. 20a)[23] due to a measurement error; however, its debonding behavior was in line with the other samples and was, therefore, included in the analysis. The debonding zone width varied between a sharp peak (no discernible debonding zone) and approximately 2 mm in displacement among the samples. A majority of the samples in all groups showed slip hardening behavior beyond the debonding zone (supplementary material, Figs. 19 and 20).[23]

E. Calcium adsorption on the filament surface after pull-out

The control samples had a relative coverage area of Ca(II) of 11 ± 7 % of the total area analyzed, Plasma had an average of 17 ± 10 % Ca (II), and ASP showed an average of 29 ± 17 % Ca (II), (Table I). The coverage of calcium was significantly higher ($p = 0.002$) between the ASP and the control group. No significant difference was found between ASP and Plasma ($p = 0.054$) or Plasma and the control group ($p = 0.08$) regarding calcium coverage (Fig. 4). No significant difference in calcium concentration was observed with regard to the position of the measurement in the sample (top/bottom/center) ($p \geq 0.69$).

IV. DISCUSSION

A. Surface functionalization

The observed 50 % increase in retained barium on the ASP treated surface after rinsing, compared to control, agrees with the
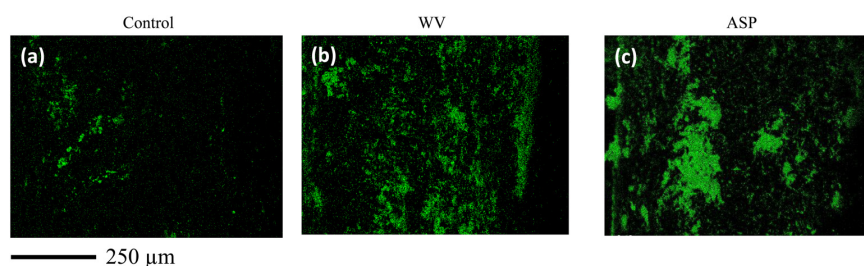

FIG. 4. EDX images of the distribution of calcium (green) on different PLA monofilament areas after pull-out testing. Untreated control (a), water vapor plasma treated (Plasma, b), and functionalized with aspartic acid (ASP, c); different amounts of calcium phosphate are visible as green areas on the monofilament surface.

results obtained by Rautaray and co-workers. They observed a strong bonding between the divalent calcium ions and ASP coated gold nanoparticles.[12] The ratio of calcium ions adsorbed from solution can be assumed to be similar to the ratio of adsorbed barium due to the same mechanism of adsorption. The increased oxygen to carbon ratio in the sample suggests an increased presence of carboxyl groups stemming from the ASP and carbonyl groups caused by unreacted NHS. A lower barium and a higher oxygen concentration were measured in the HMD, NTA, and EDTA groups compared to ASP. This suggests that a higher reaction yield of chelating groups was obtained in ASP compared to all other groups. This is due to the additional reaction step required to attach the groups to the surface, resulting in an overall lower concentration of chelating groups on the surface and a higher concentration of retained NHS. Regarding the reaction efficiency, both ASP and NTA were present in bidentate form, where the third arm of NTA was linked to the surface. However, approximately a fivefold concentration of barium was present on the ASP samples compared to the NTA; it can, therefore, be assumed that five times more ASP was present on the surface compared to NTA. Assuming a similar reaction yield of NTA and EDTA, the EDTA covered surface had approximately a twofold concentration of barium. Since ETDA is present in the tridentate form, with the fourth arm linked to the surface, it can be assumed that EDTA had double the chelation strength of NTA and ASP. Thus, ASP presents a compromise between reaction efficiency and chelation strength. The reason for low concentration of barium on the Plasma samples compared to control, despite the increase in oxygen concentration, is unclear. It is possible that the carbonyl groups were not in a chelating, i.e., bidentate, form, thus providing less sites for barium to remain adsorbed after the rinsing step. The results from the functionalization step showed different residual elements stemming from the glassware and buffering solution. The presence of these residuals suggests a need for an optimized rinsing procedure that at the same time does not damage the coating.

B. Hydrophilicity

All functionalized samples (ASP, HMD, NTA, and EDTA) showed distinctly reduced water contact angles. However, this increase in surface hydrophilicity did not result in an increase in barium concentration on the surface of all groups. In fact, the two groups with the lowest water contact angle, namely EDTA and NTA, had a lower barium concentration than the control group. On the other hand, ASP, with a lower hydrophilicity than the above groups, had double the concentration of barium compared to the other groups. This supports the argument that the bond between the ASP and the barium discussed in Sec. IV A had a higher effect on barium retention than hydrophilicity alone. Indeed, the principal component analysis performed on control, Plasma, and ASP (supplementary material, Table 3)[23] showed that the highest contribution for the first component (proportion of 0.671) came from the chelation (0.584). Both surface roughness parallel and perpendicular contributed negatively (−0.456,−0.557) as well as hydrophilicity, but to a smaller degree (−0.377). Furthermore, plotting hydrophilicity against the barium concentration (supplementary material, Fig. 23)[23] shows the effect of ASP as outlier against the rest of the data. The hydrophilicity of the Plasma samples, i.e., by depositing a functional plasma polymer layer, was comparable to other typical plasma treatments used to increase hydrophilicity. For example, the PGLA samples treated with O_2 plasma by Canal and co-workers,[10] Guimond and co-workers,[17] or Körner and co-workers[21] achieved angles approximately 20° lower with their protocols than the Plasma samples considered here. This difference might be ascribed to the addition of Ar in the plasma helping to stabilize the nanoscaled plasma polymer film via crosslinking at the expense of polar functional groups. Körner and co-workers reported angles below 10°.[21] However, the surface layer treated in such a way dissolved in aqueous media. This would not be useable when mixing with a cementeous paste, which is an aqueous, generally acidic medium. Therefore, to be of use in CaP cements, the optimized, functional plasma polymer coating as a precursor step should be selected such that it remains stable in an aqueous medium. It was, thus, concluded that a decreased water contact angle did not influence the adsorption or retention of divalent species, and that the chelating effect had a stronger effect on the adsorption and retention of divalent species than increasing hydrophilicity. For that reason, the following three groups (1) ASP functionalization, and its precursor step (2) water vapor plasma coating, and (3) the unreacted control were used for further testing.

C. Surface roughness

The origin of the roughness observed can be attributed to two factors: (1) The fiber production process (filament extrusion), visible as grooves parallel to the pull-out direction (Fig. 2). The plasma treatment that resulted in an overall higher roughness both parallel and perpendicular to the pull-out direction. The effect of the surface treatments on the overall surface roughness was minimal, corresponding to a 3 % increase in the real surface of the Plasma group compared to the control. This was despite the observed twofold increase in R_a in the pull-out direction, and the threefold increase perpendicular to the pull-out direction. The surface increase of the ASP group compared to control was lower by an order of magnitude (+0.3 %). The R_a values reported in this manuscript were between 45 and 210 nm that would agree with the increase in roughness reported after O_2 plasma for 10 min treatment by Maenz and co-workers for PGLA surfaces[11] and Canal and co-workers on PLA[10] after 5 min of treatment. These R_a values were seemingly below 200 nm and below 1 μm, respectively. The decrease in surface roughness of the ASP group following the plasma reaction could be due to a partial dissolution or detachment of coated areas and/or their edges from the plasma reaction during the wet chemical functionalization step that was conducted in an aqueous solution.

D. Mechanical characterization of the interfacial strength

The analysis of interfacial modulus showed that the ASP group had, with a twofold increase compared to control, the highest values within all groups. The Plasma group showed a broad scattering and was not significantly different compared to the control or ASP group. It can be argued that the ASP coating resulted in a stiffer bonding between the CaP and the PLA that stems from the increased bonding between the ASP and the Ca ions as discussed in Sec. IV A. Regarding the interfacial strength, no significant difference was observed between the groups, which also showed a broad scattering

of the data. This is a typical behavior often observed in cements such as concrete.[22] Due to their brittle and polycrystalline nature, meaning that the defect distribution during the setting procedure within the samples has a large effect on their the behavior under load, a large variance between the samples occurs, even under identical manufacturing conditions. It was also observed that increased monofilament R_a that was induced by the plasma treatment did not have an impact on the mechanical properties, a fact already reported in previous studies.[10,11] Despite the large variances, the results with regard to interfacial strength can be considered consistent with what Canal and co-workers observed,[10] namely that the flexural strength did not increase beyond that of the untreated cement matrix. This finding and the partial coverage of the monofilaments with CaP suggest that the matrix and the interface failed at similar strengths and that part of the CaP initially attached to the surface was removed during pull-out. The results of the interfacial strength correspond to the fracture strength of the cement matrix. This is consistent with the slip hardening in the sliding/friction phase, which was observed on most of the pull-out tested samples. Such slip hardening can stem from a residual CaP remaining on the monofilaments during pull-out, resulting in an increased friction due to an increased surface of the pulled-out monofilament from residual CaP.

E. Postfracture calcium adsorption

The results of the postfracture analysis showed an almost threefold increase in calcium concentration for the ASP group, compared to control. This increase was also reported in the literature[11] for plasma treated PGLA and PLA multifilaments. This increase was reported to be originating from both an increase in hydrophilicity, resulting in an increased wetting of the filament surface with CaP cement paste, and an increase in R_a resulting in an increase of possible nucleation sites for the CaP. In this work, however, R_a did not show a significant influence; therefore, the effects from the surface chemistry were dominant. The difference between ASP and Plasma was nonsignificant, seemingly due to the broad scattering observed between the individual samples as discussed previously in Sec. IV D. No significant difference in calcium concentration was measured between the different areas of the monofilament, which is an indication for a similar distribution of the cement along the fiber surface.

V. SUMMARY AND CONCLUSION

We demonstrated the successful grafting of aspartic acid groups onto the surface of PLA monofilaments, which resulted in a 50 % increase in adsorption and retention of divalent elements on the surface using barium as exemplary element and in an almost threefold increase in calcium coverage observed postfracture. This treatment resulted in a twofold increase in interfacial stiffness between the PLA monofilament and the CaP matrix. No significant increase in mechanical interfacial strength of the interface was observed, apparently due to the weakness of the CaP matrix. The minimal increase in the real surface of the monofilaments following

plasma treatments revealed that the use of monofilaments allows for a good comparability between the groups.

REFERENCES

[1]N. Döbelin, R. Luginbühl, and M. Bohner, Chimia **64**, 723 (2010).
[2]H. H. K. Xu, F. C. Eichmiller, and A. A. Giuseppetti, J. Biomed. Mater. Res. **52**, 107 (2000).
[3]B. Pukánszky, Eur. Polym. J. **41**, 645 (2005).
[4]F. Libonati, A. K. Nair, L. Vergani, and M. J. Buehler, Mech. Res. Commun. **58**, 17 (2014).
[5]Y. You, B. M. Min, S. J. Lee, T. S. Lee, and W. H. Park, J. Appl. Polym. Sci. **95**, 193 (2005).
[6]I. Engelberg and J. Kohn, Biomaterials **12**, 292 (1991).
[7]Y. Zuo, F. Yang, J. G. C. Wolke, Y. Li, and J. A. Jansen, Acta Biomater. **6**, 1238 (2010).
[8]A. A. Leal, J. C. Veeramachaneni, F. A. Reifler, M. Amberg, D. Stapf, G. A. Barandun, D. Hegemann, and R. Hufenus, Mater. Des. **93**, 334 (2016).
[9]N. Graupner, K. Albrecht, D. Hegemann, and J. Müssig, J. Appl. Polym. Sci. **128**, 4378 (2013).
[10]C. Canal, S. Gallinetti, and M. P. Ginebra, Plasma Process. Polym. **11**, 694 (2014).
[11]S. Maenz, M. Hennig, M. Mühlstädt, E. Kunisch, M. Bungartz, O. Brinkmann, J. Bossert, R. W. Kinne, and K. D. Jandt, J. Mech. Behav. Biomed. Mater. **57**, 347 (2016).
[12]D. Rautaray, S. Mandal, and M. Sastry, Langmuir **21**, 5185 (2005).
[13]X. D. Kong, F. Z. Cui, X. M. Wang, M. Zhang, and W. Zhang, J. Cryst. Growth **270**, 197 (2004).
[14]W. A. Schroeder, L. M. Kay, B. Lewis, and N. Munger, J. Am. Chem. Soc. **77**, 3908 (1955).
[15]J. Ou, Y. Jiang, and Z. Zhang, Adv. Mater. Res. **343–344**, 882 (2012).
[16]A. G. Guex, D. Hegemann, M. N. Giraud, H. T. Tevaearai, A. M. Popa, R. M. Rossi, and G. Fortunato, Colloids Surf. B **123**, 724 (2014).
[17]S. Guimond, B. Hanselmann, M. Hossain, V. Salimova, and D. Hegemann, Plasma Processes Polym. **12**, 328 (2015).
[18]U. Edlund, T. Sauter, and A. C. Albertsson, Polym. Adv. Technol. **22**, 2368 (2011).
[19]Y. Zhan and G. Meschke, paper presented at the 8th International Conference on Fracture Mechanics of Concrete and Concrete Structures FraMCoS-8, Toledo, Spain, 10–14 March, 2013 (unpublished).
[20]L. F. Friedrich and C. Wang, Lat. Am. J. Solids Struct. **13**, 1937 (2016).
[21]E. Körner, G. Fortunato, and D. Hegemann, Plasma Processes Polym. **6**, 119 (2009).
[22]B. A. Proctor, Cem. Concr. Compos. **12**, 53 (1990).
[23]See supplementary material at https://doi.org/10.1116/1.5129989 for detailed XPS survey scans, stress- strain curves, sessile drop figures and statistical analysis.

Epilogue Part IV

7 Discussion, Conclusion and Outlook

7.1 Overall Discussion

The aim of this thesis was to investigate the factors influencing the mechanical strength of ceramic matrix polymer fiber reinforced absorbable bone cements with the goal of achieving a significant improvement in compressive strength. The main findings were as follows:

In the first manuscript, a novel method to separate electrospun continuous nanofiber meshes into dispersed discontinuous fibers using cement precursor particles was developed. Regarding the first hypothesis, the particles did not act as cutting moieties, it was rather observed that the addition of particles resulted in longer fibers, with smaller particles resulting in longer fibers. Regarding dispersion, it was observed that the particles were dispersed in between the fibers after sonication, reducing the fiber-fiber bundling and fiber-fiber interaction. Thus, this hypothesis can be considered as partially accepted.

In the second manuscript, the influence of the fiber diameter, content, and dispersity, on the final cement composition and compressive strength was investigated. Regarding the second hypothesis, the fiber dispersion indeed had the largest contribution to the reinforcement of the composite. The composite containing highly dispersed fibers, as shown by fracture analysis, having almost a three-fold increase in compressive strength, compared to the composite low fiber dispersion, despite it having a similar its crystalline material composition to other low dispersity groups. This can be attributed to the microcrack bridging effect discussed in section 3.3, especially when considering the higher (+13%) porosity and surface area (+55%)of the unreinforced cement (section 4.3). The second hypothesis can thus be considered as accepted.

In the third manuscript, a novel functionalization for the fibrous phase was developed, which increased the adsorption of divalent groups such as calcium compared to the other control groups and resulted in an increase in adhesion of CaP compared to particles compared to the control group, but no significant difference was observed regarding the plasma coated group. The third hypothesis can therefore not be proven.

Within the scope of this work, other observations were noted, for instance in the first manuscript, the systematic study conducted using the particle assisted sonication technique indicated that using hexane as dispersion medium hexane resulted in the cutting and dispersion of the entangled fibrous mats into separated discontinuous fibers, presumably due to its low surface energy, which would result in a deeper penetration of the medium between the fibers in the electrospun mats thus increasing process efficiency. Depending on the factors of particle type added, sonication time and temperature, the length range of the fibers could be varied. These factors can therefore be used as variation parameters. Regarding fiber to particle ratio, no significant difference in fiber length was observed between the ratios 2:1 and 1:4; this indicates a degree of process robustness regarding fiber length when varying its content, making the process viable for manufacturing, at least within the aforementioned range. Furthermore, it was shown that the fibers remained dispersed following the cement mixing and setting reaction, and a significant, four-fold, reinforcement in compressive strength compared to the pristine cement was achieved, which allowed for a more homogeneous mix to form, and since the presence of particles influence the length range, this opens the door for future investigations with regard to particle shape and optimization of fiber aspect ratios which would allow further improvements in mechanical strength of bone cements.

In the second manuscript it was found that a low ratio of well dispersed nanofibers (5% v/v) was sufficient to have the high degree reinforcement describe earlier. This ratio consequently showed the highest degree of dispersion of the two groups. Analysis of the mechanical fracture showed that the failure mechanism was primarily fiber-pullout. It was also found that the fiber content had a significant influence on the final composition of the cement, seemingly the presence of the fibers inhibiting the water uptake of the cement matrix. Further investigations in this area combined with analysis of the fracture sites using Voronoi mapping of the fiber exit points could be useful tool for root cause analysis of material failures that occur in the clinical environment.

Finally, in the third manuscript, while no increase in mechanical interfacial strength was observed, a twofold increase in interfacial stiffness was noted compared to the control group. This was presumably due to the brittleness of the matrix, stemming from the porosity and polycrystallinity of the material and indicates only minor benefits can be gained by increasing the interfacial adhesion in brittle porous matrices and opens the field for investigating different growth kinetics that adhere more tightly to the fibrous structure that would possibly results in further gains in strength.

In summary, the factors influencing the compressive strength of a PLA-CaP cement were therefore in order by influence:

1. Dispersity of the fibers

2. Diameter of the fibers

3. Volume fraction of the fibers

4. The chemical composition of the fiber surface

7.2   Limitations of the Work and Outlook

The work in this thesis was limited in scope and resources; therefore, certain aspects and observations were not investigated or pursued further and serve as a possibility for future studies. For example, the limitation of the sample size of 3-5 due to limitations in time and resources increased the statistical noise, an increase to a sample size of at least 30 would reduce the noise present in the data. The fiber type was limited to PLA. It is possible that when using stiffer fibers such as PGA the particles would have been cut under the influence of the particles. Due to the bottleneck of the manual setup of the sonication process and its long duration, only samples of small volume that were suitable for compressive mechanical testing could be manufactured. Larger samples, for example flexural testing samples, could give further insight into the mechanical properties of the composite, for example in its tensile properties, or in assessing the similarity of its behavior regarding a discontinuous ceramic or a continuous composite. The design of the experiment was limited to two levels in the second manuscript, consequently it is not clear if for example 5% fiber volume fraction represents a maximum in strength, or if the maximum is below 5% or somewhere below 30%. The resulting crystalline composition varied among the groups, seemingly due to the presence of the dispersed fibers. A tighter control over the experimental conditions would yield a more similar composition between the groups and would increase the comparability. The Voronoi diagram analysis was limited to the fractured areas, which represent the weakest points of the samples. it is possible, by using a suitable slicing technique, that intact sections of the samples can be investigated for their fiber dispersity. Finally, the cement attachment process was investigated in bulk only, which yielded inconclusive results due to the polycrystalline discontinuous nature of the cement matrix. An investigation of the functionalization properties using a single crystal grown on the functional surface and mechanically tested using a smaller probe such as an AFM, might yield more conclusive results and separate the effect of the bulk from the actual material properties.

7.3   Conclusion

The work presented in this thesis was a systematic investigation of the factors influencing the compression strength of a fiber reinforced calcium phosphate cement. It showed the importance of fiber dispersity within reinforced cements. Despite the limits of the experimental work and proof of concepts performed, the findings in this work contributes to the further understanding of absorbable cements and opens further possible roads to achieving the goal of manufacturing load bearing CaP cements in a clinical setting.

Term / Abbreviation	Description
AMBP	Ana-Maria Buehlmann-Popa
CaP	Calcium Phosphate
CPC	Calcium Phosphate Cement
DCPA	Di Calcium Phosphate Anhydrous (Monetite), $CaHPO_4$
DCPD	Di Calcium Phosphate Dihydrate (Brushite) , $CaHPO_4 \cdot 2H_2O$
DH	Dirk Hegemann
EM	Elias Mulky
FRC	Fiber Reinforced Composite
GF	Giuseppino Fortunato
HA/HAP	Hydroxy Apatite $Ca_{10}(PO_4)_6 (OH)_2$
JS	Jorge Sague
KM	Katharina Maniura-Weber
MCPM	Mono Calcium Phosphate Monohydrate $Ca(H_2PO_4)_2 \cdot H_2O$
MF	Martin Frenz
OCP	Octa Calcium Phosphate, $Ca_8H_2(PO_4)_6 \cdot 5H_2O$
PL(L)A	Poly()-L-) Lactic Acid
RL	Reto Luginbuehl
TCP	Tri Calcium Phosphate $Ca_3(PO_4)_2$

Bibliography

[1] Y. Liu, Y. Zheng, and B. Hayes. Degradable, absorbable or resorbable—what is the best grammatical modifier for an implant that is eventually absorbed by the body? *Science China Materials*, 60(5):377–391, 2017.

[2] L. Claes, P. Augat, G. Suger, and H. J. Wilke. Influence of size and stability of the osteotomy gap on the success of fracture healing. *Journal of Orthopaedic Research*, 15(4):577–584, 1997.

[3] R. Z. LeGeros. Biodegradation and bioresorption of calcium phosphate ceramics. *Clinical Materials*, 14(1):65–88, 1993.

[4] R. Z. LeGeros. Properties of osteoconductive biomaterials: Calcium phosphates. *Clinical Orthopaedics and Related Research*, (395):81–98, 2002.

[5] S. V. Dorozhkin. Calcium orthophosphates in nature, biology and medicine. *Materials*, 2 (2):399–498, 2009.

[6] P. V. Giannoudis, H. Dinopoulos, and E. Tsiridis. Bone substitutes: an update. *Injury*, 36 Suppl 3:S20–27, 2005.

[7] W. Linhart, D. Briem, M. Amling, J. M. Rueger, and J. Windolf. Mechanisches versagen einer porösen hydroxylapatitkeramik 7,5 jahre nach implantation an der proximalen tibia. *Der Unfallchirurg*, 107(2):154–157, 2004.

[8] T. Kurien, R. G. Pearson, and B. E. Scammell. Bone graft substitutes currently available in orthopaedic practice: The evidence for their use. *Bone and Joint Journal*, 95 B(5):583–597, 2013.

[9] Synthes GmbH. chronos inject bone void filler surgical technique, 2015.

[10] M. P. Ginebra. *Cements as bone repair materials*, pages 271–308. Elsevier Inc., 2009.

[11] Stryker. Hydroset injectable ha bone substitute, 2005.

[12] L. de Ruiter, K. Rankin, M. Browne, A. Briscoe, D. Janssen, and N. Verdonschot. Decreased stress shielding with a peek femoral total knee prosthesis measured in validated computational models. *Journal of Biomechanics*, 118, 2021.

Bibliography

[13] H. A. Prentice, P. H. Chan, K. E. Royse, A. D. Hinman, N. C. Reddy, and E. W. Paxton. Revision risk in a cohort of us patients younger than 55 undergoing primary elective total hip arthroplasty. *Journal of Arthroplasty*, 37(2):303–311, 2022.

[14] U. G. K. Wegst, H. Bai, E. Saiz, A. P. Tomsia, and R. O. Ritchie. Bioinspired structural materials. *Nature Materials*, 14(1):23–36, 2015.

[15] J. Kim, S. McBride, M. Fulmer, R. Harten, Z. Garza, D. D. Dean, V. L. Sylvia, B. Doll, T. L. Wolfgang, E. Gruskin, and J. O. Hollinger. Fiber-reinforced calcium phosphate cement formulations for cranioplasty applications: A 52-week duration preclinical rabbit calvaria study. *Journal of Biomedical Materials Research - Part B Applied Biomaterials*, 100 B(4): 1170–1178, 2012.

[16] H. H. K. Xu, F. C. Eichmiller, and A. A. Giuseppetti. Reinforcement of a self-setting calcium phosphate cement with different fibers. *Journal of Biomedical Materials Research*, 52(1): 107–114, 2000.

[17] C. Bao, W. Chen, M. D. Weir, W. Thein-Han, and H. H. K. Xu. Effects of electrospun submicron fibers in calcium phosphate cement scaffold on mechanical properties and osteogenic differentiation of umbilical cord stem cells. *Acta Biomaterialia*, 7(11):4037–4044, 2011.

[18] Y. Zuo, F. Yang, J. G. C. Wolke, Y. Li, and J. A. Jansen. Incorporation of biodegradable electrospun fibers into calcium phosphate cement for bone regeneration. *Acta Biomaterialia*, 6(4):1238–1247, 2010.

[19] J. T. Elliott, J. T. Woodward, A. Umarji, Y. Mei, and A. Tona. The effect of surface chemistry on the formation of thin films of native fibrillar collagen. *Biomaterials*, 28(4):576–585, 2007.

[20] Israel Engelberg and Joachim Kohn. Physico-mechanical properties of degradable polymers used in medical applications: A comparative study. *Biomaterials*, 12(3):292–304, 1991.

[21] H. Ku, H. Wang, N. Pattarachaiyakoop, and M. Trada. A review on the tensile properties of natural fiber reinforced polymer composites. *Composites Part B: Engineering*, 42(4): 856–873, 2011.

[22] I. Rajzer, E. Menaszek, L. Bacakova, M. Rom, and M. Blazewicz. In vitro and in vivo studies on biocompatibility of carbon fibres. *Journal of Materials Science: Materials in Medicine*, 21(9):2611–2622, 2010.

[23] R. J. Egli and R. Luginbuehl. Tissue engineering - nanomaterials in the musculoskeletal system. *Swiss Medical Weekly*, 142(JULY), 2012.

[24] M. Bohner. Calcium orthophosphates in medicine: From ceramics to calcium phosphate cements. *Injury*, 31(SUPPL. 4):D37–D47, 2000.

[25] Marc Bohner. Resorbable biomaterials as bone graft substitutes. *Materials Today*, 13 (1–2):24–30, 2010.

[26] M. Bohner, U. Gbureck, and J. E. Barralet. Technological issues for the development of more efficient calcium phosphate bone cements: A critical assessment. *Biomaterials*, 26 (33):6423–6429, 2005.

[27] N. Döbelin, R. Luginbühl, and M. Bohner. Synthetic calcium phosphate ceramics for treatment of bone fractures. *Chimia*, 64(10):723–729, 2010.

[28] S. V. Dorozhkin. *Calcium Orthophosphates: Applications In Nature, Biology, And Medicine.* Pan Stanford Publishing, 2012.

[29] S. V. Dorozhkin. Nanosized and nanocrystalline calcium orthophosphates. *Acta Biomaterialia*, 6(3):715–734, 2010.

[30] M. S. A. Johnsson and G. H. Nancollas. The role of brushite and octacalcium phosphate in apatite formation. *Critical Reviews in Oral Biology and Medicine*, 3(1-2):61–82, 1992.

[31] D. Apelt, F. Theiss, A. O. El-Warrak, K. Zlinszky, R. Bettschart-Wolfisberger, M. Bohner, S. Matter, J. A. Auer, and B. Von Rechenberg. In vivo behavior of three different injectable hydraulic calcium phosphate cements. *Biomaterials*, 25(7-8):1439–1451, 2004.

[32] D. R. Carter and W. C. Hayes. Bone compressive strength: The influence of density and strain rate. *Science*, 194(4270):1174–1176, 1976.

[33] E. Charrière, S. Terrazzoni, C. Pittet, Ph Mordasini, M. Dutoit, J. Lemaître, and Ph Zysset. Mechanical characterization of brushite and hydroxyapatite cements. *Biomaterials*, 22 (21):2937–2945, 2001.

[34] Susmita Bose, Sudip Dasgupta, Solaiman Tarafder, and Amit Bandyopadhyay. Microwave-processed nanocrystalline hydroxyapatite: Simultaneous enhancement of mechanical and biological properties. *Acta Biomaterialia*, 6(9):3782–3790, 2010.

[35] P. D. Costantino, K. Jones, H. J. Pelzer, and Sr. Sisson, G. A. Hydroxyapatite cement: I. basic chemistry and histologic properties. *Archives of Otolaryngology–Head and Neck Surgery*, 117(4):379–384, 1991.

[36] F. Theiss, D. Apelt, B. Brand, A. Kutter, K. Zlinszky, M. Bohner, S. Matter, C. Frei, J. A. Auer, and B. Von Rechenberg. Biocompatibility and resorption of a brushite calcium phosphate cement. *Biomaterials*, 26(21):4383–4394, 2005.

[37] J. E. Barralet, K. J. Lilley, L. M. Grover, D. F. Farrar, C. Ansell, and U. Gbureck. Cements from nanocrystalline hydroxyapatite. *Journal of Materials Science: Materials in Medicine*, 15(4):407–411, 2004.

Bibliography

[38] I. M. Robinson and J. M. Robinson. The influence of fibre aspect ratio on the deformation of discontinuous fibre-reinforced composites. *Journal of Materials Science*, 29(18):4663–4677, 1994.

[39] K. A. Athanasiou, C. M. Agrawal, F. A. Barber, and S. S. Burkhart. Orthopaedic applications for pla-pga biodegradable polymers. *Arthroscopy*, 14(7):726–737, 1998.

[40] C. Canal and M. P. Ginebra. Fibre-reinforced calcium phosphate cements: A review. *Journal of the Mechanical Behavior of Biomedical Materials*, 4(8):1658–1671, 2011.

[41] Y. You, B. M. Min, S. J. Lee, T. S. Lee, and W. H. Park. In vitro degradation behavior of electrospun polyglycolide, polylactide, and poly(lactide-co-glycolide). *Journal of Applied Polymer Science*, 95(2):193–200, 2005.

[42] N. Bhardwaj and S. C. Kundu. Electrospinning: A fascinating fiber fabrication technique. *Biotechnology Advances*, 28(3):325–347, 2010.

[43] N. Lavielle, A. M. Popa, M. De Geus, A. Hébraud, G. Schlatter, L. Thöny-Meyer, and R. M. Rossi. Controlled formation of poly(ϵ-caprolactone) ultrathin electrospun nanofibers in a hydrolytic degradation-assisted process. *European Polymer Journal*, 49(6):1331–1336, 2013.

[44] D. H. Reneker and I. Chun. Nanometre diameter fibres of polymer, produced by electrospinning. *Nanotechnology*, 7(3):216–223, 1996.

[45] C. V. Boys. On the production, properties, and some suggested uses of the finest threads. *Proceedings of the Physical Society of London*, 9(1):8–19, 1887.

[46] Anton Formhals. Process and apparatus for preparing artificial threads, 1934.

[47] M. Chung, G. Fortunato, and N. Radacsi. Wearable flexible sweat sensors for healthcare monitoring: A review. *Journal of the Royal Society Interface*, 16(159), 2019.

[48] A. Keirouz, M. Chung, J. Kwon, G. Fortunato, and N. Radacsi. 2d and 3d electrospinning technologies for the fabrication of nanofibrous scaffolds for skin tissue engineering: A review. *Wiley Interdisciplinary Reviews: Nanomedicine and Nanobiotechnology*, 12(4), 2020.

[49] Cécilia Carron and Andrea Six. Erste transparente chirurgenmaske geht in produktion, 2020.

[50] Anthony L. Andrady. *Science and Technology of Polymer Nanofibers*. John Wiley and Sons, Hoboken, New Jersey, 2008.

[51] A. Greiner and J. H. Wendorff. Electrospinning: A fascinating method for the preparation of ultrathin fibers. *Angewandte Chemie - International Edition*, 46(30):5670–5703, 2007.

[52] S. G. Kumbar, R. James, S. P. Nukavarapu, and C. T. Laurencin. Electrospun nanofiber scaffolds: Engineering soft tissues. *Biomedical Materials*, 3(3), 2008.

[53] H. Fong. Electrospun nylon 6 nanofiber reinforced bis-gma/tegdma dental restorative composite resins. *Polymer*, 45(7):2427–2432, 2004.

[54] Robert Akins and John Rabolt. *Chapter I.2.16 - Electrospinning Fundamentals and Applications*, pages 332–339. Academic Press, 2013.

[55] J. Xue, T. Wu, Y. Dai, and Y. Xia. Electrospinning and electrospun nanofibers: Methods, materials, and applications. *Chemical Reviews*, 119(8):5298–5415, 2019.

[56] Seema Agarwal, Matthias Burgard, Andreas Greiner, and Joachim Wendorff. *Electrospinning*. De Gruyter, 2016.

[57] Geoffrey Ingram Taylor. Disintegration of water drops in an electric field. *Proceedings of the Royal Society A*, 280(1382):383–397, 1964.

[58] R. W. Nunes, J. R. Martin, and J. F. Johnson. Influence of molecular weight and molecular weight distribution on mechanical properties of polymers. *Polymer Engineering and Science*, 22(4):205–228, 1982.

[59] Gökçe Yazgan, Ruslan I. Dmitriev, Vasundhara Tyagi, James Jenkins, Gelu-Marius Rotaru, Markus Rottmar, René M. Rossi, Claudio Toncelli, Dmitri B. Papkovsky, Katharina Maniura-Weber, and Giuseppino Fortunato. Steering surface topographies of electrospun fibers: understanding the mechanisms. *Scientific Reports*, 7(1):158, 2017.

[60] C. Bordes, V. Fréville, E. Ruffin, P. Marote, J. Y. Gauvrit, S. Briançon, and P. Lantéri. Determination of poly(ϵ-caprolactone) solubility parameters: Application to solvent substitution in a microencapsulation process. *International Journal of Pharmaceutics*, 383(1–2): 236–243, 2010.

[61] S. V. Fridrikh, J. H. Yu, M. P. Brenner, and G. C. Rutledge. Controlling the fiber diameter during electrospinning. *Physical Review Letters*, 90(14):144502/1–144502/4, 2003.

[62] L. Van Der Schueren, B. De Schoenmaker, O. I. Kalaoglu, and K. De Clerck. An alternative solvent system for the steady state electrospinning of polycaprolactone. *European Polymer Journal*, 47(6):1256–1263, 2011.

[63] L. Yao, C. Lee, and J. Kim. Fabrication of electrospun meta-aramid nanofibers in different solvent systems. *Fibers and Polymers*, 11(7):1032–1040, 2010.

[64] I. Armentano, M. Dottori, E. Fortunati, S. Mattioli, and J. M. Kenny. Biodegradable polymer matrix nanocomposites for tissue engineering: A review. *Polymer Degradation and Stability*, 95(11):2126–2146, 2010.

Bibliography

[65] M. Simonet, O. D. Schneider, P. Neuenschwander, and W. J. Stark. Ultraporous 3d polymer meshes by low-temperature electrospinning: Use of ice crystals as a removable void template. *Polymer Engineering and Science*, 47(12):2020–2026, 2007.

[66] L. R. Betterman, C. Ouyang, and S. P. Shah. Fiber-matrix interaction in microfiber-reinforced mortar. *Advanced Cement Based Materials*, 2(2):53–61, 1995.

[67] M. F. Ashby. Criteria for selecting the components of composites. *Acta Metallurgica Et Materialia*, 41(5):1313–1335, 1993.

[68] A. M. Brandt. Fibre reinforced cement-based (frc) composites after over 40 years of development in building and civil engineering. *Composite Structures*, 86(1-3):3–9, 2008.

[69] T. L. Anderson. *Fracture Mechanics: Fundamentals and Applications (3rd ed.)*. CRC Press, 2017.

[70] Ted L. Anderson. Textbook figure, 2022.

[71] S. Maenz, M. Hennig, M. Mühlstädt, E. Kunisch, M. Bungartz, O. Brinkmann, J. Bossert, R. W. Kinne, and K. D. Jandt. Effects of oxygen plasma treatment on interfacial shear strength and post-peak residual strength of a plga fiber-reinforced brushite cement. *Journal of the Mechanical Behavior of Biomedical Materials*, 57:347–358, 2016.

[72] N. Graupner, K. Albrecht, D. Hegemann, and J. Müssig. Plasma modification of man-made cellulose fibers (lyocell) for improved fiber/matrix adhesion in poly(lactic acid) composites. *Journal of Applied Polymer Science*, 128(6):4378–4386, 2013.

[73] C. L. Casper, N. Yamaguchi, K. L. Kiick, and J. F. Rabolt. Functionalizing electrospun fibers with biologically relevant macromolecules. *Biomacromolecules*, 6(4):1998–2007, 2005.

[74] A. G. Guex, D. Hegemann, M. N. Giraud, H. T. Tevaearai, A. M. Popa, R. M. Rossi, and G. Fortunato. Covalent immobilisation of vegf on plasma-coated electrospun scaffolds for tissue engineering applications. *Colloids and Surfaces B: Biointerfaces*, 123:724–733, 2014.

[75] M. Sawawi, T. Y. Wang, D. R. Nisbet, and G. P. Simon. Scission of electrospun polymer fibres by ultrasonication. *Polymer (United Kingdom)*, 54(16):4237–4252, 2013.

[76] I. Perelshtein, G. Applerot, N. Perkas, J. Grinblat, E. Hulla, E. Wehrschuetz-Sigl, A. Hasmann, G. Guebitz, and A. Gedanken. Ultrasound radiation as a throwing stones technique for the production of antibacterial nanocomposite textiles. *ACS Applied Materials and Interfaces*, 2(7):1999–2004, 2010.

[77] J. Engstrand, C. Persson, and H. Engqvist. The effect of composition on mechanical properties of brushite cements. *Journal of the Mechanical Behavior of Biomedical Materials*, 29(1):81–90, 2014.

[78] E. N. Bolbasov, M. Rybachuk, A. S. Golovkin, L. V. Antonova, E. V. Shesterikov, A. I. Malchikhina, V. A. Novikov, Y. G. Anissimov, and S. I. Tverdokhlebov. Surface modification of poly(l-lactide) and polycaprolactone bioresorbable polymers using rf plasma discharge with sputter deposition of a hydroxyapatite target. *Materials Letters*, 132(0): 281–284, 2014.

[79] C. Canal, S. Gallinetti, and M. P. Ginebra. Low-pressure plasma treatment of polylactide fibers for enhanced mechanical performance of fiber-reinforced calcium phosphate cements. *Plasma Processes and Polymers*, pages 694–703, 2014.

[80] S. Guimond, B. Hanselmann, M. Hossain, V. Salimova, and D. Hegemann. Deposition of plasma polymer films from acetylene and water vapor. *Plasma Processes and Polymers*, 12(4):328–335, 2015.

[81] N. R. Davis and T. E. Walker. The role of carboxyl groups in collagen calcification. *Biochemical and Biophysical Research Communications*, 48(6):1656–1662, 1972.

Acknowledgements

This PhD Thesis would not have been possible without the support and encouragement of more people than could fit on these pages. So first of all my gratitude goes to all of those that supported me and are not mentioned here.

Acknowledgements

- Benjamin Andreatta and Dr. Jorge Sague for their help and introduction to chemical methods.

- Prof. Dr. Marc Bohner and Dr. Nicola Döbelin for their valuable input and support regarding calcium phosphate cements.

- Josiane Meister, Myriam Herger, and Thomas Imwinkelried for the good times at lunch and the great yoga lessons.

- Gökçe Yazgan Panosetti for the great inputs, times and conversations on and off the road.

- Christian May for the valuable discussions, ideas, help, great puns, Maultäschle and correcting my thesis.

- Nadia Zbären for her constant support throughout the years.

- Michael Müller for his optimism, great ideas and always giving me the extra push out of my comfort zone.

- My mother who never stopped believing in and standing by me.

- and many, many more …

Rümlang, February 27, 2022   E. M.

List of Publications

Mulky, E., G. Yazgan, K. Maniura-Weber, R. Luginbuehl, G. Fortunato and A.-M. Bühlmann-Popa. 2014. Fabrication of biopolymer-based staple electrospun fibres for nanocomposite applications by particle-assisted low temperature ultrasonication. Materials Science and Engineering: C 45: 277-286.

Mulky, E., K. Maniura-Weber, M. Frenz, G. Fortunato and R. Luginbuehl. 2018. Absorbable mineral nanocomposite for biomedical applications: Influence of homogenous fiber dispersity on mechanical properties. Journal of Biomedical Materials Research - Part A 106(3): 850-857.

Mulky, E., G. Fortunato, D. Hegemann, J. Sague, R. Heuberger and M. Frenz. 2020. Grafting of calcium chelating functionalities onto PLA monofilament fiber surfaces. Biointerphases 15(1): 011006.

Declaration of Originality

Last name, first name: Mulky, Elias

Matriculation number: 00-922-104

I hereby declare that this thesis represents my original work and that I have used no other sources except as noted by citations.

All data, tables, figures and text citations which have been reproduced from any other source, including the internet, have been explicitly acknowledged as such.

I am aware that in case of non-compliance, the Senate is entitled to withdraw the doctorate degree awarded to me on the basis of the present thesis, in accordance with the "Statut der Universität Bern (Universitätsstatut; UniSt)", Art. 69, of 7 June 2011.

Place, date

Bern, 27. February 2022

Signature

Elias Mulky
Digitally signed by Elias Mulky
Date: 2022.02.27 22:04:15 +01'00'